SMALL SCALE ALFVÉNIC STRUCTURE IN THE AURORA

K. STASIEWICZ[1], P. BELLAN[2], C. CHASTON[3], C. KLETZING[4], R. LYSAK[5],
J. MAGGS[6], O. POKHOTELOV[7], C. SEYLER[8], P. SHUKLA[9], L. STENFLO[10],
A. STRELTSOV[11] and J.-E. WAHLUND[1]

[1]*Swedish Institute of Space Physics, Uppsala, Sweden*
[2]*California Institute of Technology, Pasadena, U.S.A.*
[3]*Space Sciences Laboratory, University of California, Berkeley, U.S.A.*
[4]*Department of Physics and Astronomy, University of Iowa, U.S.A.*
[5]*School of Physics and Astronomy, University of Minnesota, U.S.A.*
[6]*Physics Department, University of California, Los Angeles, U.S.A.*
[7]*Institute of Physics of the Earth, Moscow, Russia*
[8]*School of Electrical Engineering, Cornell University, U.S.A.*
[9]*Institut für Theoretische Physik, Ruhr-Universität, Bochum, Germany*
[10]*Department of Plasma Physics, Umeå University, Sweden*
[11]*Thayer School of Engineering, Dartmouth College, U.S.A.*

Abstract. This paper presents a comprehensive review of dispersive Alfvén waves in space and laboratory plasmas. We start with linear properties of Alfvén waves and show how the inclusion of ion gyroradius, parallel electron inertia, and finite frequency effects modify the Alfvén wave properties. Detailed discussions of inertial and kinetic Alfvén waves and their polarizations as well as their relations to drift Alfvén waves are presented. Up to date observations of waves and field parameters deduced from the measurements by *Freja*, Fast, and other spacecraft are summarized. We also present laboratory measurements of dispersive Alfvén waves, that are of most interest to auroral physics. Electron acceleration by Alfvén waves and possible connections of dispersive Alfvén waves with ionospheric-magnetospheric resonator and global field-line resonances are also reviewed. Theoretical efforts are directed on studies of Alfvén resonance cones, generation of dispersive Alfvén waves, as well their nonlinear interactions with the background plasma and self-interaction. Such topics as the dispersive Alfvén wave ponderomotive force, density cavitation, wave modulation/filamentation, and Alfvén wave self-focusing are reviewed. The nonlinear dispersive Alfvén wave studies also include the formation of vortices and their dynamics as well as chaos in Alfvén wave turbulence. Finally, we present a rigorous evaluation of theoretical and experimental investigations and point out applications and future perspectives of auroral Alfvén wave physics.

Table of Contents

1. Introduction

1.1. ALFVÉN WAVES

Alfvén waves are low-frequency, electromagnetic waves in a conducting fluid with a background magnetic field. In the Alfvén wave the background magnetic field tension provides the restoring force, whereas the ion mass provides the inertia. The existence of such waves was theoretically predicted by Alfvén (1942). Before the discovery of these waves only sound or acoustic waves were known to exist due to the compressibility of a fluid. This theoretical prediction was of great importance because it opened new possibilities to transport energy in a medium. The experimental confirmation of this extremely fruitful idea appeared several years later, when experiments in the (now) Alfvén laboratory in Stockholm proved the existence of these waves in mercury and in liquid sodium. The first experimental evidence for the existence of Alfvén waves in a plasma appeared 10 years after Alfvén predicted their existence. A standing wave of the appropriate frequency was observed first by Bostick and Levine (1952) in a pulsed toroidal device. Wilcox *et al.* (1960) in a laboratory plasma experiment verified the Alfvén speed and

reflections of the wave from a conducting and insulating end-plates. The wave represents a perturbation of the perpendicular electric and magnetic field, traveling along the applied magnetic field. Upon reflection from the conducting end, the wave reversed sign of the electric signal and retained the sign of the magnetic perturbation. A reflection from a non-conductive end resulted in preserving the sign of the electric field and reversing the magnetic perturbation.

Let us recall briefly the major results of magnetohydrodynamic theory (see e.g. Alfvén and Fälthammar, 1963). Assume that the background magnetic field is oriented along the z-axis and consider plane waves propagating obliquely at an angle θ to the applied field. For waves at frequency below the ion gyrofrequency, $\omega_{ci} = q_i B_0 / m_i$, the linear analysis of MHD equations leads to three wave modes. The first one is the Alfvén wave which has the frequency

$$\omega = k_z v_{\mathrm{A}} \, , \tag{1}$$

where

$$v_{\mathrm{A}} = \frac{B_0}{(\mu_0 \rho)^{1/2}} \, , \tag{2}$$

v_{A} is the Alfvén velocity, $k_z = k \cos \theta$, and $\rho = n_i m_i$ is the mass density. The other two modes are fast and slow magnetosonic modes.

The dispersion relation for the Alfvén wave does not depend on the elastic properties of the fluid. In a wave of this type there are no fluctuations of the density and the pressure, i.e., $\delta n = 0$ and $\delta p = 0$. The perturbation vector $\mathbf{b}$ is perpendicular to the planes of the vectors $\mathbf{B}_0$ and $\mathbf{k}$; the electric field $\mathbf{E}$ is perpendicular to $\mathbf{B}_0$ and lies in the $\mathbf{B}_0$, $\mathbf{k}$ plane. The fluid velocity $\mathbf{u}$ is connected with the perturbation of the magnetic field $\mathbf{b}$ by $\mathbf{u} = \mp \mathbf{b}/(\mu_0 \rho)^{1/2}$, where the upper (lower) sign refers to the case $\mathbf{k} \cdot \mathbf{B}_0 > 0$ ($\mathbf{k} \cdot \mathbf{B}_0 < 0$).

1.2. Dispersive Waves and Their Relation to Aurora

Ideal MHD, by definition, has no field-aligned electric field and thus the waves derived above cannot provide parallel energization of particles which are a known feature of the coupling between the ionosphere and magnetosphere. After Stefant (1970) pointed out that inclusion of kinetic effects related to finite ion gyroradius produces Alfvén wave dispersion and magnetic field-aligned electric field, the dispersive waves became increasingly important in the study of magnetosphere-ionosphere interactions. The parallel electric field is produced by low-frequency ($\omega < \omega_{ci}$) dispersive Alfvén waves when the wavelength perpendicular to the background magnetic field becomes comparable either to the ion gyroradius at electron temperature, $\rho_s = (T_e/m_i)^{1/2}/\omega_{ci}$, the ion thermal gyroradius, $\rho_i = (T_i/m_i)^{1/2}/\omega_{ci}$ (Hasegawa, 1976), or to the collisionless electron skin depth $\lambda_e = c/\omega_{pe}$ (Goertz and Boswell, 1979).
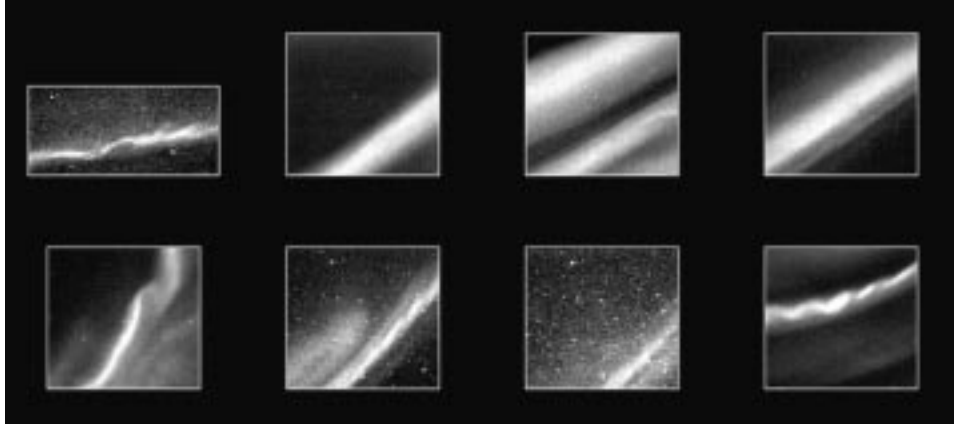
Figure 1. Discrete optical auroral forms with thickness of 0.1–1 km. (Courtesy of T. S. Trondsen, University of Calgary.)

The most natural way of launching Alfvén waves, which is usually realized in space plasmas is through a sheared plasma flow across the background magnetic field. A typical example of such a process is the plasma expansion to the inner regions of the Earth's magnetosphere during magnetic storms or forcing of the magnetopause boundary by the solar wind. Also, any impulsive reconfiguration of the magnetic field (e.g., reconnection) would launch a spectrum of Alfvén waves. As the waves created by these processes propagate towards the ionosphere, they generate filamentary structures extending along the magnetic field lines that connect spatial gradients in the magnetosphere and the ionosphere providing an efficient magnetosphere-ionosphere coupling. It is believed that auroral forms and vortex structures with a thickness of 0.1–10 km are related to the nonlinear Alfvén wave phenomena. A characteristic thickness of ~ 100 m corresponds to a typical electron inertial length in the topside ionosphere. High resolution optical observations of the thickness of auroral forms (Maggs and Davis, 1968) have shown that the most probable value for the thickness of optical arcs is about 100 m. These results have been recently corroborated by Trondsen *et al.* (1997) and Trondsen and Cogger (1998) who find a similar mean value. Figure 1 shows examples of thin auroral forms (0.1–1 km) which are most likely related to nonlinear inertial Alfvén wave structures.

We shall adopt the following convention in this paper. Inertial Alfvén Waves (IAW) are $\omega < \omega_{ci}$ Alfvén waves in a medium where the electron thermal velocity, $v_{te} = (2T_e/m_e)^{1/2}$, is less than v_A. As will be elaborated later, in such a case, the parallel electric field is supported by the electron inertia. Kinetic Alfvén Waves (KAW) are waves in a medium where $v_{te} > v_A$. In this case, the parallel electric force is balanced by the parallel electron pressure gradient. The term Dispersive Alfvén Waves (DAW) would cover these two cases. Clearly, the IAW arises in a low-beta plasma with $\beta = 2\mu_0 nT/B_0^2 < m_e/m_i$, whereas the KAW appear in an

intermediate beta plasma with $m_e/m_i < \beta < 1$. Here, $T = (T_e + T_i)/2$ is the plasma temperature. The dispersive properties of the waves become increasingly important when the perpendicular wavelength, or characteristic scale of spatial inhomogeneities become comparable with ρ_s, ρ_i, or λ_e.

Alfvén waves, and particularly DAW, play important role in space electrodynamics for several reasons. They are responsible, or related to:

(1) Energy transport in the form of the Poynting flux $\mathbf{S} = \mu_0^{-1}\mathbf{E} \times \mathbf{B}$ over large distances in space.

(2) Global oscillations and resonances.

(3) Mutual magnetosphere–ionosphere coupling.

(4) Turbulence, energy cascading over wide range of spatial scales.

(5) Structuring, filamentation of plasma, creation of vortices and solitons; chaos and self-organization.

(6) Ponderomotive effects.

(7) Transverse ion energization and bulk heating.

(8) Parallel electric field, the electron acceleration, and the formation of discrete aurora.

1.3. PLASMA PARAMETERS ON AURORAL FIELD LINES

In the study of Alfvén waves in the auroral zone, the background plasma parameters play a critical role in setting the Alfvén speed v_A as well as the wave dispersion characteristics through the electron skin depth, the electron thermal speed, and ion gyro-radius. Neither the plasma density nor the temperature on the auroral field lines has been extensively reported in the literature, but we briefly summarize the reported observations here.

In situ measurements of the plasma density have been determined primarily either through the analysis of wave modes with a density dependent dispersion relation or through swept or fixed-bias Langmuir probes. Topside sounding of the plasma frequency at high latitude from ISIS 1 found density cavities associated with auroral kilometric radiation (AKR). The cavities had densities of the order of a factor of 10 less than the background density in narrow latitudinal bands (Benson and Calvert, 1979; Benson et al., 1980).

At higher altitudes most measurements have used the wave techniques. Among the earliest in the auroral zone are those from the S3-3 satellite which showed one of the few published altitudinal distributions of density in the auroral zone at altitudes between 1000 and 8000 km determined from measurements of the lower hybrid frequency (Mozer et al., 1979). The dependence of density on altitude was fit to an inverse power law form (Lysak and Hudson, 1979). The altitudinal extent of the density profile at high latitudes was greatly extended by a study of DE 1 wave data in which a large number of measurements of the upper cutoff of whistler mode radiation at the electron plasma frequency was used to determine density at radial distances of $2-5$ R_E (Persoon et al., 1983).
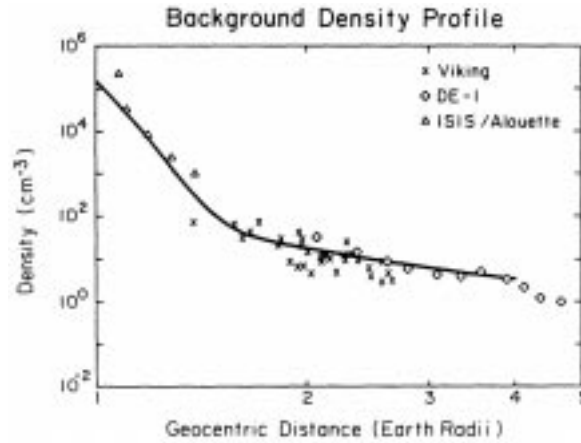
Figure 2. Model profile of electron density compared with data from several spacecraft. (Taken from Kletzing and Torbert, 1994.)

More recently, results from the Viking satellite provided additional information on the density at high latitudes and altitudes up 13 000 km. Hilgers (1992), using a swept Langmuir probe, found a density profile that agreed well with the composite profile from DE 1, Allouette II and ISIS 1 data. The same Viking measurements also found very low densities in the AKR-producing regions which could be as low as 1 cm^{-3} (Hilgers, 1992; Hilgers *et al.*, 1992). These low plasma densities were also reported in a study of Viking wave data by Perraut *et al.* (1990). Kletzing and Torbert (1994) summarized these density measurements, adding low altitude data from rocket measurements to find a model profile given by

$$n(r) = n_a e^{-(r-r_0)/h} + n_b(r-1)^{-1.5} , \tag{3}$$

where n, n_a, n_b are given in cm^{-3} and r (measured from the center of the earth), r_0, and h in R_E. Typical parameters are $r_0 = 1.05$, $h = 0.06$, $n_a = 6 \times 10^4$, $n_b \approx 17$. A comparison of this profile with data from several satellites is displayed in Figure 2.

Published profiles of the plasma temperature above 2000 km at high latitude are exceedingly rare. At low latitudes a temperature profile appropriate for the plasmasphere was determined by Kasha (1969). Reports of the temperature determination anywhere at high latitude are difficult to find. Kintner *et al.* (1978) determined plasma temperature from the electrostatic hydrogen cyclotron wave spectrum in the auroral zone and found a characteristic temperature near 3 eV. Mozer *et al.* (1979) found an electron temperature of 0.4 eV at an altitude of 6400 km. They also state that temperatures in the auroral zone are typically of the order of 1–5 eV. More recently, Perraut *et al.* (1990) found that Viking measurements, combining wave spectra with active relaxation sounding and a mutual impedance probe, showed that the plasma on the auroral field lines is cold with temperatures of the order of 1 eV. They also found that this plasma was dominated by ionospheric plasma with
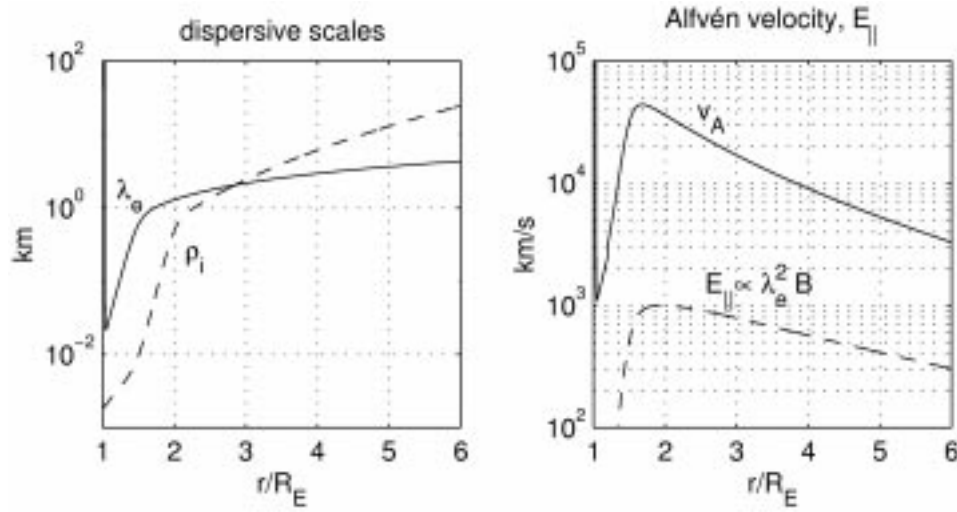
Figure 3. Profiles of the dispersive scales (λ_e, ρ_i), the Alfvén velocity v_A and a scaling factor for the parallel electric field $E_\parallel \propto \lambda_e^2 B$, as functions of geocentric distance.

ratios of cold to hot plasma of $100-1000$. Most recently, Kletzing *et al.* (1998) presented a statistical study of Langmuir sweep data which showed that for the auroral zone and polar cap, the background plasma outside acceleration regions is quite cold. The bulk of the measurements showed electron temperatures less than 5 eV up to 8000 km altitude, the highest altitude measured. This suggested that up to this altitude, the background, unperturbed plasma is dominated by cold, ionospheric plasma.

The above does not apply to active regions with Alfvén wave turbulence. As will be elaborated further, *Freja* results show (Section 3.3) that in regions with broadband turbulence, a bulk ion heating is observed, and the ion temperature can be a factor of 10 larger than the electron temperature. Also, recent measurements on FAST show that in localized regions related to Alfvén waves at altitudes as low as 1000 km, the cold electrons below ~ 10 eV can be completely evacuated or heated to higher energies (see Section 3.4).

At higher altitudes, it is known that the auroral zone connects to the plasma sheet which has characteristic electron temperatures of $100-3000$ eV. Typical plasma sheet densities vary from $0.05-1.0$ cm^{-3}. Thus as the cold ionospheric plasma falls off exponentially, the power-law component begins to dominate and temperature rises to plasma sheet values.

One implication of these variations in the temperature and the density is that two different forms of the dispersive Alfvén wave exist depending on altitude. At low altitude, up to $3-4$ R_E in geocentric distance, the Alfvén speed is greater than the electron thermal speed (Lysak and Carlson, 1981) and the inertial Alfvén wave is the appropriate wave mode. However at higher altitude, the electrons become

sufficiently hot and their thermal velocity exceeds the Alfvén speed, and the kinetic Alfvén wave is the appropriate limit.

Thus, in the auroral acceleration region the electron inertial effects are the most important. The inertial length, given by $c/\omega_{pe} = 5.3$ km$/\sqrt{n}$, where the number density n is given in cm^{-3}, is plotted in Figure 3 for the density profile given in (3). Also plotted in this figure are an average ion gyroradius, the Alfvén velocity v_{A}, and a normalized value of $\lambda_e^2 B$. To compute these distributions we assumed that the average ion energy varies from 0.5 eV in the ionosphere to 1 keV in the magnetosphere with a weighting function corresponding to the two terms in Equation (3). In a similar manner the average ion mass was assumed to vary from 16 a.m.u. in the ionosphere to 1 a.m.u. in the magnetosphere. The scaling factor $\lambda_e^2 B$ is proportional to the magnitude of the parallel electric field carried by an Alfvén wave as implied from Equation (61), under assumption $J_{\parallel}/B = $ const. It can be seen that the scaled parallel electric field peaks at an altitude just under 2 R_E geocentric distance. This altitude corresponds to the typical altitude of the auroral acceleration region, suggesting that the parallel electric field of Alfvén waves plays a role in the auroral acceleration process.

2. Two-Fluid Theory of Dispersive Alfvén Waves

Solutions for dispersive Alfvén waves can be obtained from the two-fluid momentum equations for the particle species $j = \{e, i\}$

$$\frac{\partial \mathbf{u}_j}{\partial t} + \mathbf{u}_j \cdot \nabla \mathbf{u}_j = \frac{q_j}{m_j}\big(\mathbf{E} + \mathbf{u}_j \times \mathbf{B}\big) - \frac{1}{m_j n}\nabla P_j \,, \tag{4}$$

combined with the continuity equation

$$\frac{\partial n}{\partial t} + \nabla \cdot (n\mathbf{u}_j) = 0 \,, \tag{5}$$

and Maxwell's equations

$$\nabla \times \mathbf{E} = -\frac{\partial \mathbf{B}}{\partial t} \tag{6}$$

and

$$\nabla \times \mathbf{B} = \mu_0 \mathbf{J} + \frac{1}{c^2}\frac{\partial \mathbf{E}}{\partial t} \,. \tag{7}$$

Here, the standard notation is used with $\mathbf{u}_j$ denoting the flow velocity of species j, $n = n_e = n_i$ the number density, q_j the particle charge, P_j the pressure, and $\mathbf{J} = ne(\mathbf{u}_i - \mathbf{u}_e)$ the electric current density, $e = |q_e|$, and c is speed of light. The displacement current, $\epsilon_0 \partial E/\partial t$, in (7) is usually neglected for the low-frequency waves, $\omega \ll \omega_{pe}, kc$. However, the auroral zone density is sometimes low enough so that the displacement current may become important. In such cases, v_{A} must be

replaced by $v_A(1+v_A^2/c^2)^{-1/2}$, which ensures that the wave group velocity remains less than the speed of light.

For $\omega \ll \omega_{ci}$ both electron and ion perpendicular motion are well approximated by drift theory. To zeroth order in ω/ω_{cj}, both the electrons and ions have the perpendicular drift $\mathbf{u}_E = \mathbf{E} \times \mathbf{B}/B^2$, and to first order in ω/ω_{cj} have the polarization drift $\mathbf{u}_{pj} = (m_j/q_j B^2)d\mathbf{E}_\perp/dt$, where $d_t = \partial_t + \mathbf{u}_E \cdot \nabla$. Since the $\mathbf{u}_E$ drifts are identical for the electrons and ions the $\mathbf{u}_E$ drifts do not result in any net current. However, being proportional to mass the ion polarization drift provides the main contribution to the perpendicular current, which is

$$\mathbf{J}_\perp = nq_i\mathbf{u}_{pi} = \frac{nm_i}{B_0^2}\frac{d\mathbf{E}_\perp}{dt} = \frac{1}{\mu_0 v_A^2}\frac{d\mathbf{E}_\perp}{dt} \ . \tag{8}$$

It is convenient in the discussion of dispersive Alfvén waves to introduce the scalar potential ϕ and a vector potential $\mathbf{A} = A_z\hat{\mathbf{z}}$, so that the wave electric field can be written as

$$\mathbf{E} = -\nabla\phi - \frac{\partial A_z}{\partial t}\hat{\mathbf{z}} \ . \tag{9}$$

In view of the low-beta approximation ($\beta \ll 1$), we have neglected the perpendicular component of the vector potential. Thus, the wave magnetic field perturbation is $\mathbf{b} = \nabla \times (A_z\hat{\mathbf{z}}) = \nabla A_z \times \hat{\mathbf{z}}$. It follows from (9) that the parallel and perpendicular components of the wave electric field are, respectively,

$$E_\parallel = -\frac{\partial\phi}{\partial z} - \frac{\partial A_z}{\partial t} \tag{10}$$

and

$$\mathbf{E}_\perp = -\nabla_\perp\phi. \tag{11}$$

The dependence of the electric field on both an electrostatic and a vector potential means that the inertial wave cannot be neatly categorized as an electrostatic wave (i.e., function of ϕ only) or as an electromagnetic wave (i.e., function of vector potential only). This intertwining of both ϕ and A_z means that the conventional simplifying intuitive descriptions of electric fields are inappropriate since these intuitive descriptions typically assume that the electric field is either completely electrostatic or completely inductive. For example, in the electrostatic approximation it is assumed that the electric field is conservative so that the difference in potential between two points is just $\Delta\phi = -\int_a^b \mathbf{E} \cdot d\mathbf{l}$ and independent of the path between points a and b. However, when there is a vector potential, the integral is path-dependent since $\oint \mathbf{E} \cdot d\mathbf{l} \neq 0$. In fact, Faraday's law shows that $\oint \mathbf{E} \cdot d\mathbf{l}$ equals the rate of change of the magnetic flux linked by the path of integration. These considerations show that when Alfvén wave propagation is important, integration of the electric field, i.e., $\int \mathbf{E} \cdot d\mathbf{l}$ will *not* produce a system of closed electrostatic equipotentials.

The total wave current is given by

$$\mu_0 \mathbf{J} = \nabla \times \nabla \times (A_z \hat{\mathbf{z}}) = \nabla \nabla \cdot (A_z \hat{\mathbf{z}}) - \nabla^2 A_z \hat{\mathbf{z}} , \tag{12}$$

so that the parallel and perpendicular components of the current densities are, respectively,

$$\mu_0 J_\parallel = -\nabla_\perp^2 A_z \tag{13}$$

and

$$\mu_0 \mathbf{J}_\perp = \nabla_\perp \frac{\partial A_z}{\partial z} . \tag{14}$$

2.1. PARALLEL ELECTRON INERTIAL EFFECTS

We first discuss the inertial Alfvén waves (IAW). These waves appear in low β plasma when $\beta < m_e/m_i$, i.e., $v_A > v_{te}, v_{ti}$. When $\beta \ll m_e/m_i$ the dominant mechanism for driving the magnetic field-aligned electric field is associated with the parallel electron inertia. The parallel motion is simply a quiver in response to the parallel electric field and since this quivering motion is inversely proportional to the particle mass, the electron parallel motion dominates. Because for IAW $\omega/k_z \gg v_{te}$, the parallel electron pressure gradient is discarded from the electron parallel equation of motion (4), which becomes simply

$$m_e \, \partial u_{e\parallel}/\partial t = q_e E_\parallel . \tag{15}$$

Substituting $E_\parallel$ from (10) and $J_\parallel (= n q_e u_{e\parallel})$ from (13) into (15) we obtain

$$(1 - \lambda_e^2 \nabla_\perp^2) \frac{\partial A_z}{\partial t} = -\frac{\partial \phi}{\partial z} , \tag{16}$$

where $\lambda_e = c/\omega_{pe}$ is the collisionless electron skin depth. On the other hand, combination of (8), (11), and (14) gives

$$\nabla_\perp \frac{\partial A_z}{\partial z} = -\frac{1}{v_A^2} \nabla_\perp \frac{\partial \phi}{\partial t} , \tag{17}$$

which gives

$$\frac{\partial A_z}{\partial z} = -\frac{1}{v_A^2} \frac{\partial \phi}{\partial t} . \tag{18}$$

Differentiation of (16) with respect to time and then inserting (18) leads to the inertial Alfvén wave equation

$$(1 - \lambda_e^2 \nabla_\perp^2) \frac{\partial^2 A_z}{\partial t^2} = v_A^2 \frac{\partial^2 A_z}{\partial z^2} . \tag{19}$$

Fourier transform of (19) yields the inertial Alfvén wave dispersion relation (Drell *et al.*, 1965; Goertz and Boswell, 1979)

$$\omega^2 = \frac{k_\parallel^2 v_A^2}{1 + k_\perp^2 \lambda_e^2} \; . \tag{20}$$

In the limit $k_\perp^2 \lambda_e^2 \ll 1$ this reduces to the MHD Alfvén wave dispersion relation. On the other hand, for $k_\perp^2 \lambda_e^2 \gg 1$ the IAW looses its electromagnetic character, and (20) reduces to the modified convective cells (Okuda and Dawson, 1973), $\omega = (k_\parallel / k_\perp)\omega_{gm}$, where $\omega_{gm} = (\omega_{ce}\omega_{ci})^{1/2}$ is the geometric mean of the electron and ion gyro-frequencies.

Propagation characteristics of inertial Alfvén waves differ significantly from the predictions of MHD models. The inclusion of nonzero values of $k_\perp$ results in two important consequences, a spreading of the wave energy across magnetic field lines and a nonzero parallel electric field. The energy (ray path) propagates along the group velocity, given by

$$\frac{\partial \omega}{\partial \mathbf{k}} = \hat{\mathbf{z}}\frac{v_A}{(1 + k_\perp^2 \lambda_e^2)^{1/2}} - \hat{\mathbf{x}}\omega\lambda_e\frac{k_\perp \lambda_e}{1 + k_\perp^2 \lambda_e^2} \; . \tag{21}$$

The electron inertia leads to a decrease of the field-aligned group velocity of the inertial Alfvén wave, i.e., the wavepackets are always sub-Alfvénic. The perpendicular group velocity for these waves is in the negative $\mathbf{k}_\perp$ direction and goes to zero at $k_\perp \lambda_e = 0$. That is, the wave is a backward wave for propagation across the magnetic field. As can be seen from (20) inertial Alfvén waves must have $\omega^2 \leq k_\parallel^2 v_A^2$, so that they propagate inside a conical region with apex angle satisfying

$$\tan \theta_r = \frac{\omega}{\omega_{ci}} \left(\frac{m_e}{m_i}\right)^{1/2} , \tag{22}$$

as implied from (21). Waves with $k_\perp \lambda_e \gg 1$ have a group velocity very close to the angle θ_r. In this regime the group and phase velocities are nearly orthogonal.

2.2. KINETIC EFFECTS

In the other limiting case when the plasma electron β_e is larger than the mass ratio, and the Alfvén wave speed is much slower than the electron thermal speed the electron inertia is small and the parallel electric field is balanced by the parallel electron pressure gradient. When $T_e \gg T_i$ the corresponding wave equation can be obtained by using considerations similar to those used for inertial waves. From the parallel component of the electron motion (4) we have, assuming the temperature does not vary along the field,

$$E_\parallel = -\frac{T_e}{en_0}\frac{\partial n_{e1}}{\partial z} = -e\mu_0\rho_s^2 v_A^2\frac{\partial n_{e1}}{\partial z} \; , \tag{23}$$

where n_{e1} is a small perturbation in the equilibrium density n_0, $\rho_s = c_s/\omega_{ci}$, and $c_s = (T_e/m_i)^{1/2}$ is the sound speed. From (10) and (23) we obtain

$$e\mu_0 \rho_s^2 v_{\mathrm{A}}^2 \frac{\partial n_{e1}}{\partial z} = \frac{\partial A_z}{\partial t} + \frac{\partial \phi}{\partial z} \, . \tag{24}$$

The variation of the electron density is coupled to the field aligned current density according to the electron continuity Equation (5), which combined with (13) gives

$$\frac{\partial n_{e1}}{\partial t} + \frac{1}{e\mu_0} \frac{\partial}{\partial z} \nabla_\perp^2 A_z = 0 \, . \tag{25}$$

Combining Equations (18), (24), and (25) we have

$$\frac{\partial^2 A_z}{\partial t^2} - \frac{\partial}{\partial z} v_{\mathrm{A}}^2 \frac{\partial A_z}{\partial z} + v_{\mathrm{A}}^2 \rho_s^2 \nabla_\perp^2 \frac{\partial^2 A_z}{\partial z^2} = 0 \, , \tag{26}$$

which describes the propagation of the kinetic Alfvén wave. Fourier transforming (26) we obtain the frequency of the KAW

$$\omega = k_\parallel v_{\mathrm{A}} \left(1 + k_\perp^2 \rho_s^2\right)^{1/2} \, . \tag{27}$$

The frequency of the nondispersive Alfvén wave is recovered from (27) in the limit $k_\perp \rho_s \ll 1$. The perpendicular group velocity for the kinetic Alfvén wave is in the positive $\mathbf{k}_\perp$ direction as can be seen from the relation

$$\frac{\partial \omega}{\partial \mathbf{k}} = \hat{\mathbf{z}} v_{\mathrm{A}} \left[1 + k_\perp^2 \rho_s^2\right]^{1/2} + \hat{\mathbf{x}} \omega \rho_s \frac{k_\perp \rho_s}{1 + k_\perp^2 \rho_s^2} \, . \tag{28}$$

Thus, the kinetic Alfvén wave is forward wave across the magnetic field in contrast to the inertial Alfvén wave. The propagation angle is given by

$$\tan \theta = \left(\frac{\omega \rho_s}{v_A}\right) \frac{k_\perp \rho_s}{[1 + k_\perp^2 \rho_s^2]^{3/2}} \le \frac{\omega}{\omega_{ci}} \frac{(2\beta_e)^{1/2}}{3^{3/2}} \, . \tag{29}$$

The maximum angle of propagation is for $k_\perp \rho_s = 2^{-1/2}$ and is larger than the corresponding value for inertial waves (22) because kinetic waves exist for $\beta_e > m_e/m_i$.

2.3. FINITE LARMOR RADIUS AND FINITE FREQUENCY EFFECTS

The equation describing the behavior of a plane wave in a uniform plasma has the general form

$$\mathbf{n} \times (\mathbf{n} \times \mathbf{E}) + \bar{\varepsilon} \cdot \mathbf{E} = 0 \, , \tag{30}$$

where $\mathbf{n} = c\mathbf{k}/\omega$ and $\bar{\varepsilon}$ is the dielectric tensor. In a cold plasma (30) takes the form

$$\begin{bmatrix} \varepsilon_\perp - n_z^2 & \varepsilon_{xy} & n_x n_z \\ -\varepsilon_{xy} & \varepsilon_\perp - n^2 & 0 \\ n_x n_z & 0 & \varepsilon_\parallel - n_x^2 \end{bmatrix} \begin{bmatrix} E_x \\ E_y \\ E_z \end{bmatrix} = 0 \, , \tag{31}$$

where $\mathbf{n} = n_x \hat{\mathbf{x}} + n_z \hat{\mathbf{z}}$ and the dielectric tensor elements are

$$\varepsilon_\parallel = 1 - \sum_j \frac{\omega_{pj}^2}{\omega^2}, \qquad \varepsilon_\perp = 1 - \sum_j \frac{\omega_{pj}^2}{\omega^2 - \omega_{cj}^2} ,$$

$$\varepsilon_{xy} = -i \sum_j \frac{\omega_{cj}}{\omega} \frac{\omega_{pj}^2}{\omega^2 - \omega_{cj}^2} . \tag{32}$$

The off-diagonal element ε_{xy} arises from currents carried by the $\mathbf{u}_E$ drifts. In the $\omega \ll \omega_{ci}$ limit no current results from $\mathbf{u}_E$ drifts in which case $\varepsilon_{xy} \to 0$. In this limit (31) reduces to two decoupled systems, namely

$$\begin{bmatrix} \varepsilon_\perp - n_z^2 & n_x n_z \\ n_x n_z & \varepsilon_\parallel - n_x^2 \end{bmatrix} \begin{bmatrix} E_x \\ E_z \end{bmatrix} = 0 , \tag{33}$$

and

$$\left(\varepsilon_\perp - n^2 \right) E_y = 0 . \tag{34}$$

Equation (34) describe the fast mode (compressional Alfvén wave). Setting the determinant of (33) equal to zero gives the shear Alfvén wave dispersion relation (Bellan, 1994)

$$\left(n_z^2 - \varepsilon_\perp \right) \varepsilon_\parallel + n_x^2 \varepsilon_\perp = 0 , \tag{35}$$

which in the cold plasma, $\omega \ll \omega_{ci}$ limit reduces to

$$\left(\frac{c^2}{v_A^2} - \frac{c^2 k_z^2}{\omega^2} \right) \frac{\omega_{pe}^2}{\omega^2} + \frac{c^2 k_x^2}{\omega^2} \frac{c^2}{v_A^2} = 0 , \tag{36}$$

which is just a rearrangment of (20).

The warm plasma generalizations of the parallel and perpendicular dielectric tensor elements are (Gekelman *et al.*, 1997b; Lysak and Lotko, 1996)

$$\varepsilon_\parallel = -\frac{\omega_{pe}^2}{\omega^2} \xi^2 Z'(\xi), \qquad \varepsilon_\perp = \frac{\omega_{pi}^2}{\omega_{ci}^2 - \omega^2} [1 - e^{-\mu} I_0(\mu)] \mu^{-1} . \tag{37}$$

Here $\xi = \omega / k_\parallel v_{te}$, and $\mu = k_\perp^2 \rho_i^2$, where ρ_i is the ion gyroradius. Z' is the derivative of the usual plasma dispersion function $Z(\xi) = \pi^{-1/2} \int e^{-z^2} (z - \xi)^{-1} dz$ and I_0 is the modified Bessel function. For small μ, the factor containing the Bessel function is approximated as $[1 - e^{-\mu} I_0(\mu)]/\mu \approx 1 - 3\mu/4$ by Hasegawa (1976). However, a Padé approximation $[1 - e^{-\mu} I_0(\mu)]/\mu \approx 1/(1 + \mu)$ is applicable for the whole range of μ, with error about 6% (Johnson and Cheng, 1997; Streltsov et al., 1998). Using the Padé approximation, which is valid for arbitrary μ, Equations (35)–(37) can be written as

$$Z'(\xi) \left[(1 - \frac{\omega^2}{\omega_{ci}^2})(1 + k_\perp^2 \rho_i^2) \frac{v_A^2}{v_{te}^2} - \xi^2 \right] = k_\perp^2 \lambda_e^2 . \tag{38}$$

The above equation represents the full dispersion relation for linear dispersive Alfvén waves (DAW) with arbitrary electron velocity, large ion gyroradius and finite frequency effects. The factor before $v_A^2/v_{te}^2 = (m_e/m_i)(1/\beta_e)$ represents effects of large ion gyroradius and finite frequency. For the plasma with cold electrons, β_e is less than the electron to ion mass ratio, we can use a large argument approximation, $Z'(\xi) \to \xi^{-2}$, and (38) then becomes

$$k_\parallel^2 v_A^2 = \frac{\omega^2(1 + k_\perp^2\lambda_e^2)}{(1 - \omega^2/\omega_{ci}^2)(1 + k_\perp^2\rho_i^2)} \, , \tag{39}$$

which in the limit of low frequency reduces to the familiar equation

$$\omega = k_\parallel v_A \sqrt{\frac{1 + k_\perp^2\rho_i^2}{1 + k_\perp^2\lambda_e^2}} \, . \tag{40}$$

Note, that retaining finite frequency terms in (39) leads to Equation (40) with the denominator replaced by $1 + k_\parallel^2\lambda_i^2 + k_\perp^2\lambda_e^2$, where $\lambda_i = c/\omega_{pi}$.

In the opposite limit, for higher beta the argument ξ is small ($\omega/k_\parallel \ll v_{te}$) and $Z' \approx -2$. The dispersion relation (38) for the kinetic Alfvén waves with finite frequency is then

$$\omega = k_\parallel v_A \sqrt{1 + k_\perp^2(\rho_s^2 + \rho_i^2) - \frac{\omega^2}{\omega_{ci}^2}(1 + k_\perp^2\rho_i^2)} \, . \tag{41}$$

The above equation coincides with the original derivation (Hasegawa, 1976) in the limit $\omega \ll \omega_{ci}$, except for the term ρ_i^2 in the brackets instead of $\frac{3}{4}\rho_i^2$ because of the Padé approximation used in (37). We should emphasize here, that in the inertial limit, $\xi \gg 1$, and in the kinetic limit, $\xi \ll 1$, so that formally, λ_e and ρ_s should not appear in the same dispersion equation. However, a hybrid dispersion with $\rho^2 = \rho_s^2 + \rho_i^2$ in the numerator and $1 + k_\perp^2\lambda_e^2$ in the denominator of (40) is consistent with numerical solutions of the full dispersion equation (Lysak and Lotko, 1996).

The parametric dependence of the solutions to Equation (38) for the case $T_i/T_e = 1$ is illustrated in Figure 4. Contours of the phase velocity, $\omega/k_\parallel v_{te}$, are shown as a function of $k_\perp\lambda_e$ and v_{te}^2/v_A^2. Small v_{te} values correspond to the inertial limit given by Equation (39), and large v_{te} values correspond to the kinetic limit of Equation (41).

2.4. WAVE POLARIZATION

The wave polarization in the general case can be obtained from the first row of (33), and using (37)

$$\frac{E_\parallel}{E_\perp} = \frac{n_\parallel^2 - \varepsilon_\perp}{n_\parallel n_\perp} = \frac{k_\parallel}{k_\perp}\left(1 - \frac{\omega^2}{k_\parallel^2 v_A^2(1 + k_\perp^2\rho_i^2)}\right) \, . \tag{42}$$
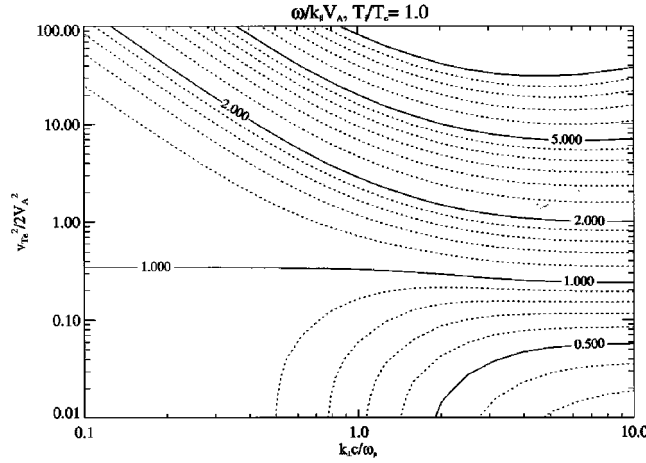
Figure 4. Contours of phase velocity for Alfvén waves obtained by numerical solution of Equation (38). (After Lysak and Lotko, 1996.)

For cold electrons we use dispersion (40) in Equation (42) to obtain

$$\frac{E_\parallel}{E_\perp} = \frac{k_\parallel k_\perp \lambda_e^2}{1 + k_\perp^2 \lambda_e^2} \ . \tag{43}$$

Note that when $k_\perp \lambda_e \gg 1$, we find $E_\parallel = (k_\parallel/k_\perp)E_\perp$ and the wave becomes electrostatic.

For the kinetic Alfvén wave, using low frequency limit of (41) we get

$$\frac{E_\parallel}{E_\perp} = -\frac{k_\parallel k_\perp \rho_s^2}{1 + k_\perp^2 \rho_i^2} \ . \tag{44}$$

Note that the parallel electric field in this case is opposite in sign to that in the inertial case, as noted by Goertz and Boswell (1979).

Another important quantity is the ratio $E_\perp/b_\perp$ which can be derived from Equation (6) under assumption of a plane wave $\partial/\partial x \to ik_\perp$, $\partial/\partial z \to ik_\parallel$, $\partial/\partial t \to -i\omega$. We find easily that

$$k_\perp E_\parallel - k_\parallel E_\perp = \omega b_\perp \ , \tag{45}$$

and using again the polarization Equation (33), and (37) we obtain generally, for DAW type

$$\left|\frac{E_\perp}{b_\perp}\right| = v_A^2 \left|\frac{k_\parallel}{\omega}\right| (1 + k_\perp^2 \rho_i^2) \ . \tag{46}$$

In the cold electron limit of the DAW we use dispersion (40) to obtain

$$\left|\frac{E_\perp}{b_\perp}\right| = v_A \sqrt{(1 + k_\perp^2 \lambda_e^2)(1 + k_\perp^2 \rho_i^2)} \ . \tag{47}$$

Thus, the electric to the magnetic field ratio for inertial waves with short perpendicular wavelengths can be much larger than the local Alfvén speed.

For the kinetic wave we substitute the low-frequency limit of (41) into (46) to obtain

$$\left|\frac{E_\perp}{b_\perp}\right| = v_A(1 + k_\perp^2 \rho_i^2)[1 + k_\perp^2(\rho_s^2 + \rho_i^2)]^{-1/2}. \tag{48}$$

2.5. DRIFT ALFVÉN WAVES

In the presence of the density gradient, $\partial n_0/\partial x$, both the electrons and ions acquire an equilibrium diamagnetic drift $\mathbf{v}_{Dj} = \hat{\mathbf{y}}(T_j/q_j B_0 n_0)\,\partial n_0/\partial x$. Here, we have the possibility of coupling DAW with the drift waves. In order to derive the local dispersion relation (Shukla *et al.*, 1984) for coupled dispersive Alfvén – drift waves with $|\partial/\partial t| \ll \omega_{ci}$, we use the electron continuity equation

$$\frac{\partial n_{e1}}{\partial t} - \frac{1}{B_0}\frac{\partial n_0}{\partial x}\frac{\partial \phi}{\partial y} + \frac{1}{\mu_0 e}\frac{\partial}{\partial z}\nabla_\perp^2 A_z = 0, \tag{49}$$

the ion vorticity equation

$$\left(\frac{\partial}{\partial t} + u_{i*}\frac{\partial}{\partial y}\right)\nabla_\perp^2\phi + v_A^2\frac{\partial}{\partial z}\nabla_\perp^2 A_z = 0, \tag{50}$$

and the parallel component of the electron momentum equation

$$\left(\frac{\partial}{\partial t} + u_{i*}\frac{\partial}{\partial y}\right)A_z - \lambda_e^2\frac{\partial}{\partial t}\nabla_\perp^2 A_z + \frac{\partial}{\partial z}\left(\phi - \frac{T_e}{en_0}n_1\right) = 0, \tag{51}$$

where $u_{i*} = (T_i/eB_0 n_0)\partial n_0/\partial x$ and $u_{e*} = -(T_e/eB_0 n_0)\partial n_0/\partial x$ are the unperturbed ion and electron diamagnetic drifts, respectively. Equations (49)–(51) are the generalizations of Equations (16), (17), and (25).

Supposing that n_1, ϕ and A_z are proportional to $\exp(ik_y y + ik_z z - i\omega t)$, where $\mathbf{k} = k_y\hat{\mathbf{y}} + k_z\hat{\mathbf{z}}$ is the wave vector and ω the frequency, we obtain from (49), (50), and (51)

$$\omega n_1 + \frac{\partial n_0}{\partial x}\frac{k_y}{B_0}\phi + \frac{1}{\mu_0 e}k_z k_y^2 A_z = 0, \tag{52}$$

$$(\omega - \omega_{i*})\phi - k_z v_A^2 A_z = 0, \tag{53}$$

and

$$\left[\omega_{e*} - (1 + k_y^2\lambda_e^2)\omega\right]A_z + k_z\left(\phi - \frac{T_e}{en_0}n_1\right) = 0, \tag{54}$$

where $\omega_{j*} = k_y u_{j*}$. In deriving the above equations, we have assumed that the wavelength is much smaller than the density gradient.

Combining (52) to (54) we obtain the linear dispersion relation for coupled drift Alfvén waves

$$\left(\omega^2 - \omega\omega_m - \omega_{IA}^2 k_y^2 \rho_s^2\right)(\omega - \omega_{i*}) = \omega_{IA}^2(\omega - \omega_{e*}) , \tag{55}$$

where $\omega_m = \omega_{e*}/(1+k_y^2\lambda_e^2)$ is the magnetic drift wave frequency, $\omega_{IA} = k_z v_A/(1+k_y^2\lambda_e^2)^{1/2}$ the frequency of the inertial Alfvén waves, $\rho_s = c_s/\omega_{ci}$ the ion Larmor radius at the electron temperature.

Several comments are in order. First, in a homogeneous plasma, (55) correctly reproduces the spectra of the dispersive Alfvén waves, namely, $\omega = \omega_{IA}(1 + k_y^2\rho_s^2)^{1/2}$. Second, for $k_y\lambda_e \ll 1$, we observe that the dispersive Alfvén waves are linearly coupled with the drift mode $\omega = \omega_{e*}$. Third, when the perpendicular wavelength is much shorter than λ_e, we have $\omega_{IA} = (k_z/k_y)\omega_{gm} \equiv \omega_{DO}$ and $\omega_m = \omega_{e*}/(k_y\lambda_e)^2 \equiv \omega_{c*}$. Hence, (55) is replaced by

$$\left(\omega^2 - \omega\omega_{c*} - \omega_{DO}^2 k_y^2 \rho_s^2\right)(\omega - \omega_{i*}) = \omega_{DO}^2(\omega - \omega_{e*}) , \tag{56}$$

which for a homogeneous plasma becomes

$$\omega = \frac{k_z}{k_y}\omega_{gm}(1 + k_y^2\rho_s^2)^{1/2} . \tag{57}$$

Equation (57) is the frequency of short wavelength (with respect to λ_e) modified convective cells (Okuda and Dawson, 1973).

3. Observations and Measurements

We now turn to *in situ* observations of phenomena associated with Alfvén waves in the auroral zone. First the basis for identifying Alfvén waves is established along with some of the earlier observations of these waves. We then turn to more recent, detailed spacecraft measurements to show the rich variety of phenomena associated with these waves.

3.1. IDENTIFICATION OF ALFVÉN WAVES

When examining *in situ* measurements of a purely propagating Alfvén wave, we expect to find correlated perturbations in both the electric and magnetic fields. We would also expect correlated electric and magnetic fields for a quasi-static structure which drives a parallel current that closes in the ionosphere. To distinguish between these two cases, we examine the ratio of the electric field to the magnetic field. For inertial Alfvén waves the ratio is given by (47) and it is larger than the local Alfvén speed. In contrast, for quasi-static, auroral arc-like structures, the magnetic field is related to the field-aligned current, which for a sheet current gives

$$\frac{1}{\mu_0}\frac{\partial b_\perp}{\partial s} = J_\perp = \sigma_P E_\perp , \tag{58}$$

where σ_P is the Pedersen conductivity in the ionosphere. Integration over height in the ionosphere where σ_P is non-negligible yields

$$\frac{E_\perp}{b_\perp} = \frac{1}{\mu_0 \Sigma_P} ,$$

(59)

where $\Sigma_P = \int \sigma_P \, ds$. For the Earth's magnetic field, there is a small correction factor of order unity due to the fact that flux tubes are generally anisotropic, so that latitudinal and longitudinal fields map differently. For typically encountered ionospheric conditions $\Sigma_P \sim 5$–40 S (Sugiura, 1984; Weimer *et al.*, 1985) Equation (59) gives $E/b \approx 18$–140 km s^{-1}. The value of Σ_P for the background ionosphere is sufficiently large so that E/b is a small fraction of that expected for an Alfvén wave. Thus this ratio provides a useful experimental test of in situ measurements to determine the presence of Alfvén waves. However, a interference of incident and the reflected waves from the ionosphere or presence of short $\lambda_\perp$ Alfvén waves can modify the local E/b ratio and make difficult identification of the Alfvén mode. The wave reflections from the ionosphere will be discussed in Section 4.1.

3.2. EARLY MEASUREMENTS

Early measurements of magnetic fields in space have revealed the existence of perturbations $\mathbf{b}_\perp$ perpendicular to the main geomagnetic field. The large-scale features in the data have been interpreted as signatures of field-aligned (Birkeland) currents by Iijima and Potemra (1978). The smaller scales, or higher frequency components in the measured field have been regarded as ELF turbulence or magnetic noise of lesser importance than *dc* structures. However, the measurements on DE-2, ICB-1300, and Arcad-3 satellites revealed a high degree of correlation between the electric and magnetic field components (Maynard *et al.*, 1982; Gurnett *et al.*, 1984; Sugiura, 1984; Dubinin *et al.*, 1985; Berthelier *et al.*, 1991; Ishii *et al.*, 1992) which indicated presence of small scale currents or Alfvén waves.

Measurements on ICB-1300 at an altitude of 850 km provided convincing evidence of rich phenomena related to Alfvén wave structure (Dubinin *et al.*, 1985, 1988; Chmyrev *et al.*, 1988). One of the main results was identification of spatial vortex structures possibly associated with auroral curls. Figure 5 shows example of the vortex street observed in the electric field data. The magnetic perturbations had amplitude of 200 nT and the E/b ratio was about the Alfvén speed. The spectral maximum was observed at the frequency 0.5 Hz. Additional analysis of oscillation hodograms revealed not only the vortex chains in the auroral plasma but dipole and monopole Alfvén vortices as well. The transverse dimension of a single vortex was of the order of a few kilometers. The measured waveforms of the orthogonal magnetic and electric field components most often did not show visual similarity. Dubinin *et al.* (1990) have shown that in many cases there is a clear correspondence between $B_x(t)$ and $H[E_y(t)]$, where operator H is a reversed Hilbert transform which corresponds to $\pi/2$ phase shift of all Fourier harmonics in the signal $E_y(t)$.

To explain these observations, comprehensive theories have been developed for Alfvén vortex structures (Shukla *et al.*, 1985, 1986a; Chmyrev *et al.*, 1988),
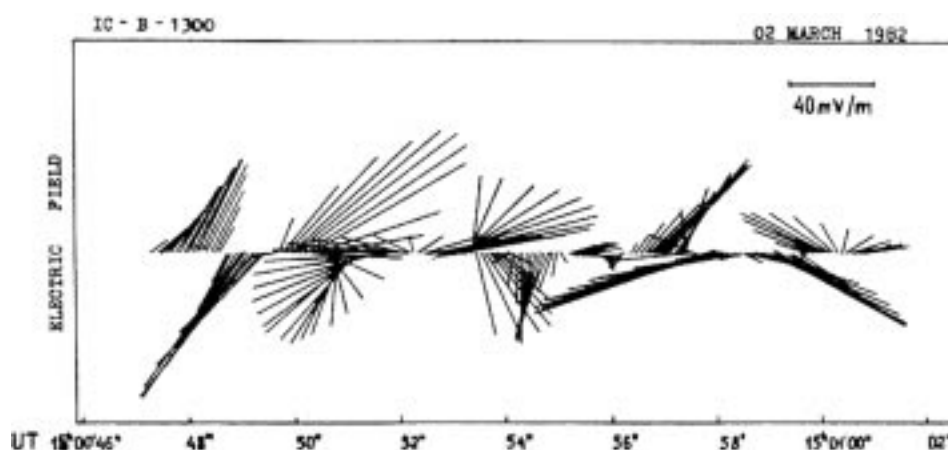
Figure 5. Variations of the horizontal component of the electric field in the frequency range 0.1–1 Hz observed on ICB-1300 which show vortex structures. (After Chmyrev *et al.*, 1988.)

and turbulence (Volokitin and Dubinin, 1989). Discussions of various theories will appear in Section 5.

Rocket measurements by Boehm *et al.* (1990) also showed a very clear example of the E/b relationship which made identification of the Alfvén wave unambiguous. Figure 6 shows an example from that paper. The eastward component of the magnetic field (middle panel) and the northward component of the electric field (second panel from bottom) for the interval 296–298 s show similar signal (the electric field is inverted) and the ratio was calculated to be that expected for the Alfvén speed. Kletzing (1994) suggested that the two bursts of 0.6 keV electrons which occur just before the waves arrive are signatures of direct acceleration by the Alfvén wave. Clear signatures of the Alfvén waves can only be observed if they are narrow enough that convection can separate the initial wave and its reflection from the ionosphere so as to prevent them from interfering with one another (making the determination of admittance difficult).

The E/b ratio often attains values intermediate between the Alfvén speed and the value expected from the Pedersen conductivity. Knudsen *et al.* (1990) performed a spectral analysis of the E/b ratio as a function of frequency for measurements from the HILAT satellite and found that for the lowest frequencies, the ratio was that expected for a quasi-static electric field structure. As frequency increases, the E/b ratio clearly increases to values above those expected for ionospheric conductivity. Further analysis was conducted using a model of ionospheric conductivity which properly handled reflection of the waves from the ionosphere. It was found that destructive interference of upgoing and downgoing waves causes the intermediate value of the Alfvén ratio.
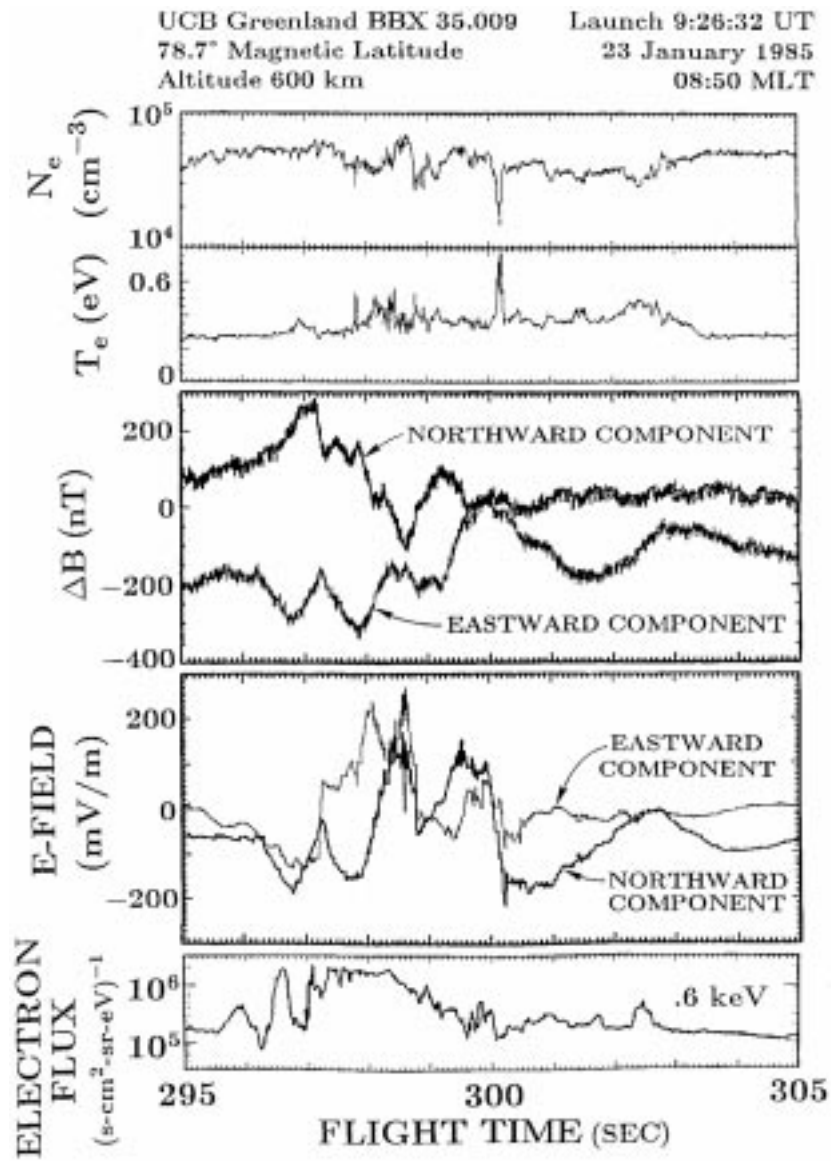
Figure 6. Figure from Boehm (1990) which shows a clear signature of an Alfvén wave between 296 −298 s in the northward component of the electric field and eastward component of the magnetic field.

3.3. FREJA OBSERVATIONS

The *Freja* satellite was especially designed for fine-structure plasma measurements with a high temporal/spatial resolution of the auroral processes in the topside ionosphere, 600–1750 km (Lundin *et al.*, 1994). Unfortunately, due to a malfunction of the south pole downlink receiver, the altitude coverage of the high bit-rate data became limited to above about 1200 km in the North polar region. Launched in October 1992 and operated until 1995, *Freja* carried out measurements during declining solar activity conditions, and with an inclination of 63° the spacecraft traversed the auroral oval almost tangentially in the East-West direction.

The *Freja* experiments allowed 3D measurements of both the *dc* (128 Hz sampling rate) and the *ac* (32 kHz sampling rate) magnetic fields with a set of fluxgate and search coil magnetometers (Zanetti *et al.*, 1994; Holback *et al.*, 1994). Similarly, 2D electric *dc* (768 Hz sampling rate) and *ac* (32 kHz sampling rate) electric fields are measured by a set of probe pairs mounted on wire-booms 7.6–21 m apart from each other (Marklund *et al.*, 1994). These measurements provided, together with the sampling of 32–64 ms resolution electron distribution functions (Boehm *et al.*, 1994) and the full 3D ion distributions every 3 s (Eliasson *et al.*, 1994; Whalen *et al.*, 1994) excellent means of observing the micro-physics within small-scale Alfvénic features.

3.3.1. *The Alfvén Waves Turbulence*
The easiest way to identify Alfvénic activity in the *Freja* data is through a filtered $f \geq 1$ Hz component of the magnetic field, where electromagnetic fluctuations with amplitudes of a few to several tens of nT show widespread magnetic turbulence (Gary *et al.*, 1998; Stasiewicz and Potemra, 1998). The fluctuating fields can be identified as Alfvén wave turbulence (AWT) in the frequency range ~ 1–7 Hz because the observed ratio $\delta E/\delta B$ is about the local Alfvén velocity v_A (Aikio *et al.*, 1996; Stasiewicz *et al.*, 1998). The cusp and dayside cleft are found to be regions of almost permanent Alfvénic activity, while its appearance in the nightside auroral oval is closely related to periods of auroral activity.

Figure 7 shows an example of a large region of Alfvén turbulence observed in the cleft region. One can notice a general correlation between large scale density depressions and Alfvén wave intensity. Similar behavior is seen in virtually the whole *Freja* data set, which indicates that Alfvén waves play a major role in heating and evacuating the plasma along the magnetic field lines.

The Alfvén wave turbulence is most often associated with broadband ELF emissions from ~ 10 Hz reaching sometimes few kHz, up to the lower hybrid frequency. Other associated phenomena include suprathermal electron bursts with energies reaching a few hundred eV, and transverse ion acceleration to similar energies. These phenomena are often situated in larger scale cavity regions depleted in plasma. An example of such a large scale region filled with Alfvénic activity and plasma energization is displayed in Figure 8.
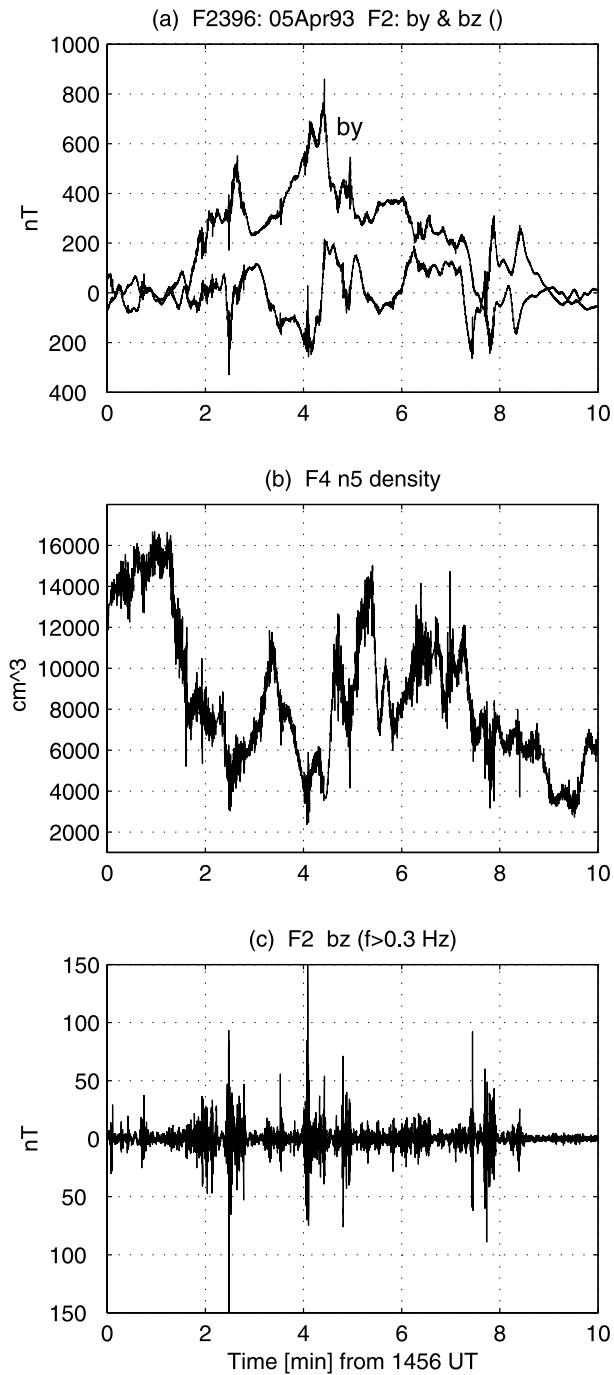
Figure 7. A large region of Alfvén turbulence in the post-afternoon region (a) perpendicular compo-nents of the magnetic field, (b) plasma density derived from the Langmuir probe, (c) AC component of the magnetic field. (Stasiewicz and Potemra, 1998.)
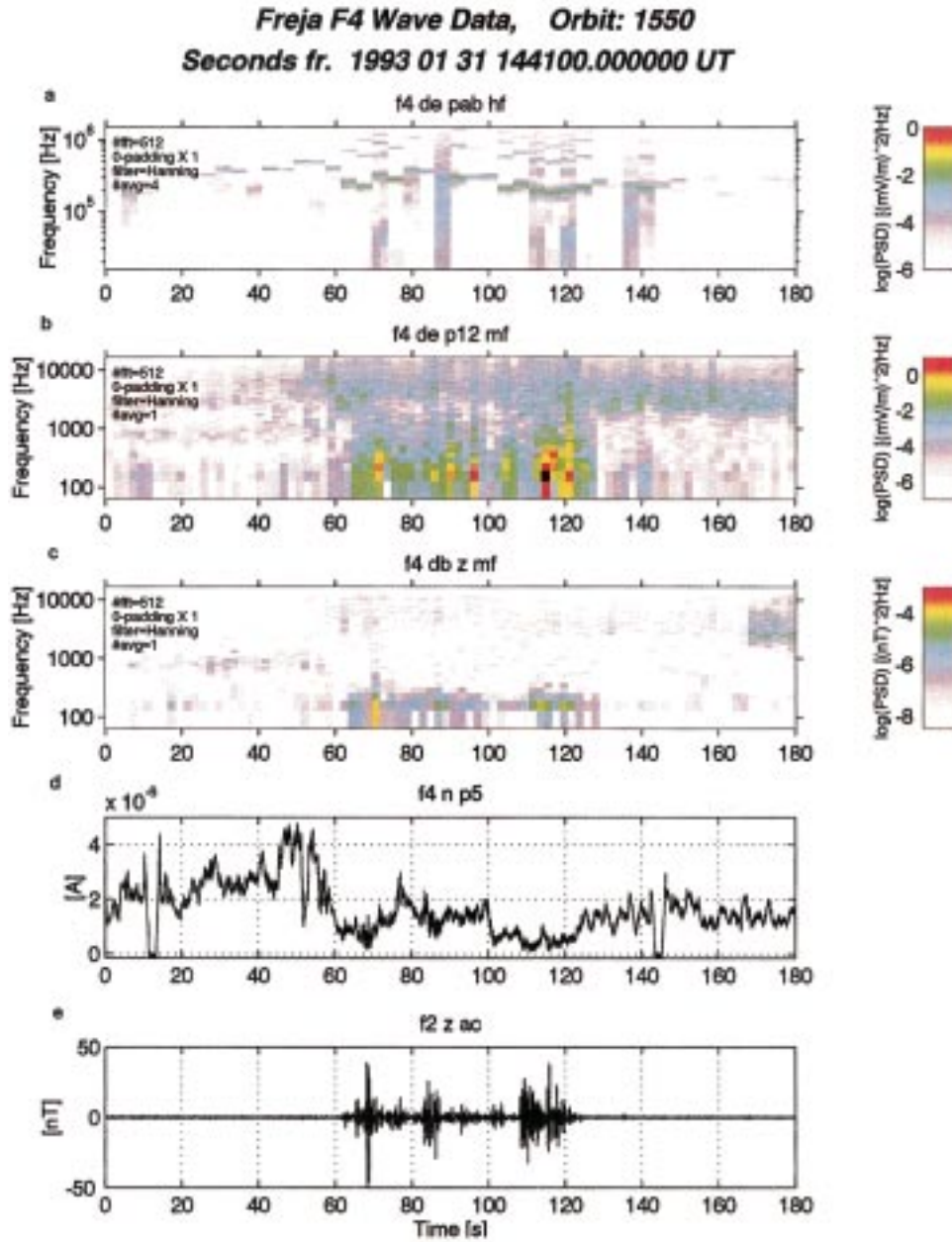
Figure 8. Overview of the plasma wave measurements during an auroral event. The magnetic fluctuations (e), which are typical for Alfvénic activity, are situated in the larger scale density cavity (d). The predominantly electrostatic broadband ELF emission (b) up to the lower hybrid cutoff is detected simultaneously with the transversely accelerated ions and electron precipitation. (From Wahlund *et al.*, 1998.)

It can be pointed out that the exact wave modes and the wave frequency in the broadband turbulence are difficult to identify with measurements on board a single spacecraft traversing the plasma with ~ 7 km s^{-1}. The Alfvén mode should have frequency much lower than the ion cyclotron frequency ($f_{cO+} \sim 25$ Hz in *Freja* environment). There are indications that Fourier spectrum of electromagnetic signals around 1 Hz corresponds to Alfvén wave frequencies. The lower limit for the Alfvén wave frequency is ~ 10 mHz which can be associated with a fundamental mode of global field line oscillations.

As we shall discuss later in this section, the presence of short-length dispersive Alfvén waves in the regions of AWT produces a spectrum equivalent to broadband ELF waves. For example, low frequency Alfvén waves, $\omega < \omega_{ci}$, with perpendicular wavelengths ~ 10 m up to ~ 7 km would be Doppler shifted ($f = V_s/\lambda$) in the spacecraft reference frame and observed as waves in the frequency range $\sim 1\text{–}700$ Hz. For this reason, one should be aware that the frequency vs time spectrograms as that shown in Figure 8 apply to the satellite reference frame, and generally do not correspond to the wave frequency spectrum in the plasma reference frame.

3.3.2. *Solitary Kinetic Alfvén Waves*

Within the extended regions of AWT there frequently exist singular, localized waveforms with large magnetic perturbations (several tens of nT), large perpendicular electric fields (up to 500 mV m^{-1}), and complex density perturbations (several tens of %). The origin of these structures is a subject of current research and considerable debate in the literature as well as among the authors of this review. When these strong pulse-like electromagnetic signals were first detected in the *Freja* data (Louarn *et al.*, 1994; Wahlund *et al.*, 1994a) they were dubbed Solitary Kinetic Alfvén Waves (SKAW) since the waveforms contained features with scales of the order of the ion acoustic gyroradius and therefore kinetic (thermal) effects were expected to play a role. The authors made it clear though, that inertial Alfvén waves were also considered, with scales of a few electron inertial lengths (~ 10 Hz in the spacecraft frame of reference). In this review we shall replace SKAW with a more precise term dispersive Alfvén wave (DAW) structure which may include both inertial and kinetic effects. Many of these structures at the inertial scale of a few λ_e are so strong, that term IAW singularities seems to be the most appropriate description (see Figure 11). The importance of these structures for auroral processes was properly recognized and the compatibility of the spatial scales with the thickness of discrete auroral arcs noted. An example of a dispersive Alfvén wave structure is shown in Figure 9.

3.3.3. *Polarization Patterns*

The polarization studies concerned the behavior of the perpendicular perturbation vector $\mathbf{b}_\perp = (b_x, b_y)$ which is also used to infer field-aligned currents. In a study by Volwerk (1996), the DAW have been found to have mainly a rotational mag-
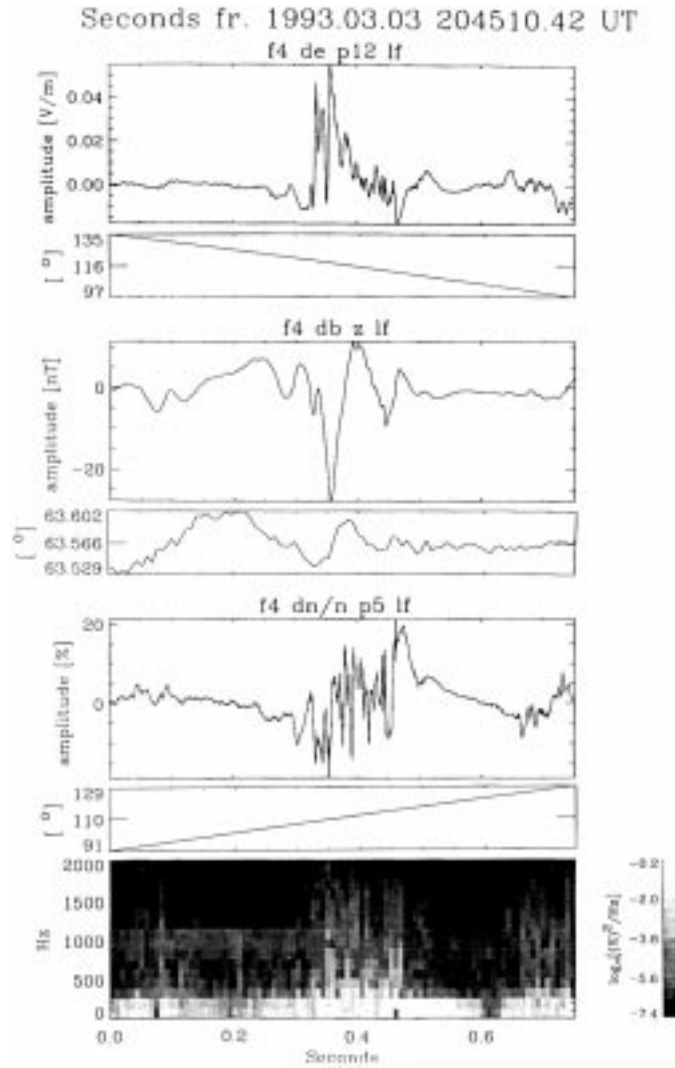
Figure 9. A clear example of a small scale Alfvénic structure filled with broadband electrostatic turbulence. (Wahlund *et al.*, 1994a.)

netic field together with a small compressional component of less then 5%. The polarization results on the existence of tubular current structures were similar to the earlier results from ICB-1300 data on auroral vortex structure (e.g., Chmyrev *et al.*, 1988).

A multiresolution wavelet analysis applied to the magnetic field records within IAW regions (Stasiewicz *et al.*, 1998; Stasiewicz and Potemra, 1998) showed that polarization patterns are strongly scale dependent. Larger scales (∼10 km) exhibit more linear polarization while the smaller scales (≤ 1 km) show frequently circular/elliptical polarization, consistent with vortex structure. Many IAW singularities

Figure 10. Electron spectrogram and *ac* magnetic activity along the spacecraft velocity vector from a pre-midnight *Freja* passage. A clear correlation between supratermal electron bursts and the Alfvén wave signatures is observed. (From Gary *et al.*, 1998.)

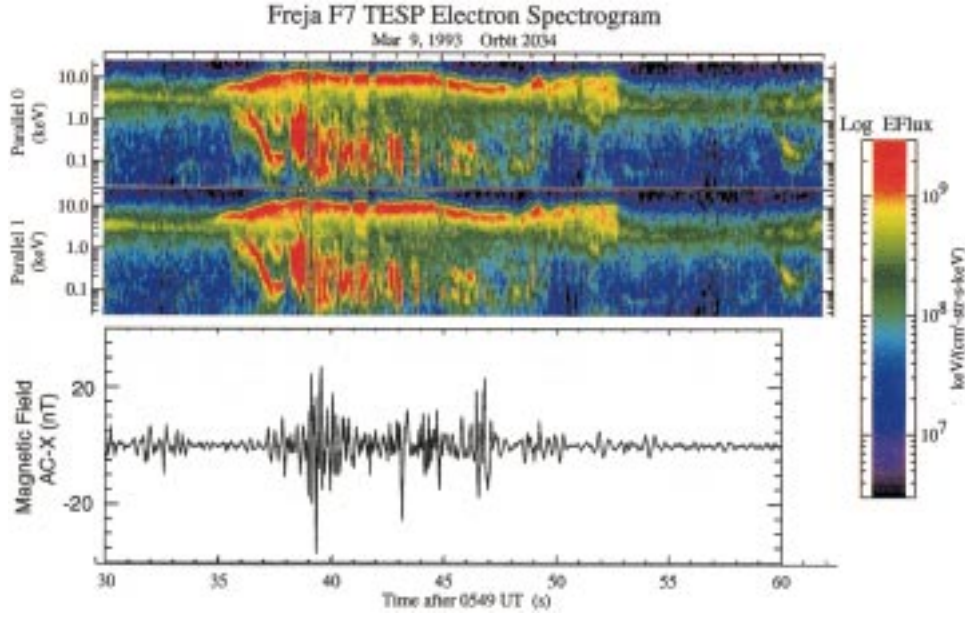show, however, linear polarization, consistent with current sheets (Stasiewicz *et al.*, 1998).

3.3.4. *Poynting Flux and Suprathermal Electron Bursts*

Suprathermal electron bursts are intense short-lived bursts of precipitating fluxes of electrons with energies usually below 1 keV and with pitch-angles often very close to the geomagnetic field direction. Numerous observations of these electron bursts have been carried out with rocket and satellite instrumentation within the auroral region. The bursts are most often found at the edges of inverted-V arc precipitation or may occur alone. The upper energy limit of the bursts are less than the inverted-V arc energy, and it is therefore often thought that these bursts are an integral part of the inverted-V acceleration mechanism.

Based on *Freja* data several authors have reported the simultaneous occurrence of electromagnetic waveforms characterized as Alfvén waves and suprathermal electron bursts (Boehm *et al.*, 1995; Stasiewicz *et al.*, 1997, 1998; Gary *et al.*, 1998; Knudsen *et al.*, 1998; Wahlund *et al.*, 1998). A striking example of such an event is displayed in Figure 10.

The parallel component of the Poynting flux is usually suggested to be responsible for the acceleration of these electrons. It can be determined from the electromagnetic data with

$$S_{\parallel\lambda} = \mu_0^{-1}\delta\mathbf{E}_{\perp\lambda} \times \delta\mathbf{B}_{\perp\lambda} , \tag{60}$$

where subscript $\lambda = v_s/f$ refers to the largest scale, or the smallest frequency f used for filtering of the data. Because different authors used different cutoff frequency, and studied cases at different geophysical conditions, the reported values for Poynting flux differ a lot (Seyler *et al.*, 1995; Volwerk *et al.*, 1996; Stasiewicz *et al.*, 1997). Typically, the observed Poynting flux for structures less than 1 km is $\sim$1–20 mW m^{-2} in the downward direction, and it is generally larger than the associated electron energy fluxes. The parallel Poynting flux can therefore provide the necessary free energy to produce the suprathermal electron bursts (see theory section). Because the dispersive Alfvén waves are very dissipative, much of their energy is transferred into the surrounding plasma before the Alfvén wave reaches the ionosphere below. However, in most cases there is smaller upward directed Poynting flux which indicates reflection of the downgoing electromagnetic energy, or the ionospheric sources.

3.3.5. *Field-Aligned Currents and Density Cavities*
The estimation of field-aligned current densities from the measurements of magnetic field gradients onboard a single spacecraft will depend critically on the assumption of how the magnetic perturbations originate. A different result will be obtained if the magnetic perturbation is viewed as a solitary wave passing *Freja* with a large phase velocity along $\mathbf{B}_0$, or if the magnetic perturbations are an effect of a spatially localized filamentary current structure with a possible low frequency temporal evolution, $\omega \ll \omega_{ci}$, characteristic for Alfvén waves. Multipoint measurements on *Freja* with double density probes show, however, that the density structures are mainly spatial for a large range of scales from $\sim$kilometers down to $\sim$ 30 m ($\sim$ 200 Hz in satellite frame) (Wahlund *et al.*, 1998; Stasiewicz *et al.*, 2000a). Also, multiprobe electric field sensors on Fast (see next section) provide direct evidence that the IAW structures are spatial, with a perpendicular drift smaller than the satellite speed. Thus, the usual derivation of field-aligned currents from the observed gradient of the perpendicular perturbation field $\mu_0 J_z = \partial B_y/\partial x$ provides good approximation to $J_\parallel \equiv J_z$.

The reported values for $J_\parallel$ range from few tens μA m^{-2} (Louarn *et al.*, 1994; Lühr *et al.*, 1994; Seyler *et al.*, 1995) to few hundred μA m^{-2} (Stasiewicz *et al.*, 1997, 1998; Stasiewicz and Potemra, 1998). An example of very intense current structure presented in Figure 11, shows a striking correlation between the current and the density cavity. Because in the IAW parallel current is proportional to the parallel electric field (Equation (15)) *viz*.

$$\tilde{E}_\parallel = i\omega\lambda_e^2\mu_0\tilde{J}_\parallel \,, \tag{61}$$

the measurements suggest that the mechanism leading to the formation of the cavity could be related to the ponderomotive force (Bellan and Stasiewicz, 1998; Shukla *et al.*, 1999) or, alternatively, to the Joule heating in the current channel (Shukla and Stenflo, 1999b). Detailed discussion of these processes shall appear in Sec-
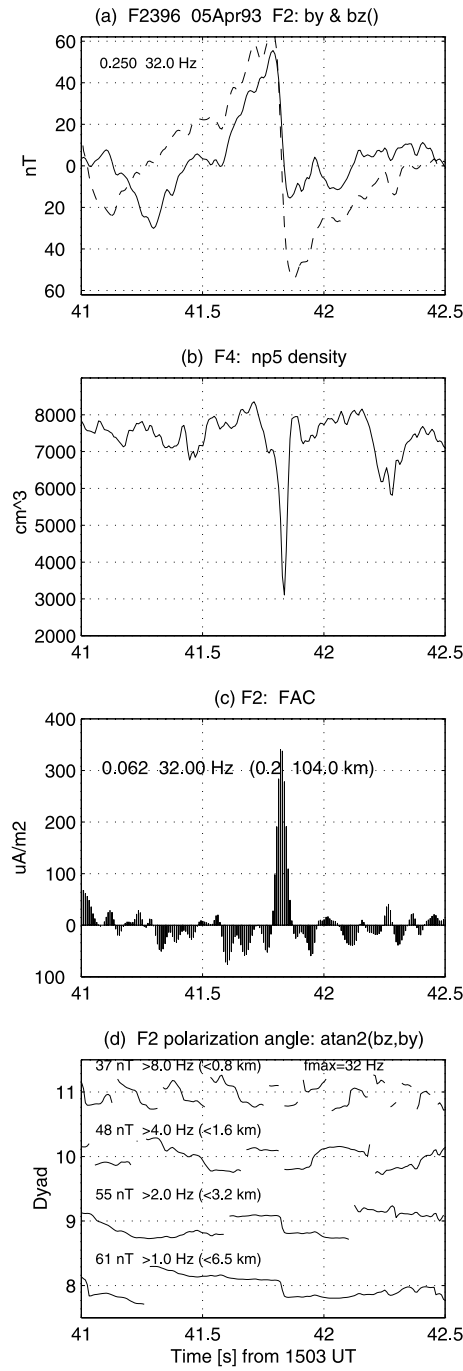
Figure 11. A singular Alfvénic structure observed in the magnetometer data. It is associated with a deep density cavity and strong field-aligned current of 300 μA m^{-2}. (From Stasiewicz *et al.*, 1998.)

tion 5.7. An altitude profile of a normalized parallel electric field (61) computed under assumption of the parallel current continuity is shown in Figure 3.

In a laboratory experiment (discussed in Section 3.5, and also by Maggs and Morales (1997)) cavities of similar width as that in Figure 11 were observed to generate spontaneously drift Alfvén waves at the edges of the cavity. The generated waves had frequency of $\sim 0.1\omega_{ci}$, which could be scaled to ~ 2 Hz in the *Freja* case. In the *Freja* data there are indeed indications that such fluctuations occur, see, e.g., Figure 12 and Figure 8 in Stasiewicz *et al.* (1998). However, the expected drift waves with a scaled period of 500 ms cannot be resolved within a 600 m cavity which is traversed by *Freja* satellite during 70 ms. Thus, the waves appear to exist, but we are unable to resolve their properties from the fast moving spacecraft.

3.3.6. *Parallel Electric Fields and Resonance Cones*

Sometimes, when the geomagnetic field is positioned within the plane of the electric field antennae (spin plane), information can be gained regarding the parallel electric field component of the small scale Alfvén wave structures. It was noted already by Louarn *et al.* (1994) and Wahlund *et al.* (1994a) that strong parallel fields seemed to exist. Two published reports (Stasiewicz *et al.*, 1997; Chust *et al.*, 1998) indicate occasional presence of the parallel electric field up to few tens of mV m^{-1}. Such fields are measured in association with deep density cavities, strong field-aligned currents and accelerated electrons, and similar phenomena are also seen on the FAST (Chaston, unpublished). No obvious instrumental effects have been found in the reported cases, but neither is a theoretical support for such large values of $E_\parallel$ at lower frequencies.

As discussed in Section 2.1, the IAW propagates obliquely to the magnetic field, and small $\lambda_\perp$ waves would concentrate on a surface inclined at θ_r given by Equation (22). If the source is localized, the locus of short $\lambda_\perp$ waves would form a conical surface. This behavior is well known from laboratory measurements (see Section 3.5) and it is also rigorously discussed in Section 5.4. If the cone is excited by a small size source, then there may be a parallel electric field singularity on the surface of the cone. Stasiewicz *et al.* (1997) suggested that the IAW singularities observed in satellite data could correspond to such a condensation of waves propagating at the resonance cone (compare also Figure 11).

3.3.7. *Association of DAW with Langmuir and Whistler Waves*

As discussed earlier, there is clear correlation between suprathermal electron fluxes and Alfvén wave intensity both in the average, statistical sense, as well as for individual events. If the electrons are accelerated locally, one would expect to see Langmuir waves generated by electron beams. Acceleration at higher altitudes above the spacecraft should be associated with whistler waves, which can propagate along the field lines. At *Freja* altitudes we observe indeed direct correlation between Alfvénic activity and Langmuir and/or whistler waves. Langmuir wave is an electrostatic emission excited by a non-thermal feature (bump-on-tail) in the

electron distribution function. The observed correlation of these, widely spaced in frequency wave modes, is an indirect evidence on the local acceleration of electrons by Alfvén waves (Stasiewicz *et al.*, 1996, 1997). The electrons are locally accelerated, form a beam which is then thermalized by emissions of Langmuir waves. An example of such situation occurring within a strong Alfvénic structure is shown in Figure 12. A pair of oppositely directed field-aligned currents are colocated with pair of oppositely directed Poynting fluxes of ~ 30 mW m^{-2} ($\delta E \approx 0.5$ V m^{-1} and $\delta B \approx 100$ nT). Strong suprathermal electron beams in both directions are colocated with electromagnetic structures. The upgoing electron beam excites strong Langmuir waves which saturate the wave instrument at 1.2 V m^{-1} of parallel field at 270 kHz.

Narrowband Langmuir waves on *Freja* are generally excited by weak electron beams $n_b \ll n_0$ with a wide velocity spread $\Delta V_b \approx V_b$. They are less frequent in the dayside cusp where instead, a strong whistler wave turbulence is observed in association with the dispersive Alfvén waves.

3.3.8. *Transverse Ion Acceleration and Bulk Heating*

Numerous studies have been carried out regarding transverse ion heating in connection with broadband ELF emissions in the auroral regions based on the *Freja* data set (Norqvist *et al.*, 1996; Andre *et al.*, 1998; Knudsen *et al.*, 1998; Wahlund *et al.*, 1998). Cyclotron heating of the ions (predominantly O$^+$) was argued to be the most important acceleration mechanism.

A most prominent feature regarding transverse ion heating events observed with *Freja* is that the whole ion population is heated to $5-30$ eV during auroral-Alfvénic active periods (Knudsen and Wahlund, 1998; Wahlund *et al.*, 1998). The ion temperatures were estimated from three independent measurement methods; the cold plasma analyzer (CPA), the hot ion detector (TICS) and indirectly from the wave measurements by using the emission characteristics of broadband ELF waves. The ion distributions had $T_{i\perp}/T_{i\parallel} \approx 2-3$, while during quiet time the ion distributions were generally isotropic and cold (below 0.5 eV, Norqvist *et al.* (1998)). The electron temperatures were found to vary between $1-2$ eV within active periods, which indicate that $T_e \ll T_i$ at *Freja* altitudes during periods of extensive broadband ELF emissions. The electron temperatures were estimated from Langmuir probe sweeps.

Knudsen and Wahlund (1998) found increased core ion fluxes (H$^+$ and O$^+$) in association with the small-scale Alfvénic waveforms by using the CPA covering energies below 20 eV. The fluxes had amplitudes in excess of 10^{13} m^{-2} s^{-1}, and could be explained by either a localized heating to several eV within the Alfvén structures or by bulk ion drifts of the order of $1-2$ km s^{-1}. Since the estimated electric field of 70 mV m^{-1} would cause an $\mathbf{E} \times \mathbf{B}$ drift in excess of 2 km s^{-1}, the results could not be used to distinguish the two possibilities.

Recent results show that the gyroresonant ion heating may not be the dominant mechanism at *Freja* altitudes (Stasiewicz *et al.*, 2000b). It has been demonstrated
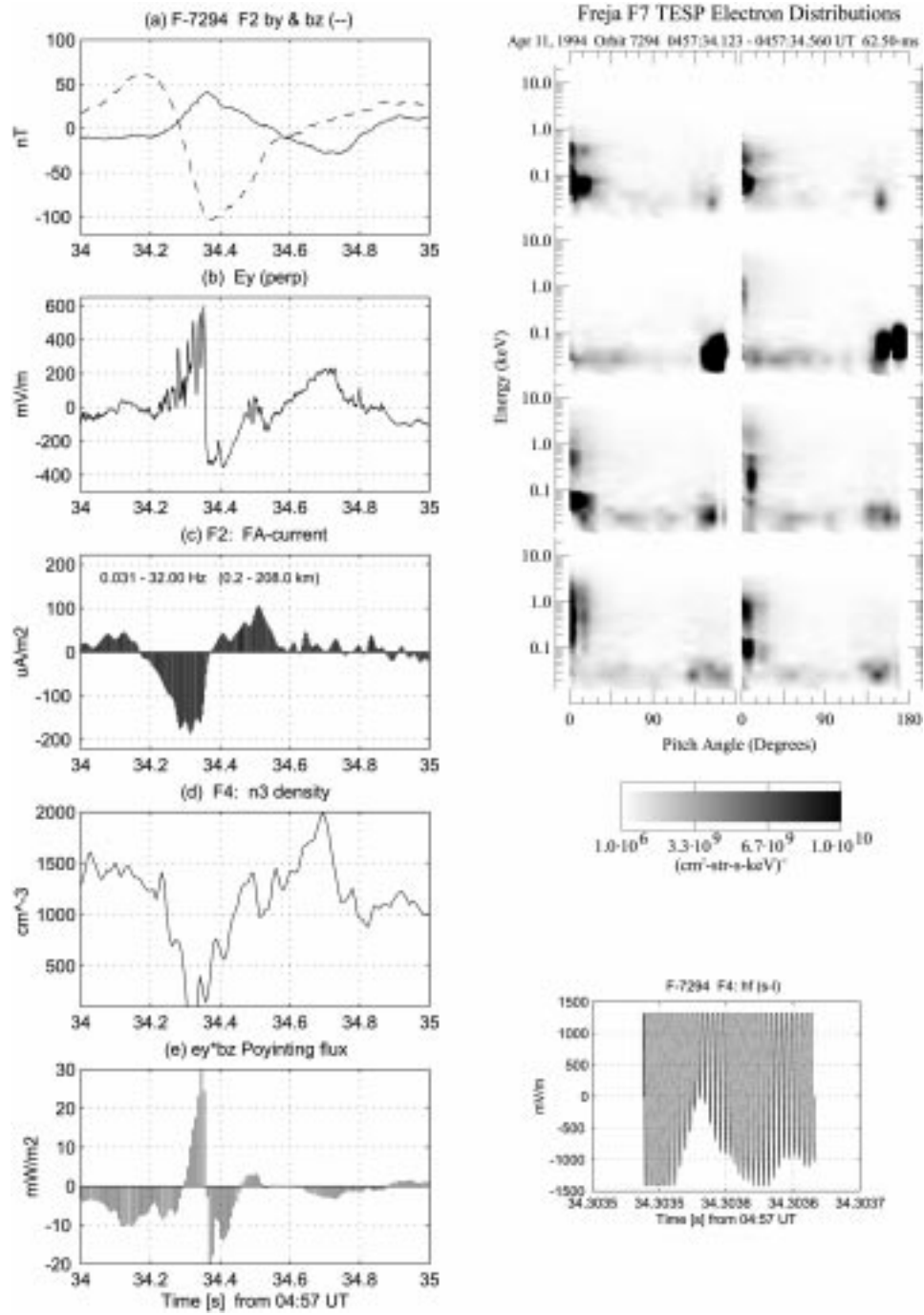
Figure 12. An example of the Alfvén wave structure which has signatures of a waveguide mode with a pair of oppositely directed currents, electron distributions, and Langmuir waves measured during this event. (Stasiewicz *et al.*, 1997.)
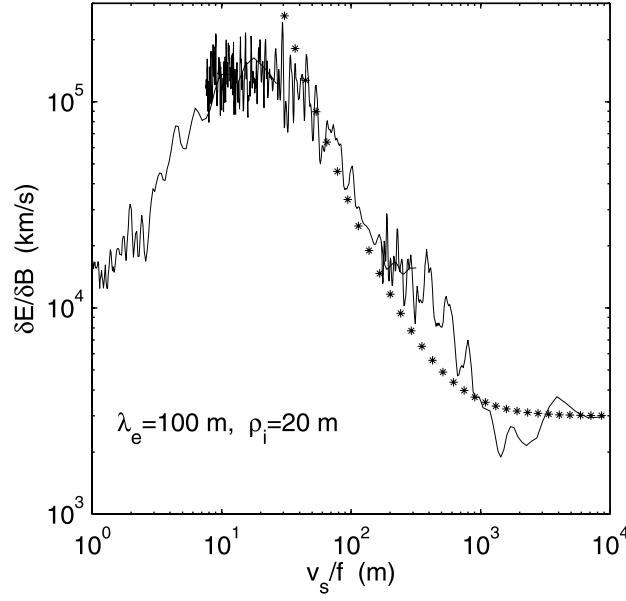
Figure 13. $\delta E/\delta B$ ratio for a DAW event related to strong ion heating. The marker line shows theoretical dispersion for DAW given by Equation (47). It shows that structures 40–10,000 m could be interpreted as spatial, broad $\Delta k_\perp$ spectrum. (From Stasiewicz *et al.*, 2000a.)

that the *Freja* observations are more likely consistent with stochastic ion heating by short perpendicular wavelength electrostatic waves and structures produced by a decay of DAW discussed in this paper.

3.3.9. *Turbulence of Dispersive Alfvén Waves (BB-ELF)*

As mentioned earlier in this section, the presence of short-length dispersive Alfvén waves broadens the spectrum and make it appear as broadband waves in the spacecraft reference frame. Recently, Stasiewicz *et al.* (2000a) have shown that the BB-ELF spectrum observed on the satellite in the frequency range ~ 1–500 Hz can be attributed to short-length DAW. The identification was made on two grounds. One was based on direct multipoint measurements of the density structures, and the other on the measured $\delta E/\delta B$ spectrum during turbulent events. It can be seen in Figure 13 that the ratio $\delta E/\delta B$ follow the theoretical curve (47) for DAW, shown here with asterisks. One can see an essentially single mode connecting large scale structures with small ones, down to $\lambda \approx 40$ m. The saturation of the $\delta E/\delta B$ spectrum at $\lambda \approx 50$ m was attributed to the characteristic scale

$$\rho_d = \frac{E_x}{\omega_{ci} B_0} \tag{62}$$

for stochastic damping of DAW due to the chaotization of ion orbits (Stasiewicz *et al.*, 2000b). It has been also noted that the spectrum below 20 m is not reliable

because large ion gyroradius effects are convoluted with antenna attenuation of the electric signal at short wavelengths.

Earlier, Wahlund *et al.* (1998) made a comprehensive analysis of similar structures based on the linear relation between the potential $\delta\phi$ and δn. The analysis was based on a generalized linear response relation between the potential and the density fluctuations derived by Seyler and Wahlund (1996) for short-scale phenomena near the ion acoustic gyroradius ($\rho_s = c_s/\omega_{ci}$) and extending down to the Debye scale ($\lambda_D = c_s/\omega_{pi}$). It has been noted that most analysis of ion-acoustic waves start out with the usual presumption of an electron Boltzmann response or equation which is valid for oblique waves that are not too close to perpendicular, but fails for propagation angles close to or smaller than the $\sqrt{m_e/m_i}$ from perpendicularity ($\approx 0.3°$ for O^+ and $\approx 1.3°$ for H^+), where parallel electron inertia is important. Generally, the relation is

$$e\delta\phi = \frac{\theta^2 T_e - T_i - (T_e + T_i)(k_\perp^2 \rho_s^2)^{-1}}{1 + \theta^2} \frac{\delta n}{n} , \qquad (63)$$

where $\theta = (k_\parallel/k_\perp)\sqrt{m_i/m_e}$. For the limit $\theta \gg 1$, the density response is electron Boltzmann for all $k_\perp$, i.e., $\delta n/n \approx e\delta\phi/T_e$. For $\theta \ll 1$ the density response is ion Boltzmann when $k_\perp\rho_s \gg 1$, so that $\delta n/n \approx -e\delta\phi/T_i$. When $\theta \ll 1$ and $k_\perp\rho_s \ll 1$ the response relation becomes $\delta n/n \approx -(B_0\Omega_i)^{-1}k_\perp^2\delta\phi$ which is the ion polarization response characteristic of Alfvén waves. There are four distinct classes of low frequency waves that can exist on the Alfvén-ion cyclotron dispersion branch: For long perpendicular wavelengths there are ion cyclotron waves which have ($k_\perp\rho_s < 1$) and inertial Alfvén waves having ($\theta < 1$), and for short wavelengths ($k_\perp\rho_s > 1$) there are ion acoustic waves ($\theta > 1$, fast ion acoustic) and ($\theta < 1$, slow ion acoustic (SIA or electron acoustic).

On the basis of the $\delta E(\delta n/n)^{-1}$ analysis of the experimental data Wahlund *et al.* (1998) conclude that waves in the frequency range 30–400 Hz exhibit an ion Boltzmann relation, which is consistent with SIA waves in a plasma where $T_i \gg T_e$. Note that this frequency range in the spacecraft frame would correspond to structures 20–350 m in Figure 13. The perpendicular phase velocity of SIA/electron acoustic waves is significantly lower than the acoustic speed, on the order of 1 km s^{-1}, and therefore is significantly smaller than the spacecraft velocity. Thus it is likely that SIA waves are spatial with respect to the satellite frame since the Doppler frequency is probably considerably larger than the wave frequency (for sounding rockets the Doppler and wave frequencies are comparable). The transition from inertial Alfvén wave behavior having an ion polarization response to SIA wave behavior having an ion Boltzmann response affects the E/b ratio in a manner than can be measured. We see from (47) that the presence of SIA waves according to fluid theory should correspond to an enhancement in E/b for wavelengths below the ion gyroradius. However, parallel electron Landau damping can inhibit excitation of SIA waves if the ion temperature is not sufficiently large (Lysak and Lotko, 1996; Seyler *et al.*, 1998). So that detection of waves having

an ion Boltzmann response is a strong indication of an elevated T_i/T_e ratio unless there exists a mechanism that can excite SIA waves under conditions of strong parallel electron Landau damping.

Further confirmation of the ion acoustic/ion cyclotron nature of the higher frequency part have been obtained by the SCIFER, 1400 km (Kintner *et al.*, 1996) and the AMICIST, 450 km (Bonnell *et al.*, 1996) rocket flights within the cleft and pre-midnight aurora respectively. Especially the later work demonstrated that electrostatic H^+ cyclotron mode with $0< |k_\parallel/k_\perp| <0.22$ could explain some of the broadband wave features.

3.3.10. *Conclusions from the Freja Observations*

The *Freja* spacecraft has confirmed the existence of widespread electromagnetic turbulence associated with auroral electron precipitation. In the frequency range 1 −7 Hz (spacecraft reference) the turbulent spectrum has $\delta E/\delta B \approx v_A$ characteristic for the Alfvén wave turbulence (AWT). At higher frequencies, the ratio $\delta E/\delta B$ increases. It has been found that the measured spectrum obeys the theoretical relation (47) valid for dispersive Alfvén waves and therefore broadband ELF waves 10– 500 Hz can be attributed to DAW turbulence at spatial scales 20−700 m. Within the broadband turbulence *Freja* often encounters distinct, intermittent electromagnetic pulses which have the following characteristics:

– $\delta E \approx 10$–500 mV m^{-1},
– $\delta E/\delta B \geq v_A$; indicative of IAW,
– $\delta B_\perp \gg \delta B_\parallel$,
– non-sinusoidal waveforms; often with monopolar and bipolar electric field signatures,
– deep density cavities on the inertial scale,
– associated broadband ELF emissions, consistent with short wavelength DAW.

Occurrence: During auroral activity at the boundaries of large-scale field-aligned current systems. Almost permanent presence in the dayside cusp/cleft region.

Large scale density cavities: Alfvén activity is often situated in large scale plasma cavity depletions, possible evacuation processes: parallel electric fields acting on electrons and/or transverse ion acceleration and outflow.

Energy flow: Parallel Poynting flux 1–20 mW m^{-2}, but occasionally values as large as ~ 50 mW m^{-2} can be observed. Direction is predominantly downward, some upward reflections.

Field-aligned currents: Between tens of μA m^{-2} to hundreds of μA m^{-2}.

Energy cascade: There are indications that the DAW drive a turbulent cascade toward short-scale waves down to ~ 30 m.

Electron energization: Association with suprathermal electron bursts with energies from thermal to several hundred eV up to the inverted-V electron energies (if present)

Ion energization: Transversely accelerated ions up to energies of a few hundred eV related to either the more localized Alfvénic waveforms or the more distributed DAW (broadband ELF wave activity).

3.4. FAST OBSERVATIONS

The FAST spacecraft is well instrumented for studying the microphysics of fine scale Alfvénic disturbances observed in the auroral oval. The FAST fields experiment provides 3-D electromagnetic field measurements and multiple baseline electric field measurements thereby allowing some of the temporal/spatial ambiguity inherent in single point measurements to be removed. These features coupled with 80 ms electron and ion distribution functions allows a picture of the essential microphysics to be established. In this section we present the characteristics of impulsive plasma skin depth scale Alfvénic field fluctuations observed by the FAST spacecraft.

Skin depth size Alfvén waves are observed by the FAST satellite from perigee at 350 km up to apogee at 4180 km. The observed properties of these waves confirm the observations made by *Freja* discussed in the previous section of this review. However, FAST's high inclination orbit provides a different perspective with a generally north-south cut (rather than east-west) through the fluxtubes on which these waves exist. Furthermore the eccentricity of the orbit allows an altitude profile for these waves to be established extending from just above the ionosphere to the base of the primary auroral electron acceleration potential.

The waves are observed most commonly in and around the cusp and are often imbedded in regions of magnetosheath ion precipitation. Nightside observations are however not unusual. There appears to be no bias in occurrence with the background region I and II current systems and interestingly these waves are not seen in regions where an electrostatic potential exists below the spacecraft (i.e., where up-going ion beams are observed) and rarely in regions of inverted-V electrons.

Perhaps one of the most outstanding features of these waves in the aurora is their association with suprathermal fluxes of downgoing field-aligned electrons which have been identified from the *Freja* observations in the previous section as STEB. These accelerated electrons have energies from 10 eV up to 1 keV and sometimes higher on the nightside and may provide precipitating energy fluxes in excess of 10 mW m^{-2}. Examining high-resolution data shows that these fluxes consist of a series of bursts well correlated with the impulsive Alfvén wave field. In the following discussion we firstly present an example of a FAST dayside oval crossing typical of those when Alfvén waves are observed and then discuss in general the observed properties of these waves obtained from several orbits.
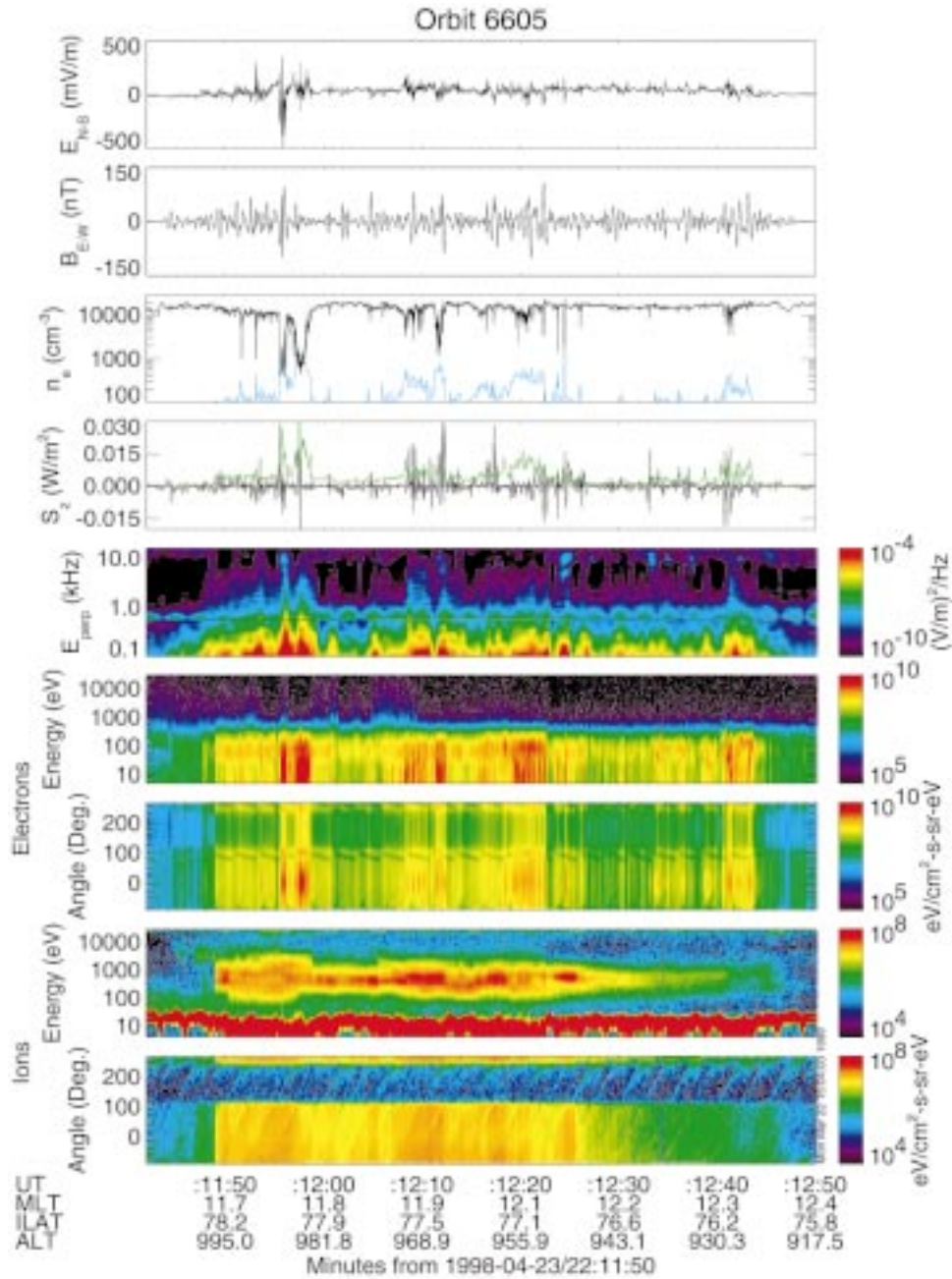
Figure 14. A FAST cusp crossing. (1) electric field N–S component, (2) magnetic field, E–W, (3) electron density from the Langmuir probe (black trace) and the ESA experiment (blue trace), (4) field-aligned wave Poynting flux (black trace, positive downwards) and integrated electron energy flux (green, multiplied by 5). Panel (5) is the spectrum of electric field fluctuations. The remaining panels show the electron and ion energy spectra and pitch angle.

3.4.1. *An Overview of an Auroral Oval Crossing*

Figure 14 presents a summary of fields and particles data recorded on the FAST spacecraft while traversing the dayside oval at an altitude of 1000 km and through a region of strong 'ELF turbulence'. The first two panels show the transverse to $\mathbf{B}_0$ electric and magnetic fields with fluctuations amplitudes of up to 500 mV m^{-1} and 100 nT, respectively, indicating E/b ratios of 5000 km s^{-1}. Close inspection of the time series data reveals that this turbulence consists of a series of impulsive $1-2$ cycle fluctuations in both E and b with periods in the spacecraft frame in the range $50-200$ ms. The third panel shows that the larger of these fluctuations are accompanied by strong density depletions. Similar cavities have been reported by Boehm *et al.*(1990) from rocket observations, and by Makela *et al.* (1998), Stasiewicz *et al.* (1998), and Wahlund *et al.* (1998) using *Freja* measurements as reported above. These density results have been obtained from the Langmuir probe which has been calibrated for this event by using the lower hybrid cutoff with the necessary composition data obtained from the plasmaspheric hiss cutoff below ω_{ci} (Chaston *et al.*, 1999). The blue trace in this panel is the hot electron density as measured by the electrostatic analyzer (ESA). Of particular interest here is the enhancements seen by the ESA and the coincident depletions seen by the Langmuir probe. Since the low energy limit of the ESA is ~ 5 eV the close agreement of the two different instruments indicates a depletion, or total absence in some cases, of the cold electron population within the Alfvén wave cavity. From the density and composition results we find the Alfvén speed of $\sim 10\,000$ km s^{-1} inside the cavities and ~ 2000 km s^{-1} outside.

The fourth panel shows the field-aligned Poynting flux with positive values indicating downward propagating waves. The green trace is the integrated electron energy flux multiplied by a factor of five for the sake of comparison. It should be noted that these integrated results correspond to a precipitating flux of up to 10 mW m^{-2} at the ionosphere which is well above the 1 mW m^{-2} ($= 1$ erg cm^{-2} s^{-1}) threshold for creating visible aurora (Stenbaek-Nielsen *et al.*, 1998). However, it should also be noted that for the majority of such structures integrated electron fluxes projected to the ionosphere are more typically just above the visibility threshold. At times the correlation/anti-correlation between enhanced energy flux and wave Poynting flux is clear. All integrated electron flux is directed downwards for this case while in general the Poynting flux is mostly downwards but some clear cases of upwards flux are apparent.

The fifth panel presents the wave electric field spectrum $0.1-10$ kHz. Throughout the interval the spectrum below the proton gyro frequency (black line) is filled with broadband emissions coinciding with the Alfvénic activity seen in the upper panels. At times the turbulence may extend to frequencies exceeding the local lower hybrid frequency. This is similar to features reported previously by Wahlund *et al.* (1994) and more recently by Knudsen and Wahlund (1998) from *Freja* observations and from the SCIFER sounding rocket (Kintner *et al.*, 1996; Bonnell *et al.*, 1996).

The electron spectra is typical of STEBs which invariably accompany intervals of Alfvénic turbulence observed on FAST. Peak energies are up to a few hundred eV and each burst is well correlated with intervals of upwards current inferred from the magnetometer deflection. The peak in the ion energy spectra at a few hundred eV is a clear signature of magnetosheath ions. These ions are isotropic apart from the clear loss cone centered at a pitch angle of 180 deg. The occurrence of Alfvénic fluctuations in the data and the presence of these ions is closely associated since the Alfvénic activity disappears in their absence. This suggests that FAST remains in the cusp throughout the time when the Alfvénic fluctuations are seen. The broad red line across the ion energy spectra below 50 eV is due to the combined effects of ion heating (TAI) and ram. These ions have been removed from the ion angle plot in the last panel by setting a low energy threshold of 100 eV.

3.4.2. *Cavities, Currents, Wavelengths*

Figure 15 presents a magnified view of the density cavity and electron distribution captured within the cavity coincident with single impulsive Alfvén wave event at 22:11:55 UT in Figure 14. The cavity has $\delta n/n$ ~1. The blue line in (a) is the density obtained from the ESA experiment and agrees well with the Langmuir probe result within the cavity. This indicates a ~ 100% depletion of the cold electron population within the cavity since all the electron density is recorded by the ESA above the low energy limit of ~ 4 eV. More typically however the energetic population accounts for less than 50% of the total electron density. The second panel, which shows the current measured by the ESA in this case, represents the total current carried by the Alfvén wave and has periodic structure within the cavity. Each of the three peaks are separated by one wavelength (or wave period) as represented in the deflection of the east–west magnetometer measurement. The electron distribution shown in (d) is that captured at the time of peak current in the centre of the cavity and is dominated by a strongly field-aligned component at 0 deg which contains most of the electron density at this time and all of the current. The angular width of the beam lies within the source cone so that most of this component precipitates into the ionosphere where it may give rise to visible aurora.

Some information about the geometry of the current system associated with the Alfvén wave can be gleaned from the form of the magnetometer time series. Figure 16 shows two examples of magnetic measurements where the first one is consistent with FAST passing through a series of current sheets and the second is consistent with the spacecraft passing across a magnetic vortex-like structure. The dashed lines are simulated magnetic fields calculated by assuming a Gaussian current profile for the geometries suggested in the schematics. For the sheet-like case, each sheet has a width of ~ 800 m with alternating directions and current densities as high as 200 μA m^{-2}. For the other case the time series is consistent with a coaxial system having a core upward current of radius ~ 300 m and a current density of 150 μA m^{-2} with a coaxial return sheath. A simple test on the
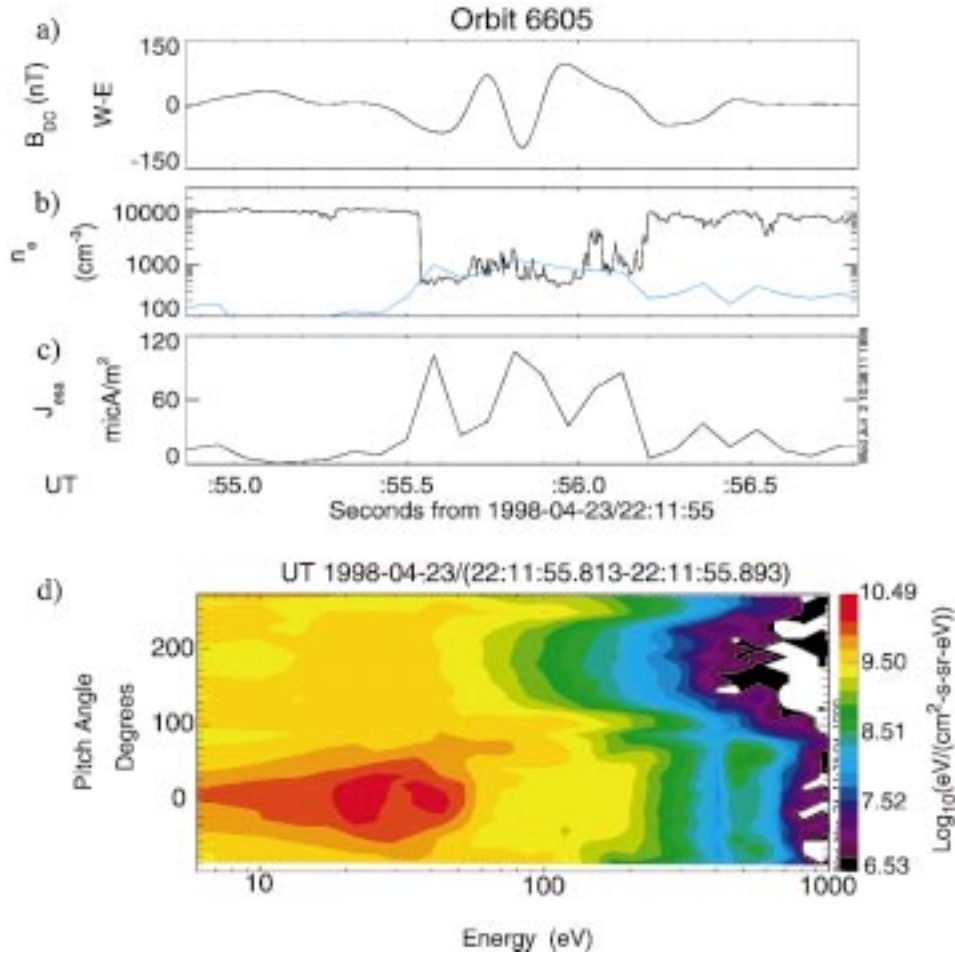
Figure 15. (a)The east–west magnetic field deflection of an individual Alfvénic disturbance from Figure (14). (b) Electron density measured within the structure by the Langmuir probe (black) and the ESA (blue). (c) The electron current as measured by the ESA. (d) The electron distribution measured within the density cavity.

sheet-like nature of the current structure is the ellipticity of the hodogram of the transverse **b** field. This is essentially the ratio of the minor to major axis of the polarization ellipse. A purely sheet-like current will have an ellipticity ~ 0 while structures containing rotation in **b** will have ellipticities greater than this value. The actual magnitude of the ellipticity (except for the sheet-like case) is determined by the trajectory of the spacecraft through the structure. In the two cases presented in Figure 16 the sheet-like case has an ellipticity of 0.06 while for the cylindrical case 0.4. Figure 17 presents the ellipticity in the transverse magnetic field for a number of events. While sheet-like currents do exist, the ellipticity in general is significantly larger than 0 with a median value of 0.3.
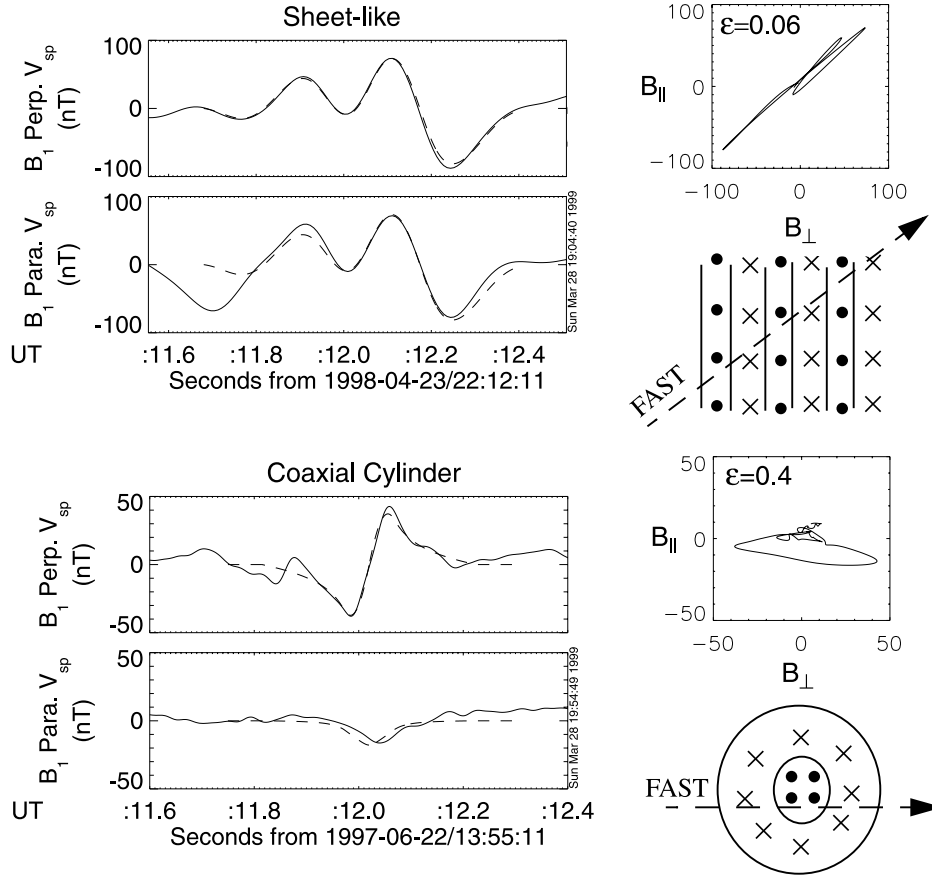
Figure 16. Two examples of an Alfvén magnetic wave field which may be interpreted in terms of static current structures through which FAST travels. The time series shows the wave field measured along and perpendicular to the spacecraft velocity vector, Vsp. The dashed lines correspond to the magnetic signals from model currents (see text).

The wave speed perpendicular to $\mathbf{B}_0$ and along the spacecraft trajectory can be determined from the time delay between two measurements of an identical waveform separated by distance $d \leq 50$ m. This distance represents the projection of the dipole separation along the spacecraft track and perpendicular to $\mathbf{B}_0$. Preliminary results of this analysis are shown in Figure 18 and indicate that the structures have perpendicular velocities of ± 1 km s^{-1} parallel and anti-parallel to the spacecraft trajectory or roughly the north-south direction. The dip at 0 km s^{-1} shows that in general these waves are not at rest in the plasma frame. Minimum variance analysis shown in Figure 17 suggests that $\mathbf{k}_\perp$ also lies along the north-south direction. This indicates that the perpendicular speeds provide an estimate of the perpendicular wave phase speed. Given that the wave frequency (of the lowest frequency component) in the spacecraft frame is known to be ~ 5 Hz, we can show that the
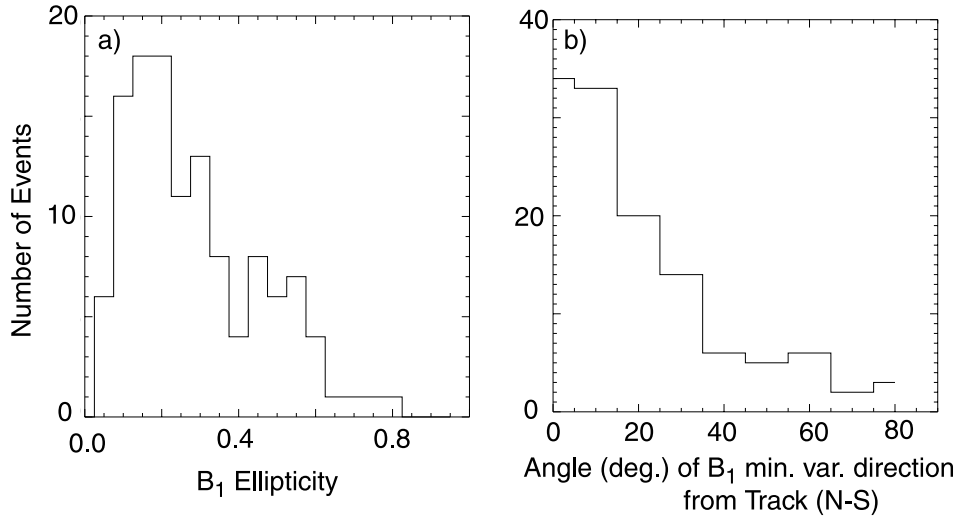
Figure 17. Histograms showing (a) the ellipticity of the hodogram of the Alfvén wave magnetic field and (b) the minimum variance direction of the magnetic field as an angle from north–south.
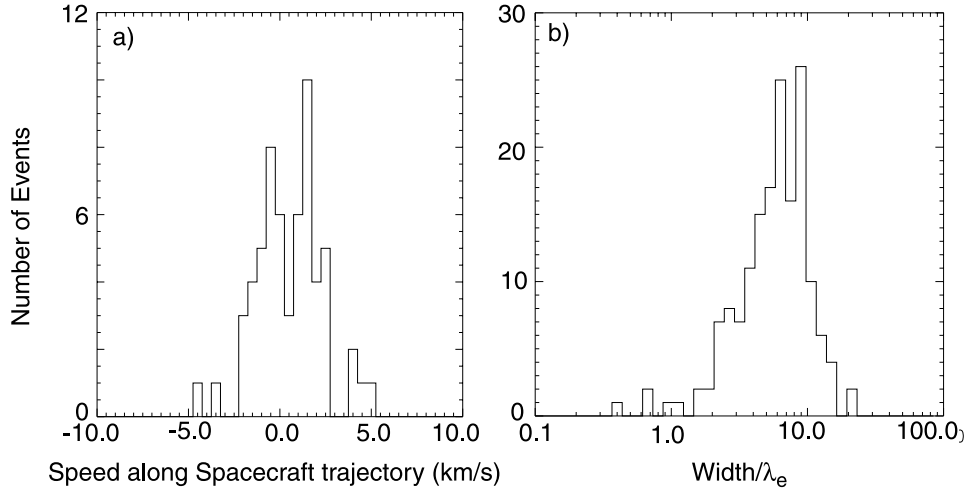
Figure 18. (a) Histograms showing the perpendicular velocities and (b) width of the Alfvén structures along the spacecraft trajectory.

wave frequency in the plasma frame is ~ 1 Hz. Such a wave frequency implies a perpendicular wavelength of 1 km. This result can be independently checked since at this frequency the waveform can be expected to vary less $\pi/2$ radians in the time it takes FAST to traverse one wavelength. Relating the distance traveled by FAST to observe one full oscillation for a number of events yields the distribution shown in Figure 18 indicating a width, or perpendicular wavelength, $(7 \pm 3)\lambda_e \approx 600$ m.
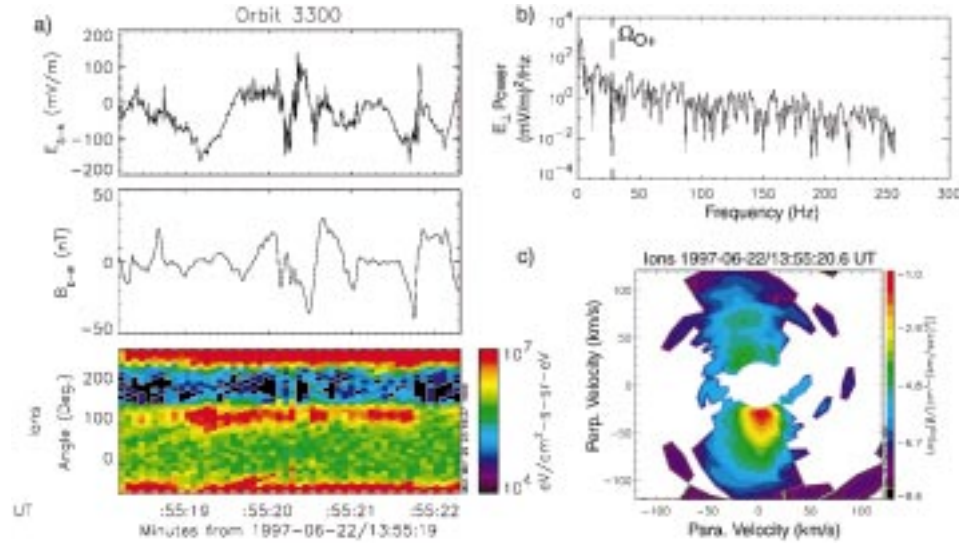
Figure 19. Transverse ion energization in an Alfvénic structure. (a) Electric field, magnetic field and ion pitch angle distribution, (b) spectrum of the electric field, and (c) ion velocity space distribution function.

3.4.3. *Ion Heating*

There is clear association between small scale Alfvénic structures and ion heating in the FAST data set. The first panel of Figure 19 shows the north-south directed electric field indicating several large amplitude Alfvénic structures which are also represented in the east−west *dc* magnetometer measurements presented in the second panel. Superimposed on these larger scale features are higher frequency fluctuations characteristic of the regions where transverse ion heating is observed. The spectrum of these field fluctuations in the spacecraft frame is displayed in panel (b). The last panel of (a) shows that coincident with these field variations are enhanced ion fluxes at a pitch angle of 90°. Ideally the pitch angle distribution should be symmetric about 0°, however the effects of spacecraft ram tends to enhance fluxes in the direction of the spacecraft velocity vector resulting an asymmetric pitch angle distribution. Figure 19 shows the classical phase space plot of the perpendicularly heated distribution. The slightly folded arms of the 'conic' show that the heating began at altitudes somewhat below the spacecraft. Inspection of the ion mass spectrometer measurements at this time show that the heated distribution is primarily oxygen.

While there is a clear association between the observation of heated ions and Alfvénic fluctuations there is often an offset between the most intense wave activity and the most strongly heated ions. For instance in the present example the most intensely heated ions occur at 13:55:19.2 UT where the amplitude of the wave is small while at 13:55:20.4 there is drop out of heated ions when the amplitudes are large. A simple explanation is that the majority of heating in the first case has

occurred at lower altitudes and the combined effect of oblique wave propagation and the $\mathbf{u}_E$ drift provides the offset. In fact, observations over the FAST altitude range from 400–4000 km suggest that ions may be continuous heated as they stream up the field line.

3.4.4. *Conclusions from FAST*
The basic characteristics of the Alfvénic structures are:
- Amplitude: $E_\perp < 1$ V m^{-1}, $b \leq 100$ nT.
- Wave frequency in plasma frame: ~ 1 Hz.
- Perpendicular wavelength: ~ 1 km or $7\lambda_e$.
- Perpendicular phase velocity: ~ 1 km s^{-1} north–south.
- Polarization: elliptical in plane perpendicular to $\mathbf{B}_0$ with major axis east–west.
- Poynting flux: mainly downwards, ~ 10 mW m^{-2}.
- Currents: up to a few 100 μA m^{-2}, usually distributed as a number of filaments.
- Density cavities: up to order of magnitude variation in density across the impulsive wave field ($\delta n/n \leq 1$), due to depletion of cold plasma within the cavity.
- Electron distribution: Down going field aligned beam with energy up to 1 keV.
- Ion distribution: Transversely accelerated ions or conics with energy up to a few 10's of eV.

3.5. LABORATORY EXPERIMENTS BY J. MAGGS

3.5.1. *Alfvén Wave Propagation*
Early laboratory experiments on Alfvén waves focused on proving their existence and verifying their predicted dispersive properties. These early efforts are described in the recent review by Gekelman (1999) and we will not cover them here. Rather, our attention will be on the properties of the dispersive Alfvén wave that are of most interest to auroral physics, namely, the propagation of energy across field lines and the effects of radiation from small sources with sizes on the order of the electron skin depth. Waves with small perpendicular wavelengths are important because they have magnetic field aligned electric fields and, therefore, interact with field aligned electron fluxes.

The first experiment to investigate the dispersive properties of the shear Alfvén waves was conducted in the limit $k_\perp \lambda_e \gg 1$ by Ono (1979). In this experiment, the Alfvén wave speed was larger than the electron thermal speed so that the wave was in the inertial regime. From (22) it is evident that, in the short wavelength limit the ratio between the parallel and perpendicular wave numbers becomes a constant (when the plasma ions are cold). That is, the wave propagates at a fixed angle relative to the magnetic field for all values of wave numbers. This behavior results in a resonance cone propagation pattern which was clearly verified by Ono. Figure 20 shows the setup Ono used to launch the waves, the detected electric
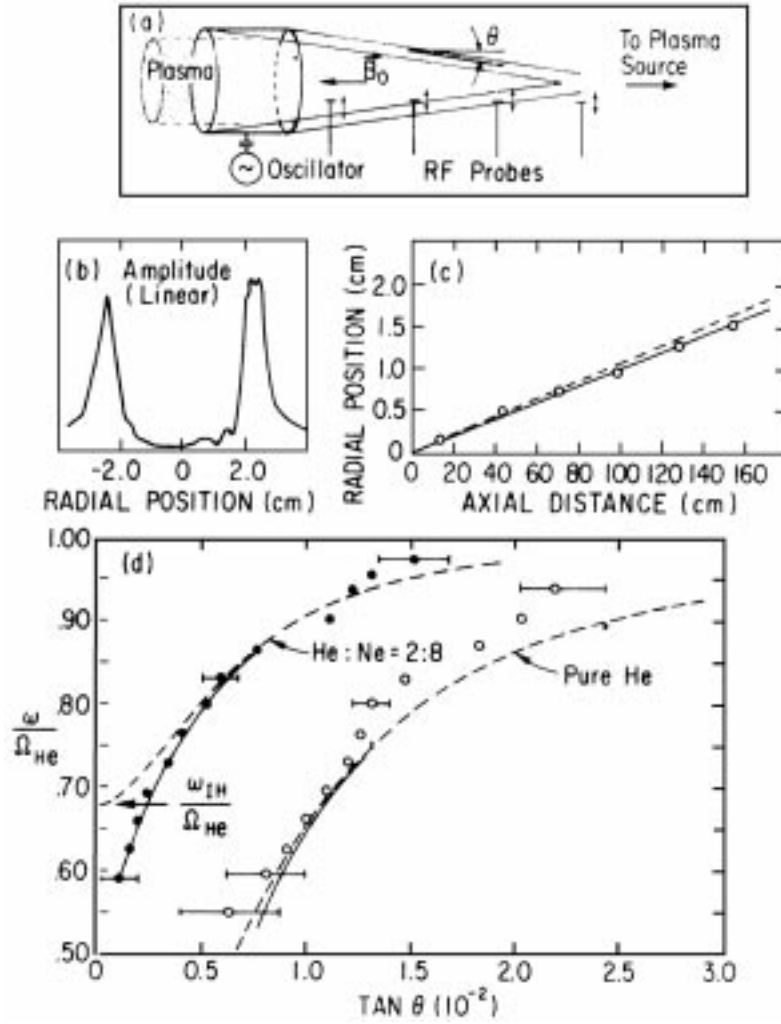
Figure 20. The experimental setup and observation of the cone-like radiation pattern for the shear Alfvén wave in the large $k_\perp \lambda_e$ limit. The electric field pattern is observed to spread from the source along a narrow conical structure at a fixed angle to the magnetic field. The observed behavior is compared to theory in panels (c) and (d). Two mixtures of gas were used in the experiments: pure helium and a neon-helium mixture. (From Ono, 1979.)

field pattern and the measured wave dispersion. The wave was launched using four, separately phased, external rings concentric to the plasma. This arrangement sets the parallel wavelength, and for each frequency used the perpendicular wave length is given by the dispersion relation. Figure 20(b–d) shows a validation of the propagation of the wave at the predicted resonant cone angle,

$$\tan \theta = \hat{\omega}(m_e/m_i)^{1/2}(1 - \hat{\omega}^2)^{-1/2} , \tag{64}$$

which is a finite frequency generalization of Equation (22) and $\hat{\omega} = \omega/\omega_{ci}$. The expression in (64) is compared to measurements (the dashed curve) in Figure 20(d) for both a pure helium plasma and a two ion species helium-neon plasma.

The experiment by Ono clearly established the perpendicular dispersive properties of the shear Alfvén wave in the $k_\perp \lambda_e \gg 1$ limit but it had shortcomings. Under the experimental parameters of density 10^{10} cm^{-3} and 4.2 kG magnetic field in a helium plasma, the Alfvén wavelength, $\lambda_A = f/v_A$, is larger than 50 m at $\hat{\omega} = 0.5$ while the experimental device was only 2.3 m in length. Thus the wave fields measured in this experiment are indicative of the near field behavior of shear Alfvén wave radiation.

The behavior of the wave at distances larger than one Alfvén wavelength from the source was investigated in an experiment by Borg *et al.* (1985) in a tokomak device. In this experiment the Alfvén speed was again larger than the electron thermal speed so that the wave investigated was in the inertial regime but the perpendicular wavelengths were longer and $k_\perp \lambda_e \approx 1$. Waves were launched into a hydrogen plasma at frequencies less than one tenth of the ion gyrofrequency using small ($\sim 3\lambda_e$) rectangular cross section solenoids oriented perpendicular to the toroidal magnetic field of the tokomak. A radiation pattern that shows the cone like propagation of the shear Alfvén wave was obtained by using a very elongated solenoid (20 cm × 3 mm) in an orientation with one small leg of the solenoid aligned along the toroidal field and the return leg located outside the device. In this orientation only one leg induced plasma current so that only a single current filament was excited. The measured radial profile (dashed line) is compared to the theoretical predictions (solid lines) in Figure 21. The theory with a single transit of the waves ($N = 1$) along the circumference of the tokamak and a pattern with 5 transits ($N = 5$) are shown for comparison. The theory assumes a cylindrical symmetry and the effects of the toroidal magnetic geometry of the tokomak are not included so that the agreement between theory and experiment is only approximate. While these experiments verify the spreading of Alfvén wave energy across the magnetic field due to perpendicular dispersive effects the tokomak magnetic geometry make it difficult to formulate a theory and obfuscate the interpretation of the data.

Studies of cross field dispersive effects on both the kinetic and inertial Alfvén waves have also been carried out in the Large Plasma Device (LAPD) at UCLA (Gekelman *et al.*, 1994, 1997a, b; Leneman *et al.*, 1999; Vincena and Gekelman, 1999). This machine is ideally suited for basic studies of shear Alfvén wave propagation because of its linear geometry, large plasma column (40 cm diameter, 9.6 m length), high plasma density (2–5 ×10^{12} cm^{-3}) and high magnetic field (1–2 kG). The magnetic field patterns of shear Alfvén waves radiated from disk shaped antennas with radii on the order of the electron skin depth was studied for various ratios of v_A/v_{te} in uniform plasmas. Such disk antennas, aligned with their normal pointing along the magnetic field, have an inherent cylindrical symmetry and radiate shear Alfvén waves with purely azimuthal magnetic fields. These antennas couple to the plasma by drawing magnetic field-aligned electron currents out of
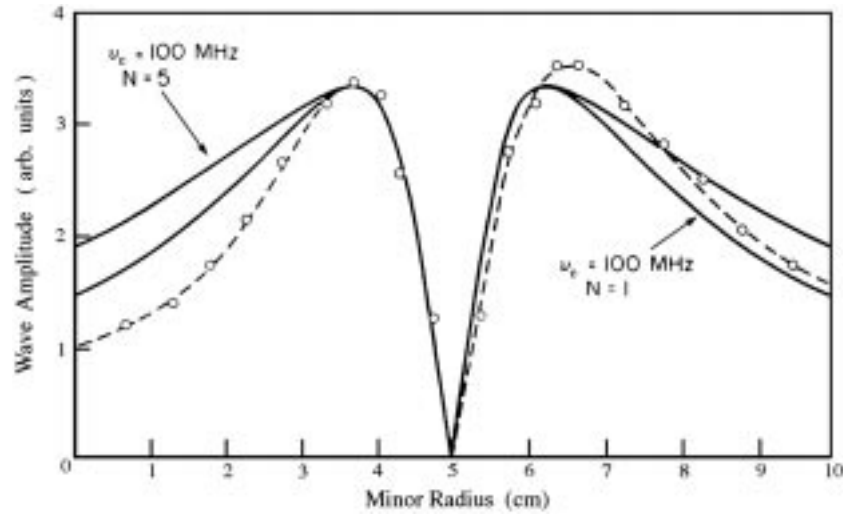
Figure 21. The field pattern of a single current channel compared to theory for one and five transits (as marked) of the wave along the circumference of the tokomak (from Borg *et al.*, 1985).

the plasma. An example of the radial pattern of the magnitude of the azimuthal magnetic field is shown in Figure 22 for a plasma with the Alfvén velocity slightly larger than the electron thermal velocity ($v_A = 1.2v_{te}$) (Gekelman *et al.*, 1994). The disk antenna used had a radius $1.51\lambda_e$. Three radial profiles are shown; one at a distance along the field line $0.5\lambda_\parallel$ from the disk antenna ($dz = 157$ cm), one at $0.8\lambda_\parallel$ ($dz = 252$ cm), and one at $1.1\lambda_\parallel$ ($dz = 346$ cm). The profiles rise steeply from a value near zero, reach a peak and then decay as r^{-1} for large r. This behavior arises because the azimuthal magnetic field is due to field-aligned electron channels which are confined inside a cone shaped region which makes an angle to the magnetic field given by (22). It is clear that the current channels broaden as the wave propagates down the field because the peak in the amplitude occurs at larger radial values as the distance from the source increases. The observed profiles are compared to the theoretically expected profiles (Morales *et al.*, 1994), as shown by the dotted curves. In the application of the theoretical analysis Gekelman *et al.* included the effects of Landau damping and electron neutral collisions but neglected Coulomb collisions (which actually are important in their experiment). The fits shown are excellent but were obtained by assuming an axially varying electron temperature which was not measured.

The radial profiles of wave magnetic field amplitude do not illustrate the perpendicular propagation of these waves. A snapshot of a shear wave magnetic field at a particular time (Gekelman *et al.*, 1997a) is shown in Figure 23 which illustrates the changes in wave magnetic field vector as a function of radius. The wave shown has a phase velocity slightly smaller than the electron thermal speed ($v_A = 0.75v_{te}$) so that the wave is in the kinetic regime The very evident circular minimum, across which the magnetic field reverses direction, is a radial phase front which moves
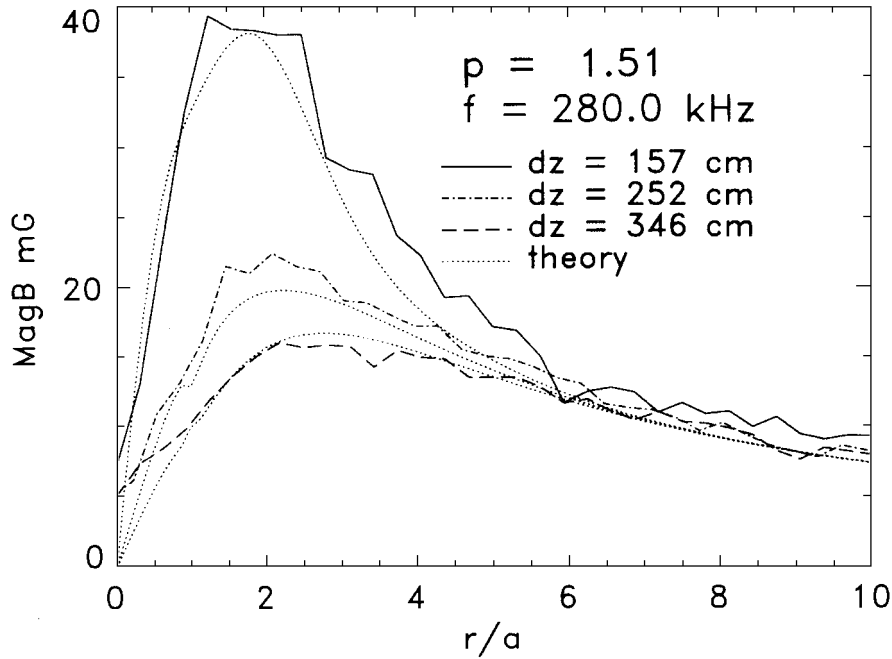
Figure 22. The observed radial profiles of the magnetic field launched by a disk antenna exciter in the LAPD are compared to theoretical predictions for an inertial Alfvén wave. (From Gekelman *et al.*, 1994.)

outwards (towards larger r) as time proceeds because as (28) indicates the kinetic Alfvén wave is a forward wave (i.e., the phase velocity is in the same direction as the group velocity) for perpendicular propagation (Morales and Maggs, 1997). As shown in Figure 24(a–c), the kinetic Alfvén wave exhibits a radial pattern (Leneman *et al.*, 1999) somewhat similar to the inertial Alfvén wave except for a secondary peak at a radial location smaller than the main peak. The radial profiles are shown for a case in which $v_{te} = 2.6v_A$ at an axial distance $0.38\lambda_\parallel$ (94 cm), $1.75\lambda_\parallel$ (440 cm), and $2.5\lambda_\parallel$ (629 cm). The behavior of the wave phase as a function of radius is shown in Figure 24(d) for this kinetic wave and for an inertial wave with $v_A = 2.1v_{te}$. The negative slope of the phase in the inertial case indicates the backward nature of the wave while the positive slope of the kinetic wave indicates it is a forward wave.

The spatial distribution of the currents associated with the kinetic wave are illustrated in Figure 25. The wave field is symmetric about the magnetic field so that only the radial and axial distribution if shown. Several techniques are used to make the current pattern easier to discern. First the axial direction has been shrunk down by a factor of 40, and the axial decay of the measured wave field has been eliminated by normalizing the maximum observed amplitude in each measurement plane to unity. Also, the product of radius times current, $rJ(r, t)$
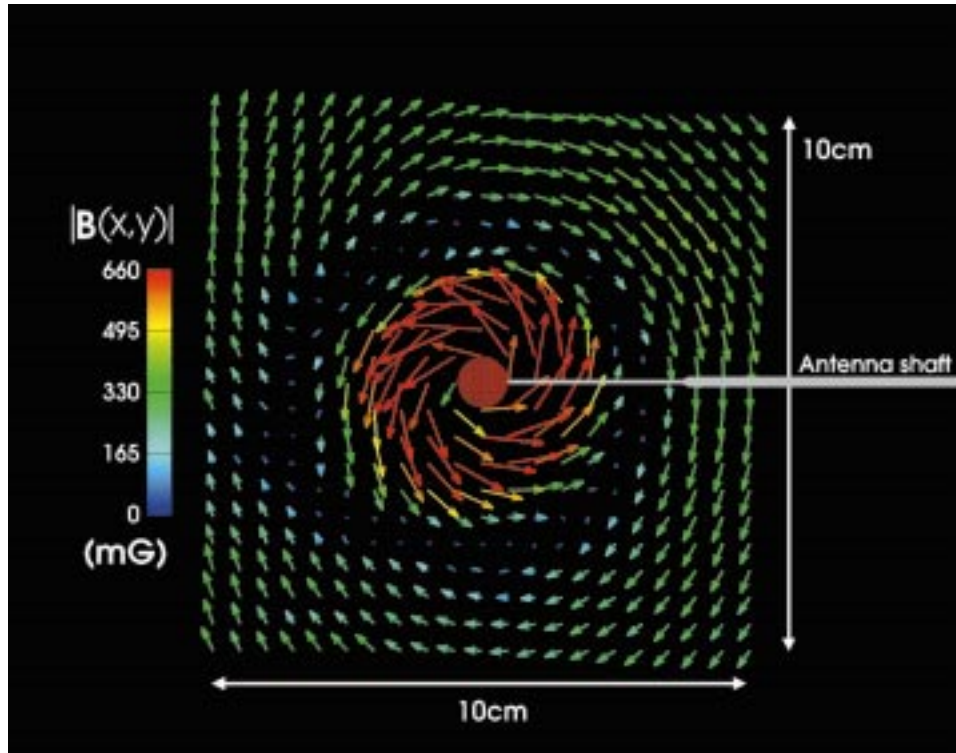
Figure 23. A time snapshot of the magnetic field vectors associated with a kinetic Alfvén wave in a plane 1.02 wavelengths from the source clearly showing a perpendicular phase front. A model of the disk antenna is also shown. (From Gekelman *et al.*, 1997.)

is shown to enhance the currents at large radial values. This figure clearly shows the parallel wave length of the wave, the spreading of the wave currents across the field, and the closure of the wave currents. The full three dimensional pattern of the inertial Alfvén wave propagating in the plasma column of the LAPD device is shown in Figure 26 (Vincena and Gekelman, 1999). The wave shown is in the kinetic limit ($v_A = 0.5v_{te}$). The measurements are taken in three planes (45 cm × 18 cm) across the magnetic field and one plane (91 cm × 25 cm) containing the magnetic field. The wave frequency is nine-tenths of the ion gyrofrequency and the parallel wave length is 90 cm. Several phase fronts associated with propagation across the field are visible as well the structure along the field.

3.5.2. *Alfvén Waves in a Density Striation*
Laboratory observations that have a direct bearing on the observation by spacecraft of density depletions with cross field scale sizes on the order of the electron skin depth and associated electric and magnetic fluctuations were made on the LAPD plasma device (Maggs and Morales, 1996, 1997; Maggs *et al.*, 1997). A magnetic field-aligned density depletion (a so called striation) was produced in a 40 cm diam-
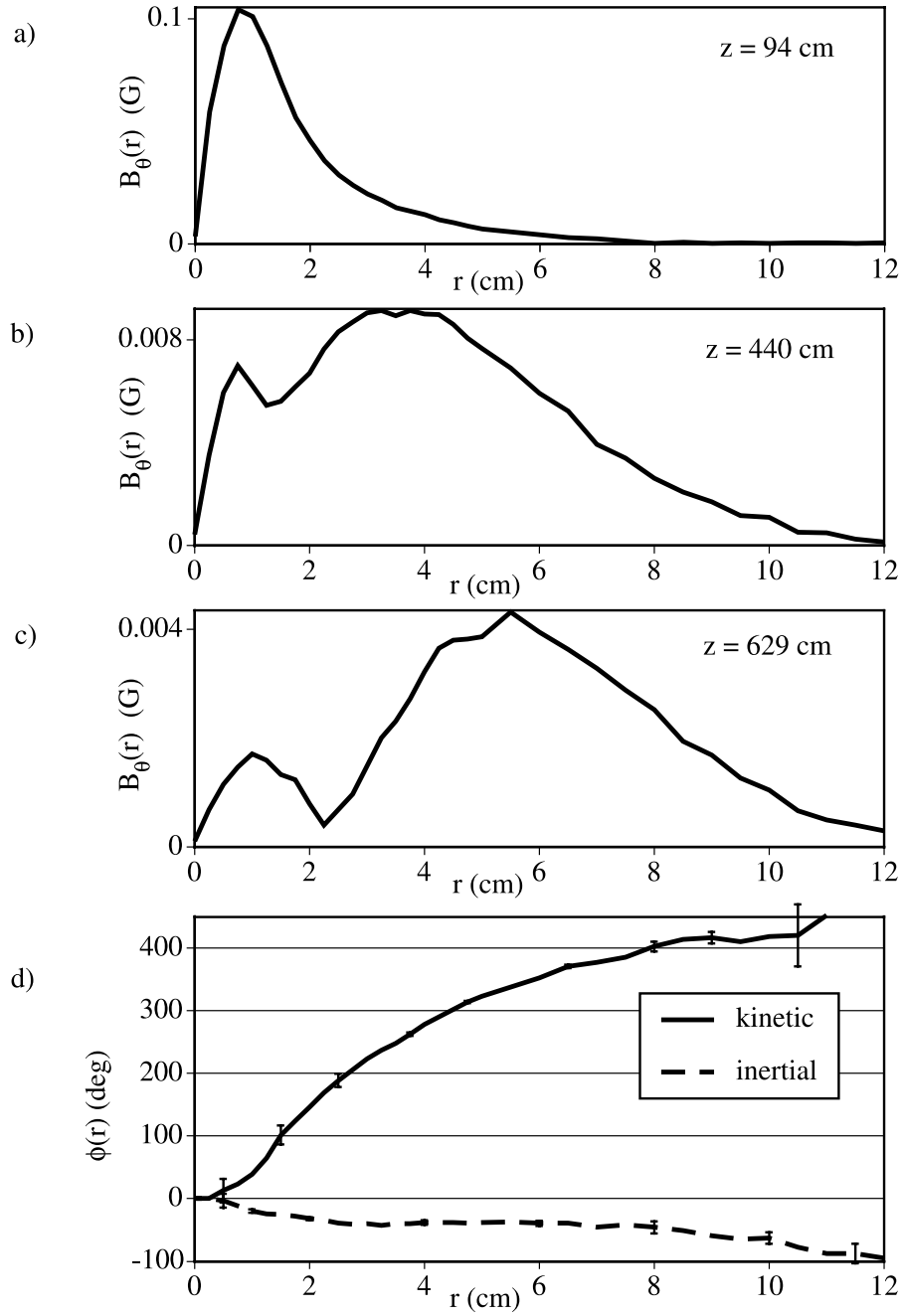
Figure 24. (a)−(c) Radial profiles of a kinetic Alfvén wave are shown at three different distances from the disk antenna source (the Alfvén wave length for this case is 2.5 m) . The spreading of wave energy across the field and the development of a secondary peak inside the main peak is evident. (d) The phase of the wave as a function of radius shows that the kinetic wave is forward and the inertial wave is backward. (From Leneman *et al.*, 1999.)
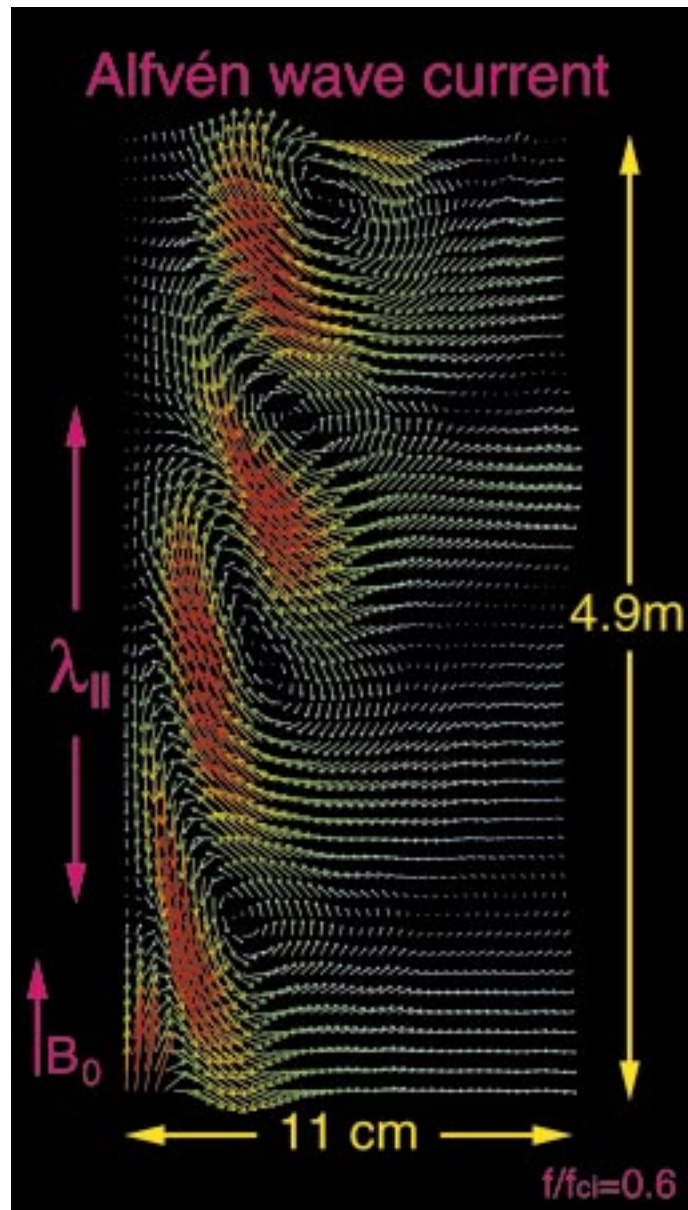
Figure 25. The current patterns (actually $rJ(r, z)$) associated with the kinetic wave shown in Figure 24. The scale along the magnetic field is reduced by a factor of forty and the wave amplitudes are normalized for ease of viewing. (From Leneman *et al.*, 1999.)
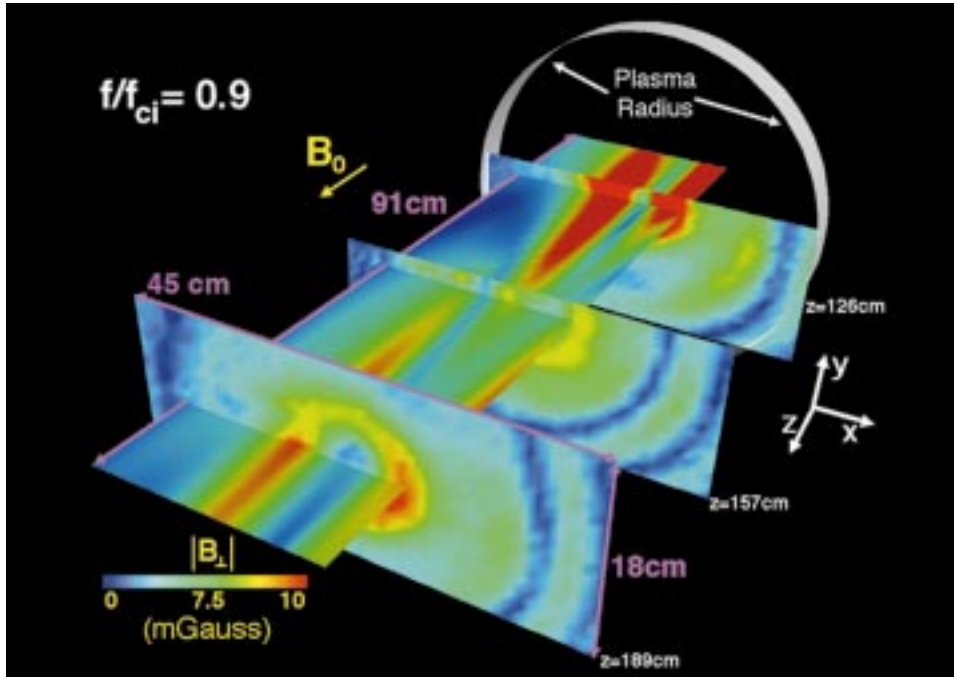
Figure 26. A three dimensional view of an inertial Alfvén wave propagating near the ion cyclotron frequency. The striking diference between the parallel and perpendicular wave structure is evident. (From Vincena and Gekelman, 1999.)
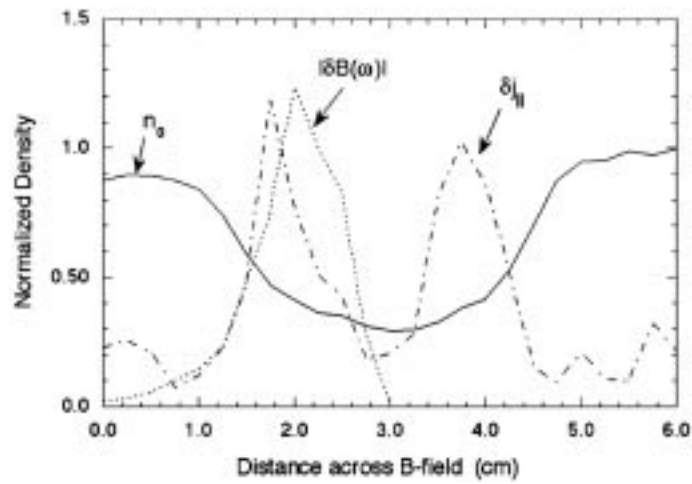
Figure 27. The pattern of the magnetic field and fluctuating magnetic field-aligned current associated with a drift Alfvén wave spontaneously generated by a magnetic field-aligned density striation. (From Maggs and Morales, 1997.)

eter, ten meter long helium plasma column by using a selective masking technique which blocks the plasma producing primary electrons emitted by the cathode. The striations produced run the length of the device, have density depletions ranging from 40 to 80%, and diameters of several electron skin depths. It was observed that as the discharge plasma is formed the striation spontaneously produces a large amplitude fluctuation in both density and magnetic field in the pressure gradient region (or wall) of the striation. These fluctuations are driven by the pressure gradient associated with the striation. Figure 27 shows the profile across the magnetic field of the fluctuating magnetic field, and the rms value of the field aligned currents, as well as the density profile of the plasma. The fluctuation profiles shown correspond to the frequency with the highest amplitude magnetic field fluctuation. This frequency is about one tenth the ion cyclotron frequency (i.e., $f \approx 0.1 f_{ci}$). The observed fluctuations are eigenmodes of the striation which is evident from the frequency spectrum shown in Figure 28. Each narrow peak corresponds to an eigenmode with different parallel wavelength, radial, and azimuthal mode number. The mode with the highest amplitude is the fundamental mode with half a parallel wavelength along the magnetic field, a radial mode number of one and an azimuthal mode number of one. The observed profiles and frequency structure agree well with theoretical predictions (Penano *et al.*, 1997). As indicated in Figure 28(a) for the case when the plasma electron beta is above the mass ratio (i.e., the kinetic Alfvén wave regime) the magnetic fluctuations are associated with density fluctuations. This behavior arises because the dispersive Alfvén wave couples to the electrostatic drift wave under these conditions producing a mode know as the drift-Alfvén wave. As the plasma beta is decreased to below the mass ratio (in the experiment the magnetic field is increased) the nature of the spontaneously generated wave changes. Figure 28(b) shows the frequency spectrum for a case when the plasma electron beta is below the mass ratio (i.e., the regime of the inertial Alfvén wave). The spectrum still has peaks but they are much broader and the magnetic fluctuations are no longer associated with density fluctuations except at very low frequency ($f \approx 0.03 f_{ci}$). Thus the driven waves at higher frequencies, in this case, are pure shear Alfvén waves. The broader spectral peaks indicates that the wave fields are becoming turbulent. Indeed as the plasma beta is lowered further the spectrum broadens to such an extent the eigenmode peaks become difficult to discern (Morales *et al.*, 1999). These observations show that density striations can give rise to trapped Alfvén eigenmodes which arise due to the pressure gradient in the wall of the striation. Therefore it should be expected that if a striation is formed by a process not initially involving Alfvén waves, then Alfvén waves may subsequently be generated by the striation. The association of narrow field aligned striations with Alfvén waves is to be expected.
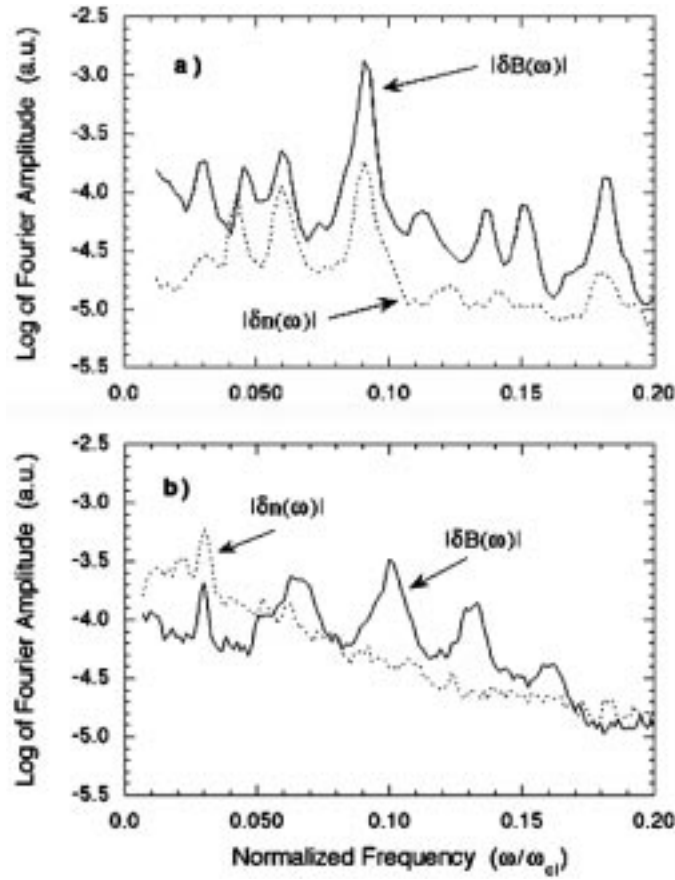
Figure 28. The frequency spectrum of the drift Alfvén waves generated by the density striation. a) The spectrum for electron plasma beta larger than the mass ratio (the kinetic Alfvén wave regime) is very coherent and shows a clear eigenmode structure. b) The spectrum for beta less than the mass ratio (the inertial Alfvén wave regime) is broader, indicative of turbulence in the plasma. (From Maggs and Morales, 1997.)

4. Alfvén Waves in Nonuniform Media

4.1. INTERACTIONS WITH THE IONOSPHERE

An important aspect of Alfvén wave propagation in the magnetosphere is the interaction of these waves with the ends of the field lines in the ionosphere. Auroral field lines may be considered to be a transmission line for shear mode Alfvén waves and, as with any transmission line, reflections will occur if the transmission line is not terminated properly. Since the ionospheric impedance is in general not matched to that of the Alfvén transmission line, reflections will occur in general. To analyze this reflection, we will follow the development of ionospheric conductivity as discussed, for example, by Kelley (1989, Chapter 6) and developed further by

Lysak (1990). We adopt the potential formalism described in Section 2.1 and, for simplicity, neglect the non-ideal MHD effects. Note that Fourier analysis of Equations (16) and (18) give a relationship between the vector and scalar potentials

$$\phi^{\pm} = \frac{\omega}{k_{||}} A^{\pm} = \pm v_A A^{\pm} \,, \tag{65}$$

where the $+$, $(-)$ signs are for propagation parallel (antiparallel) to the background magnetic field. In the ionosphere, the perpendicular currents are given by the anisotropic Ohm's law, integrated over the height of the ionosphere

$$\mathbf{I}_{\perp} = \bar{\Sigma} \cdot \mathbf{E} = \Sigma_P \mathbf{E}_{\perp} - \Sigma_H \mathbf{E}_{\perp} \times \hat{\mathbf{z}} \,, \tag{66}$$

where Σ_P and Σ_H are the height-integrated Pedersen and Hall conductivities, respectively and $\hat{\mathbf{z}}$ is the unit vector along $\mathbf{B}$. Considering the current continuity equation, the field-aligned current may be given by

$$J_{||} \sin i = \pm \nabla_{\perp} \cdot \mathbf{I}_{\perp} \,. \tag{67}$$

In this expression, i is the inclination angle of the magnetic field, which is close to $90°$ in the auroral zone so that $\sin i \approx 1$. Hence, for simplicity, we will neglect this factor in the following. The upper and lower signs in Equation (67) correspond to the northern and summer hemispheres, respectively. The sign difference arises from the fact that positive (negative) field-aligned current corresponds to current flowing parallel (antiparallel) to the magnetic field; thus, positive field-aligned current flows into the ionosphere in the northern hemisphere and out of the ionosphere in the southern hemisphere. Writing the electric field in (66) in terms of the scalar potential and using the Ampère's law (13), the current continuity Equation (67) can be written as

$$\nabla_{\perp}^2 A_z = \pm \mu_0 \nabla_{\perp} \left[\Sigma_P \nabla_{\perp} \phi - \Sigma_H \nabla_{\perp} \phi \times \hat{\mathbf{z}} \right] \,. \tag{68}$$

This equation can be further simplified if we assume that the conductivities are uniform. Under this assumption, the Hall term becomes zero, since it reduces to the curl of a gradient. Then Equation (68) can be written as

$$\nabla_{\perp}^2 \left(A_z \mp \mu_0 \Sigma_P \phi \right) = 0 \,. \tag{69}$$

If we assume a localized disturbance, so that A_z and ϕ go to zero at infinity, then the quantity in the parentheses must go to zero. A similar conclusion holds if we assume periodic boundary conditions. In this case, the fields at the ionosphere must satisfy the condition

$$A_z = \pm \mu_0 \Sigma_P \phi \,. \tag{70}$$

Let us now consider northern hemisphere conditions, in which case the ϕ^+ and A_z^+ correspond to the incident wave, and write the total wave field as

$$\phi = \phi^+ + \phi^- \ . \tag{71}$$

Using (65), the vector potential can be written as

$$A_z = \frac{1}{v_A} \left(\phi^+ - \phi^- \right) \ , \tag{72}$$

and the reflection coefficient for the electric field

$$R \equiv \frac{\phi^-}{\phi^+} = \frac{1 - \mu_0 v_A \Sigma_P}{1 + \mu_0 v_A \Sigma_P} = \frac{\Sigma_A - \Sigma_P}{\Sigma_A + \Sigma_P} \ , \tag{73}$$

where in the last step, we have introduced the Alfvén conductivity, $\Sigma_A \equiv 1/\mu_0 v_A$ (Scholer, 1970; Maltsev *et al.*, 1974; Mallinckrodt and Carlson, 1978). Note that this should properly be called an Alfvén admittance, but the conductivity terminology has taken root in the literature. It should be noted that Equation (73) also is valid in the southern hemisphere, with the $+$ and $-$ superscripts reversed. This simple model has a number of interesting properties. First of all, the Alfvén conductivity, which has a value of 0.8 mho/v_A, where v_A is given in units of 1000 km s^{-1}, is generally much smaller than the Pedersen conductivity. Thus, the reflected Alfvén wave has an electric field that is opposite to the incident wave, and so the total electric field is smaller than the electric field of the incident wave. This means that the ratio of the electric to magnetic fields is generally smaller than that usual Alfvén ratio, $|E_\perp/b_\perp| = v_A$. The interference between the incident and reflected waves will also give rise to a phase shift between the electric and magnetic components. The opposite conclusion follows if the Pedersen conductivity is lower than the Alfvén conductivity. This reflection model can also be modified to include electron inertial effects or the effects of large-scale parallel electric fields. As noted above in Equation (47), the electric to magnetic field ratio is increased in the presence of the electron inertia. This modification reduces the Alfvén conductivity to become

$$\Sigma_A = \left(\mu_0 v_A \sqrt{1 + k_\perp^2 \lambda_e^2} \right)^{-1} \ . \tag{74}$$

Another modification comes in the presence of large-scale parallel electric fields. Vogt and Haerendel (1998) have noted that the presence of such a field modifies the reflection coefficient since the electric field in the magnetosphere is not the same as that in the ionosphere. This modification can be included by introducing the approximate current-voltage relation first given by Knight (1973), which states that the field aligned current density can be related to the potential drop by the relation $J_\parallel = K\phi_\parallel$. This relationship defines a magnetosphere-ionosphere coupling length given by $L_{MI} = \sqrt{\Sigma_P/K}$, which is the order of 100 km for typical parameters. Under these conditions, the Pedersen conductivity in Equation (73) should be replaced by

$$\Sigma_{P,\mathrm{eff}} = \frac{\Sigma_P}{1 + k_\perp^2 L_{MI}^2} \ . \tag{75}$$

It should be noted that the model discussed in this section holds strictly only for a constant Alfvén speed above the ionosphere. This assumption is violated above the ionosphere since the rapidly decreasing density above the ionosphere leads to a rapid increase in the Alfvén speed. This leads to the formation of a resonant cavity above the ionosphere, as will be discussed in the next section.

4.2. THE IONOSPHERIC ALFVÉN RESONATOR

4.2.1. *Elementary Considerations*

Our previous analyses of the reflection of Alfvén waves from the ionosphere assumed that the Alfvén speed, and equivalently the Alfvén conductivity, was constant along the field line. Except for the special case where the density scales as the square of the magnetic field, this is not in general true, and there are Alfvén speed gradients. If these gradients are weak enough, WKB theory may be used to follow the propagation of the Alfvén waves. This situation may apply in the outer magnetosphere, but in the inner magnetosphere, the Alfvén speed gradient may become steep enough so the WKB theory is not valid. In such a circumstance, the Alfvén wave may be reflected by the gradient in the Alfvén speed. To illustrate this reflection, consider the extreme case of a discontinuity in the Alfvén speed. If the wave is incident from the side with Alfvén speed V_{A1}, and is transmitted to the side with speed V_{A2}, then an argument analogous to that for the ionospheric reflection yields:

$$R = \frac{E_{\text{ref}}}{E_{\text{inc}}} = \frac{\Sigma_{A1} - \Sigma_{A2}}{\Sigma_{A1} + \Sigma_{A2}} \ . \tag{76}$$

Thus, propagation into increasing Alfvén speed (decreasing Alfvén conductivity) leads to an enhancement of the wave electric field and a decrease in the magnetic field, and *vice versa*. This model has been used to calculate the propagation of Alfvén waves in inhomogeneous media by Mallinckrodt and Carlson (1978). In general, as noted above, a strong inhomogeneity in the Alfvén speed implies that we cannot use the WKB approximation and that we need to solve the complete wave equation for the wave fields. In the topside ionosphere, there is such a strong inhomogeneity due to the sharp exponential decrease in the plasma density with increasing altitude above a few hundred kilometers. This decrease takes place with a typical scale height of less than 1000 km. Since the magnetic field varies only weakly on such spatial scales, the Alfvén speed increases exponentially with a comparable scale height above the ionosphere. Above about 6000 km altitude, the density decrease becomes more gradual, and the decrease in the magnetic field leads to a slow decrease in the Alfvén speed.

4.2.2. *Alfvén Resonator Eigenmodes*

In order to analyze the eigenmodes of this system, it is useful to use a formulation of the Alfvén wave equations using scalar and vector potentials as described above:

$$\mathbf{E}_\perp = -\nabla_\perp \Phi - \frac{\partial}{\partial t} \nabla_\perp \times \Psi \hat{\mathbf{z}} , \tag{77}$$

$$\delta \mathbf{B}_\perp = \nabla_\perp \times A_z \hat{\mathbf{z}} + \nabla_\perp \partial_z \Psi , \tag{78}$$

and

$$\delta B_z = -\nabla_\perp^2 \Psi , \tag{79}$$

where $\hat{\mathbf{z}}$ is the unit vector along the background magnetic field.

In an ideal MHD plasma, these potentials satisfy the equations

$$\partial_t A_z = -\partial_z \Phi , \tag{80}$$

$$\partial_t^2 \Phi - v_A^2 \partial_z^2 \Phi = 0 , \tag{81}$$

and

$$\partial_t^2 \Psi - v_A^2 \nabla^2 \Psi = 0 . \tag{82}$$

The first of these equations represents the fact that the parallel electric field is zero, while the second and third describe the propagation of the shear Alfvén and fast modes, respectively. The inhomogeneity of the flux tube enters through the Alfvén speed in (81) and (82). In order to simplify the problem to the point where we can find analytic solutions, we shall adopt the simple profile (Greifinger and Greifinger, 1968; Trakhtengertz and Feldstein, 1984)

$$v_A^2 (z) = \frac{v_{A0}^2}{\varepsilon^2 + e^{-z/h}} , \tag{83}$$

where v_{A0} is the Alfvén speed at the ionospheric altitude, h is the ionospheric scale height, and ε is a small parameter. Here it should be recognized that the coordinate z increases in the upward direction, in contrast with our previous discussion in which z was in the direction of the magnetic field. Note that at high altitudes, $z \gg h$, the Alfvén speed simply becomes $v_A = v_{A0}/\varepsilon$. Thus the smallness of the parameter ε represents the fact that the Alfvén speed in the magnetosphere is much larger than that in the ionosphere. Note that while the density profile given by (83) does not take into account the decrease of the Alfvén speed at high altitudes, it does give a reasonable representation of the Alfvén speed profiles in the region above the ionosphere. The system given by (81) with the Alfvén speed profile (83) can be analyzed for its eigenmodes by Fourier transforming in time and in the perpendicular dimensions, leading to the wave equation:

$$\frac{\partial^2 \Phi}{\partial z^2} + \frac{\omega^2}{v_{A0}^2} \left(\varepsilon^2 + e^{-z/h} \right) \Phi = 0 . \tag{84}$$

This equation can be transformed by switching to the independent variable $x = x_0 e^{-z/2h}$, where $x_0 = 2h\omega/v_{A0}$. This transformation leads to the equation:

$$x^2 \frac{d^2\Phi}{dx^2} + x\frac{d\Phi}{dx} + \left(x^2 + x_0^2\varepsilon^2\right)\Phi = 0 \ . \tag{85}$$

This equation can be recognized as being Bessel's equation; however, in this case, the Bessel function solutions have an imaginary order, and the solutions to the wave equation take on the form:

$$\Phi = A^+ J_{ix_0\varepsilon}(x) + A^- J_{-ix_0\varepsilon}(x) \ . \tag{86}$$

It can be shown (Lysak, 1991) that these two solutions correspond to the downgoing and upgoing waves, respectively. Similarly, the solution to (82) with the Alfvén speed profile (83) yields

$$\Psi(x) = \Psi_0 J_{2k_\perp h}(x) \ , \tag{87}$$

where we have assumed $2k_\perp h \gg x_0\varepsilon$ and we have taken only the solution that decreases to zero for increasing altitude, i.e., $x \to 0$. Determination of the eigenfrequencies for these waves requires the application of the boundary condition at the ionosphere. Noting that the field-aligned current can be written as:

$$j_z = \frac{1}{\mu_0}(\nabla \times \mathbf{B})_z = -\frac{1}{\mu_0}\nabla_\perp^2 A_z \ . \tag{88}$$

If we now insert this into the current continuity equation and neglect for the moment the coupling between the shear and fast waves due to the Hall conductivity, the ionospheric boundary condition becomes:

$$\nabla_\perp^2 (A_z + \mu_0\Sigma_P\Phi) = 0 \ . \tag{89}$$

The Fourier transform in time of Equation (80) implies that:

$$A_z = -\frac{i}{\omega}\frac{\partial\Phi}{\partial z} = \frac{i}{v_{A0}}\frac{x}{x_0}\Phi' \ , \tag{90}$$

where $\Phi' = d\Phi/dx$. Evaluating the condition (89) at the ionosphere, which corresponds to $x = x_0$, we can write:

$$i\Phi' + \alpha_P\Phi = 0 \ , \tag{91}$$

where $\alpha_P = \Sigma_P/\Sigma_{AI}$ measures the Pedersen conductivity in units of the Alfvén conductivity at the ionosphere. The boundary condition (91) can be considered to be an eigenvalue equation for the parameter x_0, which is essentially the mode frequency scaled by the fundamental frequency in the problem, which is $V_{AI}/2h$. The upper boundary condition can be taken to be a radiation boundary condition, which picks out the $J_{ix_0\varepsilon}$ solution for inward propagating waves and the $J_{-ix_0\varepsilon}$ solution for outward propagating waves. It can be easily seen that the solutions are parameterized by ε, which is always much smaller than one, and α_P, which may be small or large. Detailed solutions of the eigenvalue Equation (91) have been presented in Lysak (1991). For these solutions, the outgoing wave is always damped,

and has its maximum damping at $\alpha_P \sim 1$, which is the point where the Pedersen conductance is best matched to the impedance of the Alfvén wave. The incoming wave can have a positive growth rate, but this solution is somewhat spurious due to the fact that this wave assumes an energy source for the incoming wave. The eigenmodes of this equation have the property that the normalized wave frequency x_0 has a value given by the zeroes of the Bessel function J_1 at low conductivity, and by the zeroes of the Bessel function J_0 at high conductivity. A number of improvements have been made to the simple model presented here. Lysak (1993) has presented numerical solutions for a more general Alfvén speed profile, and shown that the basic structure of the waves remains the same. More recently, Pokhotelov *et al.* (1999) have included the Hall coupling to the compressional mode. This modification changes the dispersion relation (91) to read

$$i\Phi' + \left(\alpha_P - i\frac{x_0\alpha_H^2}{4k_\perp h}\right)\Phi = 0 \,. \tag{92}$$

However, due to the large value of $k_\perp$ for typical parameters, this inclusion does not change the basic conclusions presented above.

4.2.3. *Ionospheric Feedback Instability*

Up until now, we have assumed that the ionospheric conductivity was held fixed in time and was independent of the field-aligned current. On the dayside of the ionosphere, where the conductivity is primarily produced by the impact of solar ultraviolet radiation, this may be a reasonable assumption; on the other hand, the nightside conductivity is closely connected to the precipitation energy flux. Thus, especially at night, the conductivity may be closely connected to the precipitation and thus to the field-aligned currents. If these currents are inhomogeneous, the precipitation can give rise to conductivity gradients, which, by current continuity, may then require closure by field-aligned currents. Thus the possibility of feedback between the currents and the conductivity gradients may arise. The feedback instability can be analyzed by noting that the Pedersen and Hall conductivities are simply proportional to the ionospheric plasma density (see, e.g., Kelley, 1989, for a detailed discussion of the ionospheric conductivity). The plasma density itself must evolve according to the continuity equation:

$$\left(\frac{\partial}{\partial t} + \mathbf{v} \cdot \nabla\right) n = S - R\left(n^2 - n_0^2\right) \,, \tag{93}$$

where n_0 represents the equilibrium density due to the solar radiation, R is the recombination coefficient, which is the order of 2×10^{-7} cm^3 s^{-1} (e.g., Brown, 1966), and S is the source term due to the precipitation. Note that the recombination goes as the square of the density since an electron and ion must meet to recombine. The source term S depends, again to lowest order, on the energy flux of the precipitating electrons (Rees, 1963) and corresponds roughly to a value $S = F/(H \times 35 \,\text{eV})$, where F is the energy flux and H is the effective height of

the ionosphere. This dependence of the conductivity on the precipitating electrons can give rise to an instability by the following scenario. Consider a perturbation in the ionospheric conductivity, for example, a localized enhancement, in the presence of a background electric field. In this case, the electric field must either be reduced or the current increased as a result of the larger conductivity. If the current is increased, this enhanced current must close by means of a field–aligned current. Depending on the response of the magnetosphere to this field-aligned current, which is associated with an upward propagating Alfvén wave, this interaction can go unstable, causing the conductivity perturbation to grow. We can analyze this instability by considering the source for the ionospheric density to be proportional to the field–aligned current, which can in turn be expressed in terms of the vector potential. When we add the conductivity gradients as in equation to the ionospheric boundary condition as expressed in terms of the potentials by (89), we find:

$$\nabla_\perp^2 \left(\mu_0 A_z + \Sigma_{P0} \Phi \right) = \Sigma_{P0} \mathbf{E}_0 \cdot \nabla_\perp \frac{\delta n}{n_0} + \Sigma_{H0} \hat{\mathbf{z}} \cdot \left(\mathbf{E}_0 \times \nabla_\perp \frac{\delta n}{n_0} \right) . \tag{84}$$

Similarly, we can express the linearized continuity equation for the ionospheric density as

$$-i \left(\omega - \mathbf{k}_\perp \cdot \mathbf{v}_0 + 2i R n_0 \right) \delta n = \mu_0 Q k_\perp^2 A_z . \tag{95}$$

Eliminating the density perturbation by combining (94) and (95) yields the boundary condition in terms of the potentials:

$$\left[1 - \frac{(Q/n_0) \left(\Sigma_{P0} \mathbf{k}_\perp + \Sigma_{H0} \mathbf{k}_\perp \times \hat{\mathbf{z}} \right) \cdot \mathbf{E}_0}{\omega - \mathbf{k}_\perp \cdot \mathbf{v}_0 + 2i R n_0} \right] A_z + \mu_0 \Sigma_{P0} \Phi = 0 . \tag{96}$$

Note that if the second term in the brackets is set to zero, we recover the original boundary condition (89). We may note that Equation (96) still does not say anything about the resonant cavity; this equation simply expresses the boundary condition in terms of the potentials. Following the discussion of the preceding subsection, we can write this condition in the presence of the potentials as

$$i \left(1 - \frac{\sigma}{x_0 + i\nu} \right) \Phi' + \left(\alpha_P - i \frac{x_0 \alpha_H^2}{4 k_\perp h} \right) \Phi = 0 , \tag{97}$$

where σ is the dimensionless source term:

$$\sigma = \frac{2hQ}{n_0 V_{AI}} \left(\Sigma_{P0} \mathbf{k}_\perp + \Sigma_{H0} \mathbf{k}_\perp \times \hat{\mathbf{z}} \right) \cdot \mathbf{E}_0 \tag{98}$$

and ν is the dimensionless recombination damping rate:

$$\nu = \frac{4h R n_0}{V_{AI}} . \tag{99}$$

It is interesting to note that the source term σ can be written $\sigma = (2h/V_{AI}) \mathbf{k}_\perp \cdot \mathbf{v}_{\text{eff}}$, where the effective velocity is $\mathbf{v}_{\text{eff}} = Q \left(P \mathbf{E}_0 + H \hat{\mathbf{z}} \times \mathbf{E}_0 \right)$. Recalling that $Q =$

$\gamma/(eH)$, it can be seen that for $\gamma = 1$, this effective velocity is just the relative perpendicular drift velocity between the ions and electrons, $\mathbf{v}_{eff} = \mathbf{j}_\perp /(n_0 e)$. Of course, in the limit of energetic electron precipitation where $\gamma > 1$, this effective velocity is increased by the factor γ. The numerical solution of (97) has been analyzed by Lysak (1991) for the case when the Hall coupling term is absent. These results showed that, as a function of α_P, the value of σ for maximum growth increases roughly linearly for large α_P. In addition, it may be seen that for small values of α_P, the most unstable wave occurs for $x_0 = \sigma$, or $\omega = \mathbf{k}_\perp \cdot \mathbf{v}_{eff}$, so that the unstable wave propagates at the phase velocity $\mathbf{v}_{eff}$. At higher values of α, however, the wave frequency becomes nearly constant at a value $x_0 = 3.2$ for $\varepsilon = 0.1$ and scaled growth rate $\eta \simeq 0.4$. These values are weak functions of ε. In this regime, the phase velocity is reduced since the wavelength decreases while the frequency remains constant. Thus, for small conductivity, we have a wave with a fast phase velocity, approaching v_{eff}, while for higher conductivity, the instability can have a smaller wavelength. The more general results have been considered by Pokhotelov *et al.* (1999). Just as in the large-scale case, this instability becomes unstable when the magnetospheric response becomes inductive rather than capacitive. This can be illustrated by considering the phase shift between Φ and A_z. A positive phase shift corresponds to an inductive response in this case. It has been shown (Lysak, 1991) that the phase shift at the ionosphere goes through zero when the growth rate of the instability goes through zero; therefore, the physics of this instability is essentially the same as for the global field-aligned modes described by Sato (1978). The major difference is that the growth rate of the instability now scales with $V_{AI}/2h$, which is the order of 1 Hz, rather than with the travel time to the conjugate ionosphere, which is more like periods of a few minutes. Thus the feedback instability based on the ionospheric resonant cavity is much faster than that based on the whole field line.

4.3. FIELD LINE RESONANCE BY A. STRELTSOV

The concept of field line resonance (FLR) involves excitation of standing shear Alfvén waves along geomagnetic field lines between northern and southern ionospheres. This resonant excitation occurs on the magnetic L shell where the frequency of some externally or internally driven geomagnetic oscillations matches one of the field line eigenfrequencies. Here the energy from the 'driver' is absorbed by the standing shear Alfvén wave, and as time proceeds the amplitude of this wave can reach significant magnitude.

Ultra-low-frequency (1–100 mHz) Alfvén waves standing on auroral field lines have been investigated for more than 30 years (Radoski, 1967; Cummings *et al.*, 1969) to explain low-frequency geomagnetic pulsations in Pc5–Pc6 range measured by ground-based magnetometers and HF radars in the auroral zone (Ruohoniemi *et al.*, 1991; Walker *et al.*, 1992; Samson *et al.*, 1996). Recently the interest in FLR's at high latitudes has increased significantly with new measurements

providing a good correlation between FLR's and the occurrence of small-scale, discrete auroral arcs (Samson *et al.*, 1991, 1996; Xu *et al.*, 1993; Lotko *et al.*, 1998). Although a theory of auroral structures at transverse spatial scales of the order of 10–100 km is now fairly well developed (Lysak, 1990; and Lyons, 1990, and references therein), the understanding of the formation and evolution of small-scale structures (from 10 km down to 100 m scales), including discrete auroral arcs, remains incomplete.

Small-scale, discrete auroral arcs are produced by sheet-like fluxes of precipitating electrons with energies from 100 eV up to tens of keV (McFadden *et al.*, 1986; Newell *et al.*, 1996). Direct measurements from satellites (Kletzing *et al.*, 1983; Chmyrev *et al.*, 1988; Karlsson and Marklund, 1996) and rockets (Boehm *et al.*, 1990) have shown that the discrete fluxes of keV electrons registered at the auroral zone are often correlated with small-scale, localized electromagnetic disturbances sometimes interpreted as dispersive/oblique Alfvén waves. This correlation arises naturally from dispersive Alfvén waves, which have a component of the electric field parallel to the ambient magnetic field and which can, therefore, accelerate electrons into the ionosphere (Hasegawa, 1976; Goertz and Boswell, 1979).

To explain discrete auroral arcs and other small-scale electromagnetic auroral phenomena in terms of dispersive Alfvén waves the question of how shear Alfvén waves with small transverse scales are generated must be answered. Of related interest are the conditions that allow Alfvén waves with a period in the range of 10–1000 s to produce extremely narrow and intense electric fields and currents. Auroral structures are typically on the order of or less than 1 km wide in the north-south direction and extended up to 1000 km in the east-west direction (referenced to 100 km height).

There are at least three different ways of generating shear Alfvén waves on auroral field lines. One is wave-wave or mode coupling interactions in the equatorial magnetosphere including coupling between a shear wave and an externally driven compressional wave (Chen and Hasegawa, 1974; Southwood, 1974), or coupling between a shear wave and a large-scale MHD surface wave, attached to an isolated transverse gradient in the background Alfvén speed (Hasegawa, 1976; Goertz, 1984). Large-scale compressional and incompressional surface waves can be produced by substorm activity in the central plasma sheet of the magnetotail, or by the interaction between pressure/density/magnetic field irregularities in the solar wind and the magnetosphere of the Earth. External oscillations with a broadbanded spectrum are expected to produce continuous FLRs broadly distributed across geomagnetic *L* shells (Anderson *et al.*, 1990), whereas narrowband geomagnetic oscillations will produce discrete, isolated FLRs, localized near one particular *L* shell (Greenwald and Walker, 1980).

Another possible mechanism for excitation of Alfvén waves is the onset of an internal plasma instability such as the drift mirror and drift Alfvén ballooning mirror instabilities (Pokhotelov *et al.*, 1986; Chen and Hasegawa, 1991). This mechanism is based on the fact that the periods of ULF Alfvén waves are compat-

ible with the timescale of particle bounce motion along auroral field lines, which allow the wave to efficiently absorb energy from bouncing particles. An important distinction between FLRs excited by wave-wave interactions and those excited by wave-particle interactions is the difference in the azimuthal wave number of the resonant Alfvén wave. Efficient coupling between shear and compressible or surface modes requires small but finite azimuthal wave number (say $m \leq 10$) (Kivelson and Southwood, 1986; Hasegawa, 1976; Streltsov and Lotko, 1995). Resonant energy exchange between Alfvén waves and bouncing magnetospheric protons requires $m \gg 1$. Standing Alfvén waves with low m form so-called 'toroidal' FLRs; Alfvén waves with large m form so-called 'poloidal' FLRs. The fine structure and various spatio-temporal properties of poloidal resonances was investigated analytically in a series of papers by Leonovitch and Mazur (see Leonovitch and Mazur, 1999, for references).

Sato (1978) shows that shear Alfvén waves on the auroral field lines can also be excited by the ionospheric density enhancements, drifting perpendicular to the geomagnetic field in the large-scale perpendicular electric field. This so-called 'ionospheric feedback' mechanism was investigated numerically in the context of the auroral arc formation by Watanabe *et al.* (1993). Lysak (1991) shows that the same feedback mechanism plays an important role for the excitation of 0.1–1 Hz resonance oscillations at low altitudes, in the so-called ionospheric Alfvén resonator (Polyakov and Rapoport, 1981) discussed in the previous section.

To answer the question of how shear Alfvén waves can develop subkilometer transverse scales, the fine structure of toroidal FLR layers produced by monochromatic drivers on geomagnetic field lines passing through the inner edge of the nightside plasma sheet, about $L = 7-8$, was investigated by Streltsov *et al.* (1998). Interest in this particular magnetospheric region is motivated by the fact that: (1) it maps along dipolar magnetic field lines to the ionosphere near 70° geomagnetic latitude, where large-amplitude, small-scale transverse electric fields are predominantly measured by low-altitude satellites (Bennett *et al.*, 1983; Chmyrev *et al.*, 1988; Karlsson and Marklund, 1996); (2) small-scale, discrete auroral arcs are optically observed from the ground (Xu *et al.*, 1993; Trondsen *et al.*, 1997); (3) a statistical survey of magnetospheric ULF waves by Zhu and Kivelson (1991) has shown that dominantly toroidal magnetic oscillations with characteristics indicative of fundamental or odd harmonic FLRs are most intense near the inner edge of the premidnight plasma sheet; (4) FLRs should result in conjugate aurora which have been observed in this region of the plasma sheet (Belon *et al.*, 1969).

The analysis by Streltsov *et al.* (1998) is based on the linear, reduced, two-fluid MHD model, derived in the dipole magnetic field geometry, under the assumptions that: (1) the wave frequency, ω, is much smaller than the ion cyclotron frequency ω_{ci}; (2) the wavelength of the resonant oscillations along the field line is much larger then the wavelength across the field; and (3) the plasma is relatively cool: i.e., the plasma $\beta \ll 1$. This model can be considered as the simplest in a family of nonlinear, fluid-kinetic models developed to describe dispersive ULF waves in

space plasma (Shukla and Stenflo, 1995; Cheng and Johnson, 1999) as well as in the laboratory plasma (Hazeltine *et al.*, 1987). In the two-dimensional form the model includes: the electron parallel momentum equation (linearized parallel component of Equation (4)), the density continuity equation (linearized Equation (5)), and the current continuity equation combined with the ion momentum equation:

$$(1 - \rho_i^2 \nabla_\perp^2) \nabla \cdot J_\parallel \hat{\mathbf{b}} + \epsilon_0 \nabla \cdot \left[\frac{c^2}{v_A^2} + 1 - \rho_i^2 \nabla_\perp^2 \right] \frac{\partial \mathbf{E}_\perp}{\partial t} = 0 \,, \tag{100}$$

here $\hat{\mathbf{b}} = \mathbf{B}_0/B_0$ and $J_\parallel = -(1/\mu_0) \nabla_\perp^2 A_z$ is the parallel current.

Equation (100) includes the displacement current, important when the Alfvén speed approaches the speed of light, and full ion Larmor radius correction making the model applicable even for waves with $\rho_i^2 k_\perp^2 \geq 1$. This correction comes from the kinetic treatment of the perpendicular ion motion and is not included in the classical one- or two-fluid MHD models. Formally Equation (100) contains the finite Larmor radius correction to the displacement current (term $-\rho_i^2 \nabla_\perp^2$ in the square brackets), however, analysis of the magnetospheric parameters along auroral field lines demonstrates that this term is not significant for the problem considered here since $c^2/v_A^2 \gg \rho_i^2 \nabla_\perp^2$ everywhere in the auroral flux tube. So usually in the magnetospheric applications this term is ignored (Streltsov *et al.*, 1998; Streltsov and Lotko, 1999). Dispersion relations based on this model in different parts of the auroral flux tube are identical to those given in Sections 2.1 and 2.3.

Due to the intrinsic inhomogeneity of the magnetospheric parameters transverse to the geomagnetic field lines, a monochromatic driver should excite standing Alfvén waves on a single L shell. In the ideal one-fluid MHD, the one-fluid resonant solution has a singularity at the resonance point (Southwood, 1974; Chen and Hasegawa, 1974a). This singularity can be resolved when various nonlinear or dispersive effects arise. Some possibilities include ionospheric dissipation (Newton *et al.*, 1978; Walker, 1980), the onset of an anomalous resistivity at the location where the Alfvén wave current becomes supercritical (Streltsov and Lotko, 1999), various nonlinear effects, e.g., density redistribution along the resonant field line due to the wave ponderomotive force (Rankin *et al.*, 1995; Voronkov *et al.*, 1997) and dispersive effects.

In the absence of significant nonlinearity and dissipation, the effective transverse scale size of a monochromatically driven resonant oscillation decreases as time proceeds until wave dispersion becomes important. As noted in Section 2 the dispersion modifies the properties of an ideal Alfvén wave in two ways: (a) it causes a parallel electric field in the small-scale Alfvén wave which can accelerate electrons into the ionosphere, leading in some cases to auroral arcs, and (b) it also enables a perpendicular component of the wave group velocity, allowing energy carried by dispersive Alfvén waves to propagate across the field lines away from the resonance layer. This radiative mechanism can saturate the growth in amplitude of the resonant oscillation and limit the contraction of its transverse size. The impor-

tance of the transverse propagation of dispersive Alfvén waves from the resonance surface for the FLR dynamics was emphasized by Bellan (1994, 1996a).

The dispersion of small-scale Alfvén waves is defined by the finite electron mass (inertial dispersion) at low-altitude magnetosphere ($v_A > v_{Te}$) and finite plasma temperature (kinetic dispersion) at the equatorial magnetosphere ($v_A < v_{Te}$). Formally, the location of the dispersion transition point between the inertial and kinetic limits of the Alfvén wave occurs where $\lambda_e^2 = \rho_s^2 + \rho_i^2$ (Streltsov et al., 1998). An important difference between these two types of dispersion is that the transverse group velocity of a kinetic Alfvén wave is opposite to that of an inertial Alfvén wave. Thus an oblique wave propagating toward higher L shells near the equator, for example, will begin moving toward lower L shells after passing through the transition region.

Because the inertial dispersion dominates over a larger portion of the field line on the lower magnetic L shells and kinetic dispersion dominates over larger portion of the field line on higher magnetic L shells, it is reasonable to assume that there exists an L shell where the transverse propagation of the oblique wave in the low-altitude inertial region is exactly compensated by the opposite propagation in the high-altitude kinetic region. On a such L shell the ray pattern of the dispersive wave forms a closed loop in its transit between the ionospheres (Figure 29), and hence the wave remains confined to the resonance layer. When this occurs, the dispersive FLR is termed 'nonradiative', and it can reach significantly larger amplitude and contract to much smaller transverse scale than FLRs radiating dispersive Alfvén waves. The basic concept of the nonradiative dispersive FLRs was formulated for the first time by Streltsov and Lotko (1995), and the fine structure of such resonances was investigated numerically in the series of papers by the same authors (see Streltsov et al. 1998 for references).

Their analysis shows that in the absence of dissipation, nonradiative FLR can produce dispersive Alfvén waves with transverse scales less than 1 km at 100 km altitude (Streltsov et al., 1998). The parallel electric field of the small-scale Alfvén wave can produce a 1 kV potential drop along the resonance field line between the ionosphere and ≈ 3–$4~R_E$ altitude, if the maximum amplitude of the corresponding perpendicular electric field is set equal to $200~\text{mV m}^{-1}$, which is a typical amplitude of small-scale electric fields registered in the low-altitude auroral magnetosphere (Weimer and Gurnett, 1993). As an example, the snapshots of the toroidal electric field, E_L, poloidal magnetic field, B_φ, parallel electric field, E_μ, and parallel current density, J_μ, of the fundamental FLR are shown in Figure 30.

The same physical model of the Alfvénic toroidal FLR including the effect of plasma micro-turbulence (anomalous resistivity) in the form suggested by Lysak and Dum (1983), was used to model the data measured by the FAST satellite in the nightside auroral magnetosphere (Streltsov and Lotko, 1999). Results from this numerical experiment are shown in Figure 31 with thick curves. The east-west magnetic field, north-south electric field, particle energy fluxes, and parallel current, measured by FAST crossing a discrete auroral arc in the nightside mag-
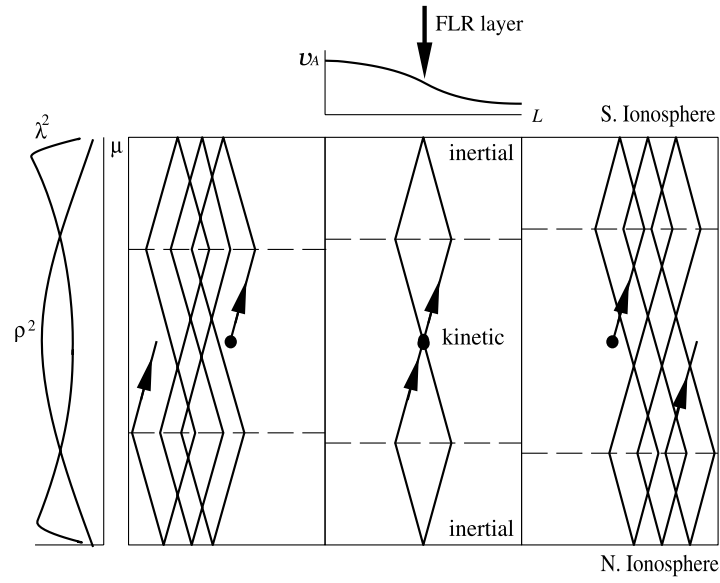
Figure 29. Schematic plot of the ray trajectories for the dispersive Alfvén wave between the ionospheres.
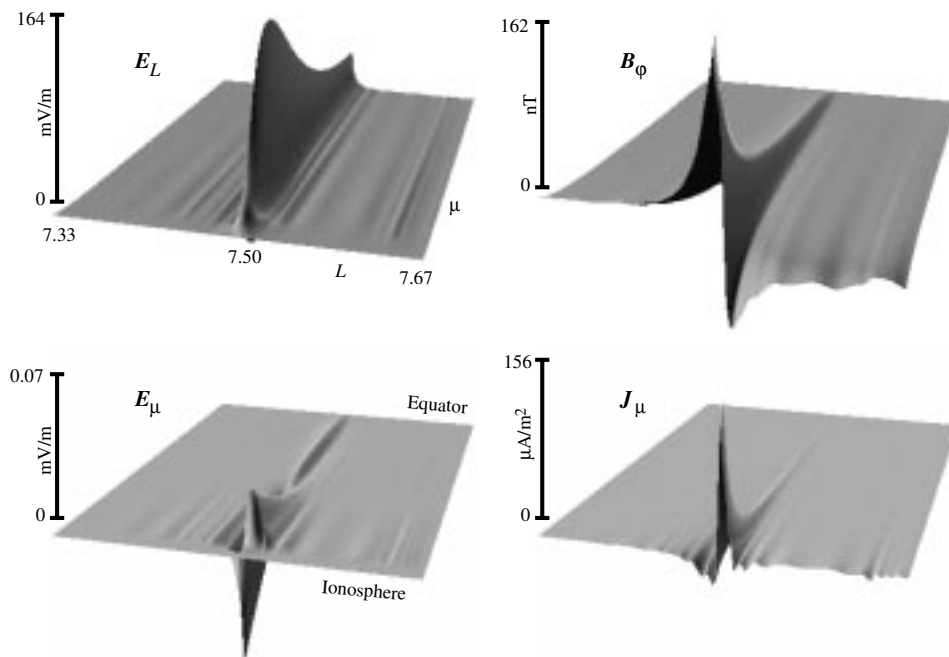
Figure 30. Snapshots of fields and currents in the fundamental, nonradiative FLR on $L = 7.5$ magnetic shell. (After Streltsov *et al.*, 1998.)
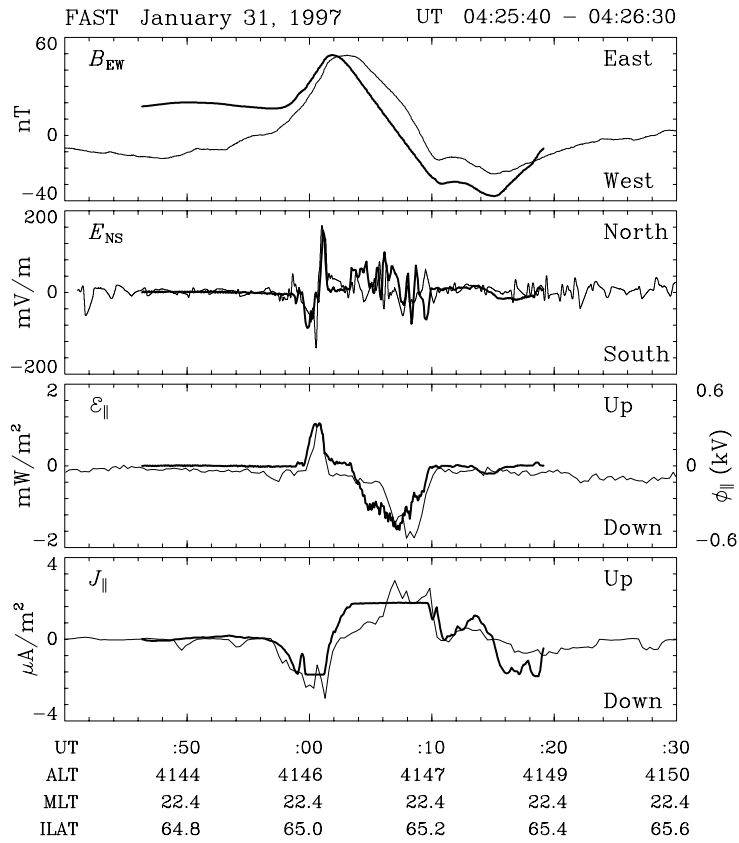
Figure 31. Comparison between FAST data (thin curves) and simulated data (thick curves) from a virtual satellite crossing numerical FLR modeled in the plasma with anomalous resistivity.

netosphere are shown in Figure 31 with thin curves. Parameters of the numerical (virtual) satellite trajectory, speed, and altitude are set to match exactly the real ones. The whole assembly of different observations by all-sky camera, magnetometers, radars, and meridional scanning photometers, performed at the same time on the ground, confirms the main features of the toroidal FLR associated with this particular FAST event (Lotko *et al.*, 1998).

Summarizing the results presented in this section we can say that the theory of small-scale toroidal Alfvénic FLRs can provides a fairly comprehensive, self-consistent explanation for a large set of electromagnetic phenomena occurring in the auroral region. These phenomena include: small-scale electric fields and currents, measured by polar orbiting satellites in the lower magnetosphere; bright, discrete auroral arcs, optically observed from the ground at the bottom of the auroral ionosphere; and magnetic pulsations in Pc3–Pc5 ranges, measured by magnetometers on the ground.

5. Advanced Models and Simulations

5.1. NONLINEAR PLANE WAVES

5.1.1. *Steady State Nonlinear Waves*

In this section we will derive nonlinear one-dimensional plane wave solutions of the Alfvén wave equations. Starting from the basic two fluid equations (4)–(7), we invoke several simplifying assumptions. First assume the existence of a strong constant applied magnetic field oriented along the z-axis and consider plane wave propagation nearly perpendicular to the applied field. The angle of propagation is taken to be of the order $\epsilon = \sqrt{m_e/m_i}$. The waves we consider have frequencies much less than the lower hybrid frequency. The electrons are assumed to predominantly carry the parallel current and the parallel ion flow is neglected.

The equations for the shear Alfvén wave in which the y coordinate is ignorable are found from (4)–(7) to be the following:

$$\frac{\partial n}{\partial t} + \frac{\partial}{\partial z}(nu_{ez}) = 0 \,, \tag{101}$$

$$\frac{\partial u_{ez}}{\partial t} + u_{ez}\frac{\partial u_{ez}}{\partial z} = -\frac{e}{m_e}E_z - \frac{T_e}{m_e n}\frac{\partial n}{\partial z} \,, \tag{102}$$

$$\frac{\partial B_y}{\partial t} = \frac{\partial E_z}{\partial x} - \frac{\partial E_x}{\partial z} \,, \tag{103}$$

$$\frac{\partial B_y}{\partial x} = -e\mu_0 n u_{ez} \,, \tag{104}$$

$$\frac{\partial u_{iy}}{\partial t} + u_{ix}\frac{\partial u_{iy}}{\partial x} = -\Omega_i u_{ix} \,, \tag{105}$$

$$\frac{e}{m_i}\left(E_x + u_{iy}B_0\right) - \frac{T_i}{m_i n}\frac{\partial n}{\partial x} = 0 \,, \tag{106}$$

$$\frac{\partial}{\partial x}(nu_{ix}) - \frac{\partial}{\partial z}(nu_{ez}) = 0 \,. \tag{107}$$

Equation (106) is the low frequency drift approximation for u_{iy}. This model was investigated by Seyler *et al.* (1995).

We now restrict consideration to one-dimensional oblique propagation in which $\partial_z = \vartheta\,\partial_x$ to eliminate the z derivatives in terms of the x derivatives and then use the quasineutrality condition (107). It can be verified that the low-frequency linear dispersion relation of (101)–(107) is given by (40) for $T_e = 0$.

From (101)–(107) a one-dimensional equation for nonlinear steady state waves is found to be

$$\frac{\mathrm{d}}{\mathrm{d}x}\left\{\left[\frac{1}{N^3} - \frac{\theta^2 c_s^2}{v^2 N}\right]\frac{\mathrm{d}N}{\mathrm{d}x}\right\} + \left(\frac{\theta^2 \Omega_i^2}{v^2} - \frac{1}{\lambda_e^2}\right)(N-1) = 0\,, \tag{108}$$

where $N = n/n_0$, $\theta = \sqrt{m_i/m_e}\vartheta$, $c_s^2 = (T_e + T_i)/m_i$, and v is the x velocity of the wave. A first integral to Equation (108) is obtained as

$$\left(\frac{\mathrm{d}N}{\mathrm{d}x}\right)^2 = \left(\frac{1}{\lambda_e^2} - \frac{\theta^2 \Omega_i^2}{v^2}\right) \times$$
$$\times \frac{N^4}{(1-\alpha N^2)^2}\left[(N-1)^2 - 2\alpha N^2(N-1) + 2\alpha N^2\,\ln N\right]\,, \tag{109}$$

where $\alpha \equiv \theta^2 c_s^2/v^2$. Equation (109) was derived in Seyler *et al.* (1995) as Equation (42) which was expressed in terms the x velocity. Related equations have been discussed by Temerin *et al.* (1979), Lee (1981) and Chang (1982) in the context of electrostatic ion cyclotron waves. It was shown in Seyler *et al.* (1995) that (109) does not possess any non-singular solitary wave solutions. In addition, it can be shown that if one ignores the $u_{ix}\partial_x u_{iy}$ term in (105) as has been done in previous calculations, one does find solitary wave solutions having a density cavity. Thus reports of solitary wave solutions that have appeared in the literature would appear to be in question since the model of Seyler *et al.* (1995) retains more physics than previous calculations. There is an open issue on whether or not the nonlinear ion polarization drift retained by Seyler *et al.* (1995) is of higher order than the linear polarization drift and thus it should not be included. This issue will have to be settled elsewhere.

5.1.2. *Time-Dependent Nonlinear Oblique Waves*

Alfvén waves that are bounded in one or both of the transverse dimensions have a parallel current. If the wave exhibits some degree of symmetry in one of these dimensions then it forms either a static or a dynamic current sheet. A static current sheet is an equilibrium in which the electric and magnetic fields are constant in time whereas a dynamic current sheet, often referred to as an Alfvén wing, has oblique symmetry and a transverse group velocity. The static current sheet is simply the $v_{g\perp} = 0$ limit of the Alfvén wing. These structures can be formed by an electric or magnetic perturbation created at some altitude which drifts relative to the magnetic field. The resulting Alfvénic disturbance propagates to a higher or lower altitude as an Alfvén wing.

The Alfvén wing differs from an Alfvénic auroral arcs such as those considered by Lysak and Dum (1983), Lysak (1985), Seyler (1988,1990), in that ionospheric and magnetospheric boundary conditions play an essential role in the formation of Alfvénic arcs, whereas Alfvén wings propagate as unbounded waves. This situation occurs when the transverse group velocity of the oblique Alfvén wave is sufficiently fast so that the reflection of the wave from the ionospheric and magnetospheric boundaries does not interfere with the propagating Alfvén wave. An Alfvénic cavity in which density gradients trap an Alfvén wave is an example

of multiple internal reflections of an Alfvén wave. Models based upon Alfvénic cavities have been proposed by Mishin and Förster (1995), Lysak (1991), Bellan and Stasiewicz (1998). An Alfvén wing incident upon a density cavity may form an Alfvénic cavity but it should be clear that an Alfvén wing is a distinctly different structure.

The Alfvén wing is the basic Alfvénic structure considered in the dynamical models of Seyler *et al.* (1995); Seyler and Wahlund (1996); Seyler *et al.* (1998); Clark and Seyler (1999). In these models it was presumed that an oblique inertial Alfvén wave propagates in a homogeneous plasma and that all the structural morphology and particle acceleration associated with observed Alfvénic structures arises from nonlinear processes, most prominently nonlinear steepening. The basic theoretical results of the Alfvén wing models will be reviewed and a discussion of the comparison to observations will be deferred to the original references.

The essential result of Seyler *et al.* (1995) was that large amplitude initial conditions of a linear oblique Alfvén wave eigenmode nonlinearly steepens and generates a negative voltage spike very similar in amplitude and spatial scale to those observed in SKAW detected by *Freja*. The origin of the spike was determined to be the ion thermal response of the plasma to density steepening.

Seyler and Wahlund (1996) investigated the ion response in more detail by considering the electrostatic limit of the Alfvén wave. They found that there existed a class of acoustic-like waves whose importance had been largely overlooked since their discovery by Stringer (1963). These waves were called slow ion acoustic (SIA) waves by the authors due to their relatively slow transverse phase velocity. A more appropriate terminology for these waves is electron acoustic since it expresses the fact that the transverse phase speed is related to the effective transverse mass of the electrons at the ion temperature. The dispersion relation for electron acoustic waves is found from (38) in the limit of small electron temperature and $k_\perp^2 \rho_i^2 \sim 1$.

Electron acoustic waves exist for propagation angles for which $k_\parallel/k_\perp < \sqrt{m_e/m_i}$ which is the same range for Alfvén waves. Nonlinear two-fluid simulations revealed that the SIA waves are emitted from sufficiently large amplitude initial conditions for inertial electrostatic Alfvén waves. The waves were found to be emitted at the Debye scale.

The transition from an ion polarization to an ion Boltzmann density response which occurs at $k_\perp \rho_i = 1$ is the main characteristic of electron acoustic waves. Electron acoustic/SIA waves can be identified by their ion-Boltzmann response in experimental data. They were in fact identified in the data for which it was determined that the ions were much hotter than the electrons. Seyler and Wahlund (1996) stated that this was to be expected since the waves would be strongly damped by parallel electron Landau damping unless their parallel phase speed significantly exceeded the electron thermal speed. This requires a temperature ratio $T_i/T_e \gg 1$. It was pointed out somewhat later and independently by Lysak and Lotko (1996) that increasing ion temperature reduced the damping of inertial Alfvén waves which exist along the same dispersion branch as the SIA waves at

higher wavenumbers such that $k_\perp \rho_i > 1$. These results are easily verified from (38).

Seyler *et al.* (1998) introduced a model in which ion kinetic effects could be included in a linear context. They argued that the dominant nonlinear effects were due to electrons, so that a linear Vlasov ion model was justified. The essential results from their fluid-kinetic simulations are that SIA waves are emitted at a scale that is not the Debye length as reported by Seyler and Wahlund (1996) but rather the scale given by $k_\perp \rho_i = 1/\theta$ where θ is the reduced angle of propagation $\theta = \sqrt{m_i/m_e}\, k_\parallel / k_\perp$. The SIA wave emission introduced intricate structure into the nonlinearly steepened and evolving inertial Alfvén wave. The authors argued that this structure gave much better qualitative and quantitative agreement with observed SKAW morphology.

Seyler *et al.* (1998) also elaborated on the kinetic theory of the waves of interest. They showed how the ion Boltzmann response emerged from a kinetic treatment and how parallel electron Landau damping of electron acoustic waves is mitigated by a large T_i/T_e ratio. They also offered an explanation of the origin of the broadband ELF waves that are always associated with Alfvénic structures as the result of wave emission due to nonlinear steepening. This is an important and unresolved issue since it has been established that ion heating and the bulk of ion outflow are associated with BB-ELF waves.

The manner in which electron acoustic/SIA waves are excited is open to debate. Emission by nonlinear steepening is only one of several possible mechanisms and not necessarily the most likely. Other possible excitation mechanisms include modulational instability (Shukla *et al.*, 1999), shear induced instability (Gavrishchaka *et al.*, 1996), magnetic tearing (Seyler, 1990) or some form of turbulent decay of DAW (Stasiewicz *et al.*, 2000a).

5.2. ELECTRON ACCELERATION BY ALFVÉN WAVES

Various proposed electron acceleration mechanisms include turbulence and anomalous resistivity related phenomena associated Alfvén waves, (Lysak and Carlson, 1981; Lysak and Dum, 1983; Stasiewicz, 1985a, b); by electromagnetic ion cyclotron waves (Temerin and Lysak, 1984); by linear Alfvén waves (Goertz and Boswell, 1979; Haerendel, 1983; Kletzing, 1994); by nonlinear Alfvén wave evolution (Seyler, 1990; Hui and Seyler, 1992; Nakamura and Tamao, 1989); and Alfvén wave resonances (Stasiewicz *et al.*, 1997; Streltsov and Lotko, 1995). However, these models, as is clear from much of this review, have usually concentrated on finding electric and magnetic field solutions. We review here those models which have explicitly shown the form of electron acceleration which results from Alfvén waves.
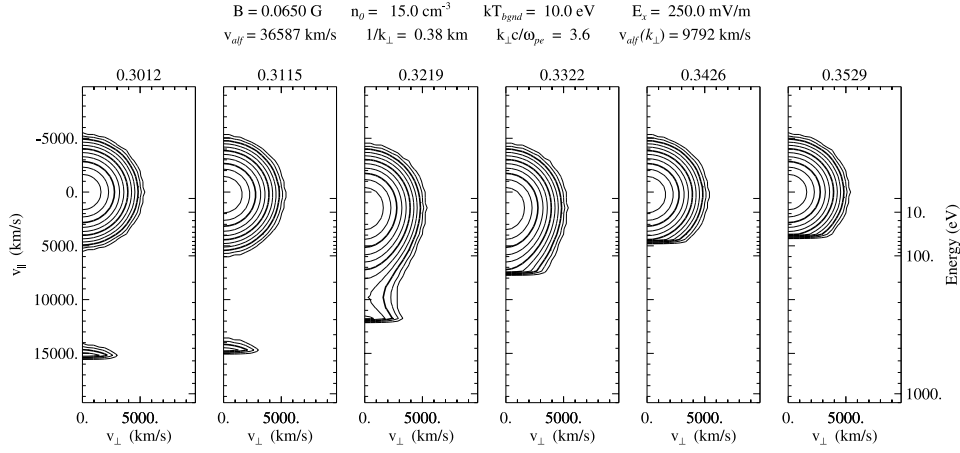
Figure 32. Time series showing the evolution of the distribution function as the 'wavefront' of the shear Alfvén wave propagates past the observation point. The panels are equidistant in time, with the first corresponding to just before the wave reaches the observation point and the last corresponding to just after the wave has passed the observation point.

5.2.1. *Linear Resonant Acceleration*

Kletzing (1994) has shown how Alfvén waves can modify the electron distribution function by resonantly accelerating a small portion of the background electrons to velocities of the order of twice the Alfvén speed. For high latitude regions this is usually a modest acceleration to energies of 0.6–1.0 keV – an often observed energy range for electrons associated with boundary processes.

Figure 32 shows a series of six panels which are snapshots of the distribution function at a single observation point as a function of time. The panels show how the distribution changes as an Alfvén wave pulse propagates past the observation point. The first panel shows the distribution just before the pulse arrives at the observation point, and the last panel shows the distribution just after the wave has passed. The middle four panels show the distribution as the wave field is passing the observation point. The plasma and wave parameters, given at the top of the figure, have been selected to represent an altitude of 7000 km in the auroral zone.

There are two features to notice. The first is the relatively small acceleration of the background distribution to an energy of about 10 eV and the subsequent deceleration of the background back to 0 eV. This is just the bulk plasma response to the bipolar parallel electric field of the Alfvén pulse; the acceleration is first in one direction and then the other. This bulk motion is just the required parallel current which, as is assumed in the derivation of the wave properties, is carried by the electrons.

Once the wave has passed, the distribution has essentially no net acceleration. The entire acceleration and deceleration process takes place in less than 50 ms.

The more interesting phenomenon involves the small bunch of electrons at about 600 eV, that can be seen in the very first panel – before the pulse has arrived.

These are resonantly accelerated electrons. These electrons have been overtaken by the wave, but have a large enough component of velocity in the wave propagation direction that they are accelerated up to the wave velocity before they fall out of the accelerating electric field in the wave front. Then, as they travel with the wave, they continue to be accelerated and gain energy and eventually emerge from the front of the wave, moving at a velocity greater than the wave. That is why they appear before the wave front passes the observation point.

The relation between initial velocity and final velocity of the resonant electrons is given by:

$$v_f = 2v_A - v_i , \tag{110}$$

where v_i is the initial velocity, v_A is the Alfvén speed, and v_f is the final velocity. This relation can be readily seen in Figure 32. Those electrons which have initial velocities sufficiently close to the wave velocity are snipped off of the distribution and reflected about the Alfvén velocity ($\sim 10\,000$ km s^{-1}), and are seen before the wave arrives. The final distribution, in the last panel, is now missing these electrons as can be seen in the piece of distribution that is missing. If one mentally reflects these electrons in the first panel about the Alfvén velocity, it can be seen that they exactly fill in the missing electrons in the final distribution.

The perpendicular scale length is quite narrow, 0.38 km. For larger scale lengths, the kinetic effects do not slow the wave as much, and it does not have a significant resonant interaction. In fact, an increase in the perpendicular length scale of only 50% is sufficient to raise the propagation speed of the Alfvén wave to the point where it moves too quickly to be resonant with the electrons.

5.2.2. *Oblique Waves and Electron Acceleration*

Hui and Seyler (1992) investigated the acceleration of electrons by short-scale inertial Alfvén wave breaking using an electromagnetic hybrid particle code, with fluid ions and parallel kinetic electrons. They found both that finite electron inertia was responsible for the wave breaking, and, similar to Kletzing (1994) described above, that cold electrons could be accelerated up to twice the Alfvén velocity when the waves broke.

Clark and Seyler (1999) continued work on small-scale nearly perpendicular nonlinear inertial Alfvén waves in the electrostatic limit with one dimensional oblique particle-in-cell simulations. These results exhibit a mechanism for electron beam generation that is operative in the limit of hot ions. Electrostatic inertial Alfvén waves (ESIAW) propagate with only weak electron Landau damping for $T_i/T_e \gg 1$. Nonlinear amplitude initial conditions convectively steepen and evolve higher wavenumber structures similar in morphology and magnitude to previous results from the fluid-kinetic model of Seyler *et al.* (1998). Shorter wavelength acoustic waves emergent during steepened ESIAW wave evolution are instrumental in exciting cold electron beams possessing kinetic energies a few hundred times that of the thermal electron population. This mechanism is one possible explanation

for suprathermal electron bursts observed in and near auroral inverted-V events as discussed earlier in this review.

The results of the oblique kinetic particle-in-cell (PIC) model of Clark and Seyler (1999) reinforces the electrostatic fluid simulation results of Seyler and Wahlund (1996) in the $T_i/T_e \gg 1$ regime, in that an initial large-amplitude inertial Alfvén wave (SIC-slow ion cyclotron wave in the terminology of Seyler and Wahlund (1996)) advectively steepens and eventually emits nearly perpendicular ion-acoustic (SIA-slow ion acoustic) waves of shorter transverse scale length. The agreement is better, however, with the fluid-kinetic model of Seyler *et al.* (1998) and simultaneously with the *Freja* data itself, with kinetic effects inducing wave emergence at the length scale $\rho_i\theta$ rather than the Debye scale (as is the case with the 2-fluid model). Associated with each SIA 'soliton' is a field-aligned thermal electron current corresponding well in magnitude with the typically observed $\approx$ 100 μA m^{-2} field-aligned current (FAC) densities, assuming *Freja*-corresponding simulation parameters. This, too, is confirmed through the kinetic model. The conjunction of steepened inertial Alfvén and emergent oblique acoustic waves resulting from the oblique kinetic simulation create distinctive SKAW-like signatures that correspond both in magnitude and scale-lengths with many observed *Freja* SKAW waveforms. This suggests that the basic physics of the model is appropriate to these waves. A primary consequence of low-frequency ($\omega \ll \omega_{ci}$) extremely perpendicular ($k_\parallel/k_\perp < \sqrt{m_e/m_i}$) waves is that they have a distinctive ion-Boltzmann character in the sense that the ion density adjusts dynamically to the potential, whereas the electrons are inhibited from doing so due to their large transverse inertia, which lends increasing inability to stream along the field lines as perpendicularity increases.

The most significant result of Clark and Seyler (1999), which is not predicted by the n-fluid theory, or fluid-kinetic model, is the generation of an electron beam, by a nonlinear electron trapping mechanism. The beam energy is appropriate for a suprathermal electron burst (STEB) (sub-keV) having a low current density (≈ 0.1 of the thermal electron current) and transverse length on the order of the acoustic gyroradius. The beam arises from the localized ion-Boltzmann response to steepened density gradients which produce an electric field spike resulting in a nonadiabatic perturbation in the electron Hamiltonian, thereby allowing electrons from the thermal population to transit across the separatrix in energy from the untrapped to the trapped region. This mechanism is termed SITE self induced trapping of electrons by Clark and Seyler (1999). This SITE acceleration mechanism has not been previously postulated for the occurrence of STEB. Nonlinear wave breaking in the cold electron limit was found to produce beams up to twice the Alfvén speed by Hui and Seyler (1991). In this case the acceleration mechanism is independent of the ion and electron temperatures.

We briefly summarize the results of Clark and Seyler (1999). There are three main stages in the acceleration process of the SITE mechanism, the wave steepening stage, the wave breaking stage and the wave relaxation stage.

An initial large amplitude sinusoidal wave begins to steepen after a few tens of cyclotron periods. The wave steepening can be interpreted as follows: parallel advection of the electron momentum projected into the perpendicular direction creates a region of enhanced electron density; since the wave is quasineutral for $k_x \rho_i < 1$, the ion density 'follows', the ions being effectively lighter than the electrons for nearly perpendicular motion. This behavior is dependent upon the 'transverse electron mass' exceeding the ion mass, which only occurs for the slow waves ($\vartheta < \epsilon$ or $\theta < 1$). Finally, associated with the steepened ion density profile is an electrostatic potential trough, as a natural consequence of the ion-Boltzmann nature of the electron acoustic wave. The 2-fluid nearly perpendicular model of Seyler and Wahlund (1996) exhibits similar steepening behavior.

At some point in time a certain population of thermal electrons will have moved across potential energy contours toward lower energies (in the wave frame) and become trapped in the wave potential well. Figure 33 shows the simulation phase space after $50\omega_{ci}^{-1} \approx 8t_i$. Here, the steepened wave is in the process of exciting an electron beam which leaves the thermal electron population at the location of the deep negative electric field 'spike' shown in Figure 33. The occurrence of a unipolar electric field spike is very commonly found in observations (Wahlund *et al.*, 1994; Seyler *et al.*, 1995).

The steep negative ion density gradient is colocated with the ion-Boltzmann negative spike in $E_\perp$. The extreme obliqueness of the wave prevents the electrons from responding in a quasineutral fashion on either side of the ion density gradient; hence, the electron density overestimates the ion density along the negative gradient in $E_\perp$. Very similar behavior results from the fluid-kinetic model Seyler *et al.* (1998), which lends credibility to both models.

Figure 33 shows that a certain population of electrons in the vicinity of the separatrix X-point, colocated with the negative spike in E_s, are forming an energetic beam. The majority of the thermal electron population remains untrapped, as before. We interpret this behavior to be a consequence of the negative electric field spike: in the wave frame, electrons in the vicinity of the negative spike decelerate and lose energy relative to the wave. At this point in time, the negative spike, generated by the convective steepening process and colocated with the positive density gradient (ion Boltzmann character), has grown sufficiently in magnitude to perturb a small population (approximately 0.25% of the total electron population) of electrons across the separatrix from an untrapped state to one in which they are trapped in the potential of the wave. As the beam electrons leave the spike-dominated region, they begin to approximately follow contours of constant energy and circulate in the wave potential.

The transition of an electron across a separatrix, from untrapped to trapped must be a consequence of the time-varying electric field. Thus the wave steepening through an ion Boltzmann response produces the negative electric field spike which non-adiabatically induces electron trapping. Hence the terminology self-induced trapping of electrons.
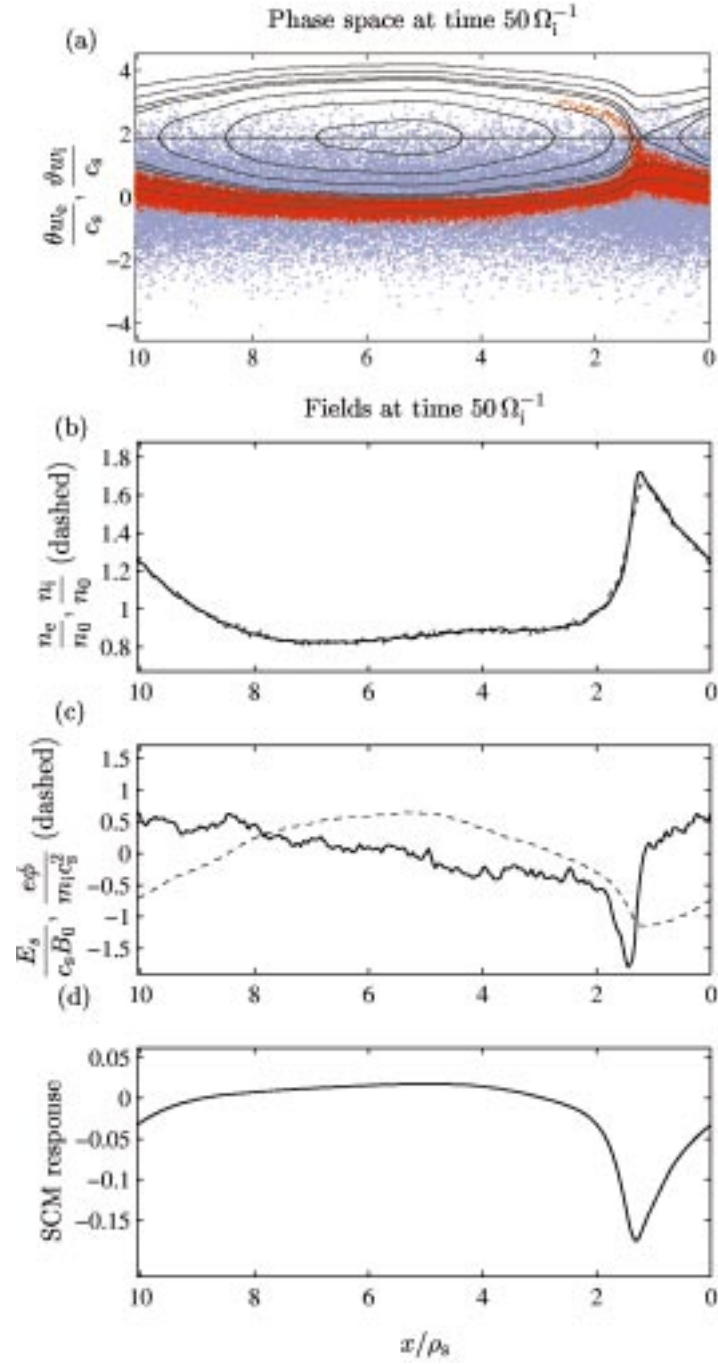
Figure 33. Electron (red) and ion (blue) phase space from an oblique particle-in-cell simulation of an electrostatic inertial Alfvén wave showing wave steepening and resultant perturbation of the electrons across the energy separatrix.

For large T_i/T_e, the density of beam electrons is not great enough to cause any noticeable density perturbations in the wave. However, associated with the wave steepening is the development of higher wavenumber ($1 < k_x < \theta^{-1}$) wave activity. However, the peak in electron density is associated with a field-aligned electron current of a few hundred μA m^{-2} created by the (locally) drifting thermal population.

Higher wavenumber structures with $k_x > \theta^{-1}$ existing on the lowest dispersion branch experience ion cyclotron damping for $\omega \approx 1$, and dissipate quickly compared to the timescale of SIC wave evolution. However, in a hot-ion ($T_i \gg T_e$) environment, we would expect electron acoustic structures with wavelengths longer than the dispersive scale length $k_x \approx \theta^{-1}$ to propagate relatively undamped. Furthermore, we should expect nonlinear steepening to create structures having the dispersive scale length as the minimal scale of the phenomenon of interest.

The electron beam is fully developed when the negative ion Boltzmann spike has relaxed. The bulk of the thermal population remains untrapped, and is associated with at least two prominent density 'humps,' one the original steepened density peak and the other a smaller peak emerging, with lower group velocity, from the former. Each peak is associated with a field-aligned current density of approximately a few hundreds of μA m^{-2} carried by the untrapped thermal electron distribution. Also, each is associated with an ion Boltzmann gradient in E_x, giving the electric field in the vicinity of the density enhancement a distinctively bipolar appearance. A number of solitary Alfvénic events have been found with bipolar electric field signatures Wahlund *et al.* (1994) and Chaston *et al.* (1999).

5.3. GENERATION OF ALFVÉN WAVES BY ELECTRON BEAMS

The dispersive Alfvén waves can by excited by linear as well as nonlinear processes. The linear process involves magnetic field-aligned electron beams (Shukla and Stenflo, 1999a) or sheared magnetic fields. On the other hand, the nonlinear processes usually require the presence of large amplitude high-frequency electromagnetic or electrostatic drivers in the plasma.

Let us consider Alfvén wave excitation in the presence of an equilibrium electron current $J_0 = -n_0 e u_0$ in a Maxwellian plasma. Here, the parallel component of the perturbed electron current density in the wave electric field is

$$J_{ez} = i \frac{\epsilon_0 \omega E_z}{2 k_z^2 \lambda_{De}^2} Z'(\xi_e) , \tag{111}$$

where E_z is the parallel component of the wave electric field, Z' the derivative of the standard plasma dispersion function with its argument $\xi_e = (\omega - k_z u_0)/k_z v_{te}$, and $\lambda_{De} = (\epsilon_0 T_e/n_0 e^2)^{1/2}$ the electron Debye radius. For $\xi_e \ll 1$, (111) becomes

$$J_{ez} = -i \frac{\epsilon_0 \omega E_z}{k_z^2 \lambda_{De}^2} \left[1 + i \sqrt{\frac{\pi}{2}} \frac{(\omega - k_z u_0)}{k_z v_{te}} \right] . \tag{112}$$

The perpendicular component of the plasma current density is

$$\mathbf{J}_\perp \approx -i \frac{n_0 e}{B_0} \frac{\omega \omega_{ci}}{\omega_{ci}^2 - \omega^2} \mathbf{E}_\perp \ . \tag{113}$$

From $\nabla \cdot \mathbf{J} = 0$, we then obtain

$$\frac{k_z c_s^2}{\omega_{ci}^2 - \omega^2} \mathbf{k}_\perp \cdot \mathbf{E}_\perp = -\left[1 + i \sqrt{\frac{\pi}{2}} \frac{(\omega - k_z u_0)}{k_z v_{te}} \right] E_z \ . \tag{114}$$

On the other hand, from the Maxwell equations we have

$$\left(k_z^2 c^2 - \frac{\omega_{pi}^2 \omega^2}{\omega_{ci}^2} \right) \mathbf{k}_\perp \cdot \mathbf{E}_\perp = k_\perp^2 k_z c^2 E_z \ . \tag{115}$$

Combining (114) and (115) we obtain the dispersion relation

$$\omega^2 \approx \omega_H^2 \left[1 - i \sqrt{\frac{\pi}{2}} \frac{(\omega - k_z u_0)}{k_z v_{te}} \right] \ , \tag{116}$$

where

$$\omega_H^2 = k_z^2 v_A^2 [1 + k_\perp^2 (\rho_s^2 + \rho_i^2)] \ . \tag{117}$$

Letting $\omega = \omega_H + i\gamma_b$ in (116), we obtain for $\gamma_b < \omega_H$ the growth rate (Shukla and Stenflo, 1999a)

$$\gamma_b = \sqrt{\frac{\pi}{8}} \omega_H \frac{|k_z u_0 - \omega_H|}{k_z v_{te}} \ , \tag{118}$$

if

$$|J_0| > \frac{n_0 e v_A (1 + k_\perp^2 \rho_s^2)^{1/2}}{(1 + k_z^2 \lambda_i^2)^{1/2}} \ . \tag{119}$$

The physical mechanism of the above instability is similar to the Cerenkov process in which the beam electrons resonantly interact with the dispersive Alfvén waves to drive the latter at non-thermal levels.

5.4. ALFVÉN RESONANCE CONES BY P. M. BELLAN

5.4.1. *Mathematical Framework for Resonance Cones*
Before discussing the specifics of IAW resonance cones it is worth developing some general properties of the relevant partial differential equation. To develop this pde we first consider a Helmholtz equation with a delta function source, i.e.,

$$\nabla^2 \psi \pm \alpha^2 \psi = \delta(x)\delta(y)\delta(z) \ . \tag{120}$$

If the minus sign is chosen, then the solution to (120) is

$$\psi(r) = -\frac{e^{-\alpha r}}{4\pi r} , \tag{121}$$

where $r = \sqrt{x^2 + y^2 + z^2}$; this is the Yukawa potential, describes Debye shielding and if $\alpha = 0$, becomes the potential of an isolated charge in vacuum. If the plus sign is chosen in (120), then the solution is

$$\psi(r) = -\frac{e^{\pm i \alpha r}}{4\pi r} . \tag{122}$$

A slightly more complicated situation occurs when the system is anisotropic and the equation has the form

$$\frac{\partial^2 \psi}{\partial z^2} - \left(\frac{\partial^2 \psi}{\partial x^2} + \frac{\partial^2 \psi}{\partial y^2} \right) + \alpha^2 \psi = \delta(x)\delta(y)\delta(z) ; \tag{123}$$

this is called the Klein–Gordon equation and the LHS has a dispersion relation formally corresponding to the IAW. Making the transformation $x \to ix'$, $y \to iy'$, $z \to z'$, Equation (123) becomes

$$\frac{\partial^2 \psi}{\partial z'^2} + \frac{\partial^2 \psi}{\partial x'^2} + \frac{\partial^2 \psi}{\partial y'^2} + \alpha^2 \psi = -\delta(x')\delta(y')\delta(z') \tag{124}$$

and so has the solution given by (122) with an extra minus sign (because of the reversal of the sign of the delta functions). Since $x'^2 + y'^2 + z'^2 = z^2 - (x^2 + y^2)$ the solution to (123) is therefore

$$\psi(x, y, z) = \frac{\exp\left(\pm i\alpha \sqrt{z^2 - (x^2 + y^2)} \right)}{4\pi \sqrt{z^2 - (x^2 + y^2)}} , \tag{125}$$

which has the peculiarity that $\psi(x, y, z)$ diverges not only at the origin, but also on the conical surface $z = \pm\sqrt{x^2 + y^2}$. Because (123) is a hyperbolic differential equation, its solutions involve propagation of information along characteristics. In particular, the information that the potential is divergent at the origin propagates along the characteristic $z = \pm\sqrt{x^2 + y^2}$. Equation (125) is relevant to IAW waves excited by a localized source and forms the basis of Alfvén resonance cones.

5.4.2. *Generation of Alfvén Resonance Cones by Localized Sources*
We now construct and solve the IAW partial differential equation for a localized source. The IAW plasma current is

$$\mu_0 \tilde{\mathbf{J}}^p = -\frac{i\omega}{c^2} \left(-\frac{\omega_{pe}^2}{\omega^2} \tilde{E}_z \hat{\mathbf{z}} + \frac{c^2}{v_A^2} \tilde{\mathbf{E}}_\perp \right) \tag{126}$$

and, in addition, it is assumed there also exists some other current which is localized and associated with some kind of discontinuity (e.g., localized magnetic reconnection). This additional current will be called $\tilde{\mathbf{J}}^a$ and acts as an antenna radiating IAW waves. Thus, Ampère's law can be written as

$$\nabla \times \tilde{\mathbf{B}} = \mu_0 \tilde{\mathbf{J}}^p + \mu_0 \tilde{\mathbf{J}}^a \;. \tag{127}$$

For simplicity we assume that the antenna current is in the z direction so that the parallel component of (127) becomes

$$\nabla \cdot \left(\tilde{\mathbf{B}} \times \hat{\mathbf{z}} \right) = \frac{i}{c^2} \frac{\omega_{pe}^2}{\omega} \tilde{E}_z + \mu_0 h \tilde{I}^a \delta(x)\delta(y)\delta(z) \;, \tag{128}$$

where $\tilde{I}^a$ is the axial current flowing in the antenna and h is the antenna length.

The perpendicular component of (127) is

$$i k_z \left(\hat{\mathbf{z}} \times \tilde{\mathbf{B}} \right) = - \frac{i\omega}{v_A^2} \tilde{\mathbf{E}}_\perp \tag{129}$$

and crossing Faraday's law with $\hat{\mathbf{z}}$ gives

$$i k_z \tilde{\mathbf{E}}_\perp - \nabla_\perp \tilde{E}_z = -i\omega \left(\hat{\mathbf{z}} \times \tilde{\mathbf{B}} \right) \;. \tag{130}$$

Equations (129) and (130) can be solved to give

$$\left(\hat{\mathbf{z}} \times \tilde{\mathbf{B}} \right) (\omega^2 - k_z^2 v_A^2) = -i\omega \nabla_\perp \tilde{E}_z \;. \tag{131}$$

If this is un-Fourier analyzed in the z direction, we see that

$$\left(\omega^2 + v_A^2 \frac{\partial^2}{\partial z^2} \right) \left(\tilde{\mathbf{B}} \times \hat{\mathbf{z}} \right) = i\omega \nabla_\perp \tilde{E}_z \;. \tag{132}$$

Applying the operator $\omega^2 + v_A^2 \partial^2/\partial z^2$ to (128) and invoking (132) yields

$$\frac{\omega_{gm}^2}{\omega^2} \frac{\partial^2 \tilde{E}_z}{\partial z^2} - \nabla_\perp^2 \tilde{E}_z + \frac{\omega_{pe}^2}{c^2} \tilde{E}_z = \frac{i\mu_0}{\omega} h \tilde{I}^a \left(\omega^2 + v_A^2 \frac{\partial^2}{\partial z^2} \right) \delta(x)\delta(y)\delta(z) \;, \tag{133}$$

where $\omega_{gm} = \omega_{pe} v_A/c = \sqrt{|\omega_{ce}\omega_{ci}|}$. Equation (133) is formally like (123) and so using (125) has the resonance cone solution

$$\tilde{E}_z(x, y, z) = \frac{i\mu_0 h \tilde{I}^a}{4\pi\omega} \frac{c}{\omega_{pe}} \left(\omega^2 + v_A^2 \frac{\partial^2}{\partial z^2} \right) \frac{\exp\left(\pm i \dfrac{\omega}{v_A} \Psi \right)}{\Psi} \;, \tag{134}$$

where $r = \sqrt{x^2 + y^2}$ is the cylindrical radius, $\Psi = \sqrt{z^2 - r^2 \omega_{gm}^2/\omega^2}$ prescribes the cone, and the plus/minus sign is chosen to give axial propagation away from the source. Comparison of (134) and (132) shows that

$$\tilde{\mathbf{B}}(x, y, z) = -\frac{\mu_0 h \tilde{I}^a}{4\pi} \frac{c}{\omega_{pe}} \frac{\partial}{\partial r} \left[\frac{\exp\left(\pm i \dfrac{\omega}{v_A} \Psi \right)}{\Psi} \right] \hat{\theta} \;, \tag{135}$$

where θ is the azimuthal angle about the z axis. Experimental observations (Ono, 1979; Borg *et al.*, 1985; Gekelman *et al.*, 1994) verifying the existence of these Alfvén resonance cones are discussed in Section 3.5. From Equations (129) and (130) it is seen that the perpendicular electric field is

$$\tilde{\mathbf{E}}_\perp = -\frac{v_A^2}{i\omega}\frac{\partial}{\partial z}\left(\hat{\mathbf{z}}\times\tilde{\mathbf{B}}\right) = \frac{\mu_0 v_A^2 h\tilde{I}^a}{4\pi i\omega}\frac{c}{\omega_{pe}}\frac{\partial^2}{\partial r\partial z}\left[\frac{\exp\left(\pm i\dfrac{\omega}{v_A}\Psi\right)}{\Psi}\right]\hat{\mathbf{r}}. \quad (136)$$

Equations (134), (135) and (136) show:

(1) $\tilde{E}_z$, $\tilde{E}_r$, and $\tilde{B}_\theta$ diverge when $\Psi = 0$, i.e., on the conical surface $r = z\omega/\omega_{gm}$.

(2) $\tilde{E}_z$ is finite on the z axis, whereas $\tilde{E}_r$, $\tilde{B}_\theta$ vanish on the z axis.

(3) $\tilde{E}_z$, $\tilde{E}_r$, and $\tilde{B}_\theta$ are all in phase giving both a net radial and a net axial Poynting flux.

(4) The drift velocity $\mathbf{u}_E$ is in the θ direction and so gives a fluid vortex motion.

(5) The field polarizations and fluid motions are consistent with the auroral arc described by (Goertz and Boswell, 1979).

(6) Since $\omega \ll \omega_{gm}$, the fields and vortex-like motion have an extremely long filamentary shape which will locally appear to be almost two dimensional (i.e., appear to have almost no z dependence).

The singularity on the resonance cone in (134), (135) and (136) is an artifact of the delta function source assumption: for a more realistic extended source, these solutions can be used as Green's functions and will be large, but finite on the conical surface $r = z\omega/\omega_{gm}$.

From a Fourier mode point of view, a localized source generates a k_z spectrum the superposition of which gives the field in the plasma. The delta function source assumed here excites all k_z equally; however, for the IAW, only k_z smaller than ω/v_{Te} propagate. For $k_z \sim \omega/v_{Te}$, Singh (1999) has shown that kinetic corrections cause a fine structure modulation of the cones similar to that of lower hybrid cones (Fisher and Gould, 1971) and prevent divergence of the fields excited by a delta function source.

If the observer is close enough to the source so that $\omega z/v_A \ll 1$ the plasma fields will have negligible phase variation and are just functions of $(z^2 - r^2\omega_{gm}^2/\omega^2)^{-1/2}$; this near-field, quasi-electrostatic limit has been experimentally measured by Ono (1979) and kinetic effects (Landau damping) were observed (see Section 3.5).

5.4.3. *Pulsed Localized Source*

So far it has been assumed that the localized source has an $\exp(-i\omega t)$ time dependence, but in reality, it is more likely that a localized source will be a temporal pulse, i.e., will be like $\delta(t)$ rather than like $\exp(-i\omega t)$. Since a single-frequency source generates

$$\tilde{E}_z \sim \frac{\exp\left(i\frac{\omega}{v_A}\sqrt{z^2 - r^2\omega_{gm}^2/\omega^2} - i\omega t\right)}{\sqrt{z^2 - r^2\omega_{gm}^2/\omega^2}} \tag{137}$$

a pulse $\delta(t) \sim \int d\omega \, \exp(-i\omega t)$ will generate a field of the form

$$\tilde{E}_z \sim \int d\omega \frac{\exp\left(i\frac{\omega}{v_A}\sqrt{z^2 - r^2\omega_{gm}^2/\omega^2} - i\omega t\right)}{\sqrt{z^2 - r^2\omega_{gm}^2/\omega^2}} \, . \tag{138}$$

Bellan (1996b) has considered excitation of IAW by a pulsed localized source and, using a temporal Laplace transform method, effectively performed the ω integration in (138). The solution was more conveniently expressed in terms of the radial electric field which was found to have the form

$$\tilde{E}_r \sim \frac{\partial^2 \tilde{\psi}}{\partial r \partial z} \, , \tag{139}$$

where

$$\tilde{\psi}(r, z, t) = z^{-1} J_0\left(\frac{\omega_{gm}r}{z}\sqrt{t^2 - z^2/v_A^2}\right) \, , \tag{140}$$

for $t > z/v_A$ and zero otherwise. Equation (140) has (i) phase fronts forming a narrow band of rays emanating from the source vicinity and continuously collapsing towards the axis and (ii) a signal envelope traveling axially from the source at the Alfvén velocity; numerical solutions confirm this picture. Fields analogous to (140) have been observed experimentally by Simonutti (1976) and by Bellan (1977) in the lower hybrid wave regime.

5.5. MAGNETIC TEARING

5.5.1. *Reconnection via IAW*

So far we have assumed that the background magnetic field is uniform. Magnetic tearing changes the field line topology and these changes typically occur in a very localized boundary layer. The dynamics of magnetic tearing involves field-aligned currents. Because realistic tearing is localized in three dimensions (patchy), the field-aligned currents are also localized in three dimensions. Since transient localized field-aligned currents radiate inertial Alfvén waves, localized tearing should involve radiation of inertial Alfvén waves. The radiated waves will have a cone pattern and since the source is typically a single transient, the radiated waves will be a superposition of Alfvén cones. Bellan (1998) noted that the radiation of Alfvén waves constitutes a power sink for the radiator and this can be construed as a radiation resistance. For highly collisionless plasmas the resistivity associated with this radiation resistance can exceed other known energy loss mechanisms (e.g.,
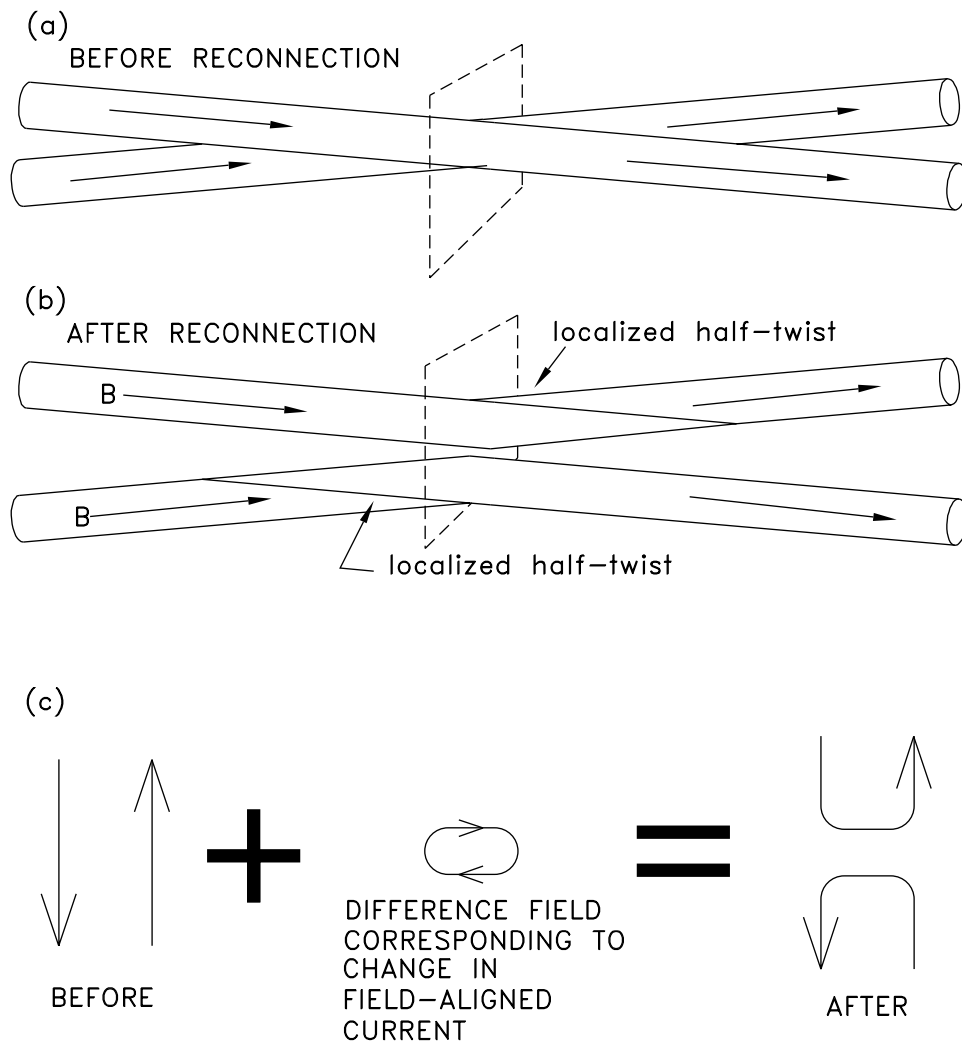
Figure 34. (a) Two adjacent, nearly parallel flux tubes before reconnection in low β plasma; (b) flux tubes after reconnection showing development of localized half-twists which correspond to axially localized field-aligned currents which act as antennas radiating dispersive Alfvén waves; (c) before and after configuration of perpendicular magnetic field in plane of square. (Figure from Bellan, 1998.)

collisions, direct acceleration of electrons) and Bellan (1998) has postulated that the IAW radiation resistivity could mediate the magnetic tearing, i.e., provide the energy sink required for tearing, a relaxation process, to proceed (see Figure 34).

5.5.2. *Tearing Modes Associated with Alfvén Waves*

The importance of the electron inertial dispersion as a means of releasing the free energy contained in the transverse magnetic field of an Alfvén wave cannot be ignored. It was pointed out by Seyler (1988, 1990) that the electron inertia can have important consequences in the small scale structuring of auroral arcs. A model which incorporates electron inertia into 3-D low-beta MHD dynamics is the reduced MHD equations which are

$$(\partial_t + \hat{\mathbf{z}} \times \nabla\phi \cdot \nabla)\nabla_\perp^2 \phi = -\frac{1}{\mu_0 m n_0}(B_0\partial_z + \hat{\mathbf{z}} \times \nabla A_z \cdot \nabla)\nabla_\perp^2 A_z \, , \tag{141}$$

and

$$(\partial_t + \hat{\mathbf{z}} \times \nabla\phi \cdot \nabla)(A_z - \lambda_e^2 \nabla_\perp^2 A_z) = -B_0\partial_z\phi \, , \tag{142}$$

where ϕ is the stream function for the flow given by $\mathbf{u}_i = \hat{\mathbf{z}} \times \nabla\phi$ and A_z is the parallel vector potential from which the magnetic field is given by $\mathbf{b}_\perp = -\hat{\mathbf{z}} \times \nabla A$.

Equations (141) and (142) exhibit magnetic tearing or spontaneous reconnection as the result of finite parallel electron inertia. Even though the system is nondissipative, the effect of dispersion can allow for slippage of the flow through the perpendicular magnetic field. Thus the classical Alfvén flux invariant does not hold and instead we have the following generalization.

$$\Phi = \int_S (\mathbf{B} - \lambda_e^2 \nabla_\perp^2 \mathbf{B}) \, \mathrm{d}\mathbf{S} \, , \tag{143}$$

where Φ is the generalized Alfvén flux and S is an open surface. The generalized magnetic flux is locally conserved along the flow. Magnetic tearing instability associated with the electron inertia was investigated by Seyler (1988, 1990). It was found that Alfvén waves with a transverse scale comparable to λ_e are unstable to electron inertial tearing modes with a growth rate given by Seyler (1990)

$$\gamma = k\lambda_e^3 \left(\frac{\Delta'}{I}\right)^2 \tau_A^{-1} \, , \tag{144}$$

where Δ' is the logarithmic derivative of the outer solution of the perturbed parallel vector potential A_z, I is the dimensionless integral with a value near unity, and τ_A is the Alfvén transit time with respect to the transverse equilibrium sheared magnetic field (b_y).

The ultimate importance of the magnetic tearing with respect to Alfvénic structures is not entirely clear at this time. It is possible that the origin of small scale Alfvén waves could be due to tearing modes or that the two-dimensional perpendicular structure often found to be associated with Alfvénic structures is the result of magnetic tearing. Alfvén waves have comparable magnitudes of energy in their transverse flow and magnetic fields.

5.6. MODE CONVERSION

Section (2.3) showed that the behavior of a plane wave in a uniform plasma is characterized by a 3×3 matrix, Equation (31), which involves the dielectric tensor elements $\varepsilon_\parallel$ and $\varepsilon_\perp$ and the refractive index $\mathbf{n} = n_x\hat{\mathbf{x}} + n_z\hat{\mathbf{z}} = c\mathbf{k}/\omega$. Because the plasma is uniform this matrix reduces to two decoupled systems, (33) and (34), which describe the shear Alfvén wave and the fast wave respectively.

If the Alfvén velocity is non-uniform in the direction perpendicular to $\mathbf{B}$ then the fast wave and the Alfvén wave can become coupled at the location where $\omega^2 = k_z^2 v_A^2(x)$; at this location $k_x \to 0$ for both the fast and Alfvén wave, WKB approximations fail, and a differential equation must be used to describe the coupling. Mode conversion of fast waves into KAW was originally discussed by Hasegawa and Chen (1975); more recently Bellan (1994, 1996a) has examined mode conversion of fast waves into IAW.

The coupling requires the existence of a finite k_y, i.e., the mode must be of the form $f(x)\exp(ik_y y + ik_z z - i\omega t)$ with k_y finite and $v_A = v_A(x)$. This is in contrast to a uniform plasma where the x and y directions are degenerate so that the coordinate system can always be defined to give $\mathbf{k}_\perp = k_x\hat{\mathbf{x}}$.

Using (126) to describe the plasma currents in the cold, low frequency limit and the complete Maxwell equations, Bellan (1994, 1996a) derived the equations describing coupling between a fast mode and an IAW in a cold plasma having a density gradient in the x direction. Denoting $P = 1/(\varepsilon_\perp - n_z^2)$, these coupled equations are

$$\frac{\mathrm{d}}{\mathrm{d}x}\left(\varepsilon_\perp P \frac{\mathrm{d}\tilde{E}_z}{\mathrm{d}x}\right) - k_y^2 \varepsilon_\perp P \tilde{E}_z + \frac{\omega^2}{c^2}\varepsilon_\parallel \tilde{E}_z = -ik_y c n_z \tilde{B}_z \frac{\mathrm{d}P}{\mathrm{d}x} \tag{145}$$

and

$$\frac{\mathrm{d}}{\mathrm{d}x}\left(P \frac{\mathrm{d}\tilde{B}_z}{\mathrm{d}x}\right) - k_y^2 P \tilde{B}_z + \frac{\omega^2}{c^2}\tilde{E}_z = ik_y \frac{n_z}{c}\tilde{E}_z \frac{\mathrm{d}P}{\mathrm{d}x} \tag{146}$$

and all transverse fields are functions of $\tilde{E}_z$ and $\tilde{B}_z$. If the plasma is uniform or if $k_y = 0$, the right-hand sides of (145) and (146) vanish while the left hand sides reduce to the uniform plasma Alfvén and fast waves respectively, i.e., to the dispersion relations given by (35) and (34). However, if $k_y \neq 0$ and $\varepsilon_\perp = c^2/v_A^2$ depends on x, there is a coupling between the Alfvén and fast modes. This coupling is highly localized to the vicinity of $\varepsilon_\perp(x) - n_z^2 = 0$, i.e., to the vicinity of $\omega^2 = k_z^2 v_A^2(x)$. Bellan (1996a) has shown that this coupling conserves the $x-$directed Poynting flux so that any energy incident on the critical layer by a fast wave will be either reflected or mode-converted into an Alfvén wave. This conservation of Poynting flux differs radically from the predictions of ideal MHD. According to ideal MHD the energy carried by a fast wave accumulates at the vicinity of $\omega^2 = k_z^2 v_A^2(x)$ leading to a field line resonance. In contrast, by taking Alfvén wave dispersion into

account, (145) and (146) show that there is in fact no energy accumulation at the
$\omega^2 = k_z^2 v_A^2(x)$ layer.

5.7. NONLINEAR EFFECTS INVOLVING DAW

5.7.1. *Ponderomotive Force and Density Perturbations*

Mikhailovskii *et al.* (1976) pointed out possible existence of kinetic Alfvén wave
(KAW) envelope solitons due to the amplitude modulation of a coherent KAW by
quasi-stationary density and magnetic field perturbations in a plasma in which the
electron and ion temperatures are equal. According to them, the magnetic pres-
sure of the KAW produces the quasistationary density and magnetic field (δB_z)
perturbations, which are given by

$$\frac{\delta n}{n_0} = \frac{\delta B_z}{B_0} = -\frac{|b_\perp|^2}{2(1+2\beta)B_0^2} \,, \tag{147}$$

where $b_\perp$ is the perpendicular component of the KAW magnetic field. We note that
the right-hand side of (147) comes from the $\mathbf{J}_\perp \times \mathbf{b}_\perp$ force, which is equivalent to
the ponderomotive force.

Recently, Bellan and Stasiewicz (1998) renewed interest in ponderomotive ef-
fects by applying them to IAW density cavities observed on *Freja* (see Section 3.3).
They have derived the ponderomotive force of the IAW wave from a general ex-
pression based on the guiding center approximation. Using the ponderomotive
force and also taking ambipolar effects into account Bellan and Stasiewicz found
that the nonlinear dependence of density on wave amplitude is given by

$$n_s \approx n_0 \exp\left[\frac{e^2}{4m_e T}\left(\frac{|\tilde{\mathbf{E}}_\perp|^2}{\omega_{gm}^2} - \frac{|\tilde{E}_z|^2}{\omega^2}\right)\right] \equiv n_0 \exp(\Psi_P) \,, \tag{148}$$

where $T = T_e + T_i$. Equation (148) shows that the electron ponderomotive force is
negative and so tends to dig density cavities whereas the ion ponderomotive force
is positive and so tends to create a density hump. It is important to recall that for
IAW $\tilde{\mathbf{E}}_\perp$ is proportional to $\nabla_\perp \tilde{E}_z$ (or equivalently to $\nabla_\perp \tilde{J}_z$ since $\tilde{E}_z$ is proportional
to $\tilde{J}_z$). Thus, if $\tilde{J}_z$ is spatially localized (as observed in the *Freja* data), $\tilde{J}_z$ will have
a local maximum and at this maximum, $\tilde{E}_z$ will also have a maximum while $\tilde{\mathbf{E}}_\perp$
will vanish. Thus, the electron ponderomotive force is the only non-vanishing pon-
deromotive force at the location of the current maximum and this ponderomotive
force produces a density depletion. If the IAW is excited by a localized source,
$\tilde{E}_z$ is finite on the field line passing through the source, whereas $\tilde{\mathbf{E}}_\perp$ vanishes on
this field line. Hence, one expects a density depletion on the field line through the
source and this density depletion will be bounded by density increases (ridges)
due to the perpendicular electric field which becomes finite as one moves away
from the field line through the source. In cylindrical geometry it is found that the
maximum of $|\tilde{\mathbf{E}}_\perp|^2/\omega_{gm}^2$ is about an order of magnitude smaller than the maximum
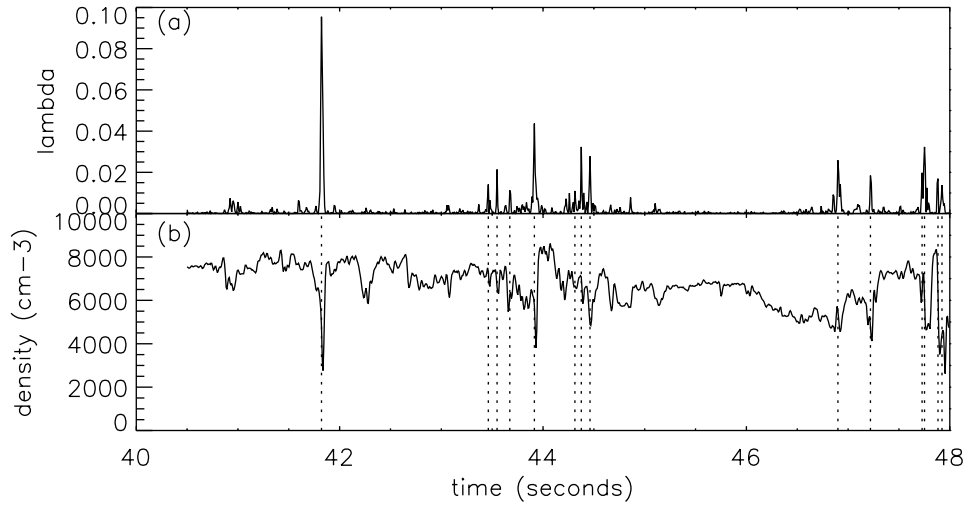
Figure 35. (a) Ponderomotive force term $e^2|\tilde{E}_z|^2/4m_eT\omega^2$ in (148) calculated from *Freja* motion across magnetic field gradients; (b) density cavities measured by *Freja*. Dotted lines show correlation between observed density cavities and calculated ponderomotive force. (Figure from Bellan and Stasiewicz (1998).)

of $|\tilde{E}_z|^2/\omega^2$ and so the density depletion is larger than the density ridges. By deducing value of E_z from the observed intensity of J_z with Equation (61) Bellan and Stasiewicz (1998) showed that (148) provides a reasonable description for the density depletions observed by the *Freja* spacecraft (see Figure 35).

Shukla *et al.* (1999) have shown that the result (148) can be obtained from two-fluid equations. The parallel component of the driving force of the dispersive IAWs can be calculated by averaging the parallel component of the convective $m_j\mathbf{v}_j \cdot \nabla v_{jz}$ and Lorentz force $q_j\left(\mathbf{v}_{j\perp} \times \mathbf{b}_\perp\right)_z$ terms over the IAW period $2\pi/\omega$, where $q_i = e$ and $q_e = -e$. The ponderomotive force of the IAW produces a space charge ambipolar potential φ and density perturbations $\delta n_{js} = n_{js} - n_0$. The magnetic field-aligned force balance equation for nonresonant electrostatic disturbances in the presence of the driving force of the IAW is (Shukla *et al.*, 1999)

$$m_j\frac{\partial v_{js}}{\partial t} + m_j\left\langle\mathbf{v}_{j\perp}^* \cdot \nabla v_{jz} + v_{jz}^*\partial_z v_{jz}\right\rangle - q_j\left\langle\hat{\mathbf{z}} \cdot \left(\mathbf{v}_{j\perp}^* \times \mathbf{b}_\perp\right)\right\rangle =$$

$$= -q_j\frac{\partial\varphi}{\partial z} - \frac{T_j}{n_{js}}\frac{\partial n_{js}}{\partial z} , \tag{149}$$

where v_{js} is the magnetic field-aligned particle velocity involved in the nonresonant electrostatic disturbances, and the angular bracket denotes averaging over the IAW period. The bracket terms in the left-hand side represents the ponderomotive force, and the asterisk the complex conjugate.

For low parallel phase velocity (in comparison with the electron thermal velocity) electrostatic waves, we can neglect the parallel electron inertial force in

(149). Adding the inertialess electron and inertial ion versions of (149) under the quasi-neutrality approximation $n_{es} = n_{is} \equiv n_s$, we obtain

$$
m_i \frac{\partial v_{is}}{\partial t} + \frac{i}{n_0 \omega} \left\langle \mathbf{J}_\perp^* \cdot \nabla E_z \right\rangle - \frac{1}{n_0} \left\langle \hat{\mathbf{z}} \cdot \left(\mathbf{J}_\perp^* \times \mathbf{b}_\perp \right) \right\rangle +
$$
$$
+ \frac{e^2}{4 m_e \omega^2} \frac{\partial}{\partial z} \left\langle |E_z|^2 \right\rangle = -T \frac{\partial}{\partial z} \ln n_s \, ,
\tag{150}
$$

where the perpendicular component of the plasma current density is given by

$$
\mathbf{J}_\perp = -i (n_0 e \omega / B_0 \omega_{ci}) \mathbf{E}_\perp \, .
\tag{151}
$$

In deriving (151) we have made use of the perpendicular and parallel components of the electron and ion fluid velocities in the IAW fields, namely,

$$
\mathbf{v}_{e\perp} \approx B_0^{-1} \mathbf{E}_\perp \times \hat{\mathbf{z}} \, ,
\tag{152}
$$

$$
\mathbf{v}_{i\perp} \approx B_0^{-1} \mathbf{E}_\perp \times \hat{\mathbf{z}} + (B_0 \omega_{ci})^{-1} \partial_t \mathbf{E}_\perp \, ,
\tag{153}
$$

and

$$
\partial_t v_{ez} = -e E_z / m_e, \qquad \partial_t v_{iz} = e E_z / m_i \, .
\tag{154}
$$

Equation (148) is recovered for the quasi-stationary ($v_{is} = 0$) density by inserting the expression for $\mathbf{J}_\perp$ into the left-hand side of (150) (Shukla *et al.*, 1999).

Shukla and Stenflo (1999b) have pointed out that the Joule heating of the electrons in the IAW can be responsible for the fine-scale density cavitations that are observed by *Freja* and FAST. When the electron thermal nonlinearity involving the Joule heating and the ponderomotive force are included, one obtains (Shukla and Stenflo, 1999c)

$$
n = n_0 \exp \left\{ \Psi_P - \frac{\sigma \omega_{pi}^2}{\omega_{ci}^2} \frac{\epsilon_0 \left\langle |\mathbf{E}_\perp^2| \right\rangle}{3 n_0 T} \right\} \, ,
\tag{155}
$$

where σ is a factor of order unity. We recall that for an IAW (with $\omega \ll \omega_{ci}$ and $k_z \lambda_i \ll 1$) we have $\mathbf{E}_\perp = (k_z \omega_{ce} \omega_{ci} / \omega^2 k_\perp^2) E_z \mathbf{k}_\perp$, and $|\mathbf{b}_\perp| = \omega |\mathbf{E}_\perp| / k_z v_A^2$, which inserted in (155) yields

$$
n = n_0 \exp[-(1 + 8 k_\perp^2 \lambda_e^2) |\mathbf{b}_\perp|^2 / 12 \mu_0 n_0 T] \, .
\tag{156}
$$

Equation (156) exhibits that the thermal nonlinearity associated with the inertial Alfvén waves can create magnetic field-aligned quasi-stationary density dips. On the other hand, when the $\sigma \omega_{pi}^2 / \omega_{ci}^2$-term in (155) is absent, which is ascribed to the Joule heating, and the relationship between $\mathbf{E}_\perp$ and $E_\parallel$, applicable for a plane wave is inserted to (155), one obtains a density hump.

5.7.2. *Parametric Instabilities of IAW*

In this section, we present an investigation of the nonlinear effects produced by finite amplitude IAW waves interacting with the plasma slow motions in a uniform magnetoplasma. Specifically, here we focus on the ponderomotive force of the IAW waves that can create magnetic field aligned ion-acoustic density fluctuations, as seen in *Freja* data (Wahlund *et al.*, 1998).

We consider the nonlinear propagation (in the $x - z$ plane) of low-frequency (in comparison with the ion gyrofrequency), long parallel wavelength (in comparison with the collisionless ion-skin depth) finite amplitude IAW waves in a magnetoplasma. In the IAW fields, the perpendicular (denoted by the subscript $\perp$) and the parallel (denoted by the subscript z) components of the electron and ion fluid velocities are given earlier by (153)–(154). The y component of the IAW magnetic field B_y and the IAW electric fields are related by Faraday's law

$$\frac{\partial B_y}{\partial t} = \frac{\partial E_z}{\partial x} - \frac{\partial E_x}{\partial z} \; . \tag{157}$$

We now derive the relevant dynamical equation for the IAW waves, taking into account the nonresonant electrostatic density perturbations δn_s that are created by the ponderomotive force of the IAW waves. For this purpose, we combine the parallel component of the Ampère law with (154) to obtain

$$\frac{\partial^2 B_y}{\partial t \, \partial x} = \frac{\omega_{pe}^2}{c^2} \left(1 + \frac{\delta n_s}{n_0} \right) E_z \; . \tag{158}$$

On the other hand, by inserting (152) and (153) into the conservation of the current density equation (viz., $\nabla \cdot \mathbf{J} = 0$) and eliminating the parallel component of the plasma current density from the Ampère law, we have

$$\frac{\partial E_x}{\partial t} = -v_{\mathrm{A}}^2 \left(1 - \frac{\delta n_s}{n_0} \right) \frac{\partial B_y}{\partial z} \; , \tag{159}$$

where $\delta n_s / n_0 \ll 1$. For large density perturbations, i. e. $\delta n_s / n_0 > 0.2$, one could extend the validity of (159) by replacing $1 - \delta n_s / n_0$ by $(1 + \delta n_s / n_0)^{-1}$.

Eliminating E_x from (157) and (159) we find (Shukla *et al.*, 1999)

$$\frac{\partial^2 B_y}{\partial t^2} - \frac{\partial^2 E_z}{\partial t \, \partial x} = v_{\mathrm{A}}^2 \left(1 - \frac{\delta n_s}{n_0} \right) \frac{\partial^2 B_y}{\partial z^2} \; . \tag{160}$$

Combining (158) and (160) we finally obtain the IAW equation

$$\left(1 - \frac{\delta n_s}{n_0} \right) \left(v_A^2 \frac{\partial^2}{\partial z^2} + \lambda_e^2 \frac{\partial^2}{\partial x^2} \frac{\partial^2}{\partial t^2} \right) B_y = \frac{\partial^2 B_y}{\partial t^2} \; , \tag{161}$$

where the last term in the left-hand side of (161) arises from the nonlinear coupling between the IAWs and the slow density perturbations that are produced by the IAW driving force. We note that (161) accounts for small amplitude density changes that are created by the ponderomotive force of the IAWs.

On the other hand, in the presence of the ponderomotive force of IAW's, the dynamics of magnetic field-aligned ion-sound waves is governed by

$$\left(\frac{\partial^2}{\partial t^2} - c_s^2 \frac{\partial^2}{\partial z^2}\right)\delta n_s = -\frac{c_s^2}{4\mu_0 T}\frac{\partial^2}{\partial z^2}\langle|B_y|^2\rangle \,, \tag{162}$$

where the perpendicular wavelength of the driven ion-acoustic waves is assumed to be much larger than the ion gyroradius at the electron temperature. Equation (162) in addition can depict supersonic density cavities produced by the IAW Ponderomotive force. Equations (161) and (162) are our desired set for studying the nonlinear propagation of IAWs in the presence of nonstationary electrostatic density perturbations.

In the following, we consider the parametric instabilities of IAWs. For this purpose, we decompose the IAW field as $B_y = B_{y0}\exp(i\mathbf{k}_0 \cdot \mathbf{r} - i\omega_0 t) +$ compl. conj. $+ B_{y\pm}\exp(i\mathbf{k}_\pm \cdot \mathbf{r} - i\omega_\pm t)$, where $B_{y0}(B_{y\pm})$ is the magnetic field of the IAW pump (sidebands), $\omega_0 = k_{z0}v_A/(1 + k_{x0}^2\lambda_e^2)^{1/2}$ the pump frequency, $\omega_\pm = \Omega \pm \omega_0$, $\mathbf{k}_\pm = \mathbf{K} \pm \mathbf{k}_0$, and $\Omega(\mathbf{K})$ the frequency (wavevector) of the low-frequency electrostatic oscillations. Thus, (161) and (162) can be Fourier transformed and combined to yield the nonlinear dispersion relation

$$\Omega^2 - K_z^2 c_s^2 = K_z^2 c_s^2 \omega_0^2 \frac{|B_{y0}|^2}{4\mu_0 n_0 T}\sum_{+,-}\frac{1}{D_{A\pm}} \,, \tag{163}$$

where $D_{A\pm} = \omega_\pm^2(1 + k_{x\pm}^2\lambda_e^2) - k_{z\pm}^2 v_A^2$. It can be shown that for $K_x \ll k_{x0}$, the latter takes the form $\pm 2\omega_0(1 + k_{x0}^2\lambda_e^2)(\Omega - K_z v_{g0} \mp \delta)$, where $v_{g0} = k_{z0}v_A^2/\omega_0(1 + k_{x0}^2\lambda_e^2)$ is the group velocity of the pump and $\delta = K_z^2 v_A^2/2\omega_0(1 + k_{x0}^2\lambda_e^2)$ a small frequency shift arising from the nonlinear interaction.

Equation (163) can be analyzed for three-wave decay and modulational interactions. For the three-wave decay interaction, we can assume D_{A-} to be resonant and ignore the upper sideband D_{A+}, which is off-resonant. Letting $\Omega = K_z c_s + i\gamma_i$ and $K_z v_{g0} - \delta \approx K_z c_s$, we obtain the growth rate γ_i from (163)

$$\gamma_i = (K_z c_s \omega_0)^{1/2}|B_{y0}|/4[(1 + k_{x0}^2\lambda_e^2)\mu_0 n_0 T]^{1/2} \,. \tag{164}$$

On the other hand, for the modulational interaction, both the upper and lower sidebands are resonant (viz., $D_{A\pm} = 0$, whereas the low-frequency perturbations are non-resonant. Here, (163) takes the form

$$(\Omega^2 - K_z^2 c_s^2)[(\Omega - K_z v_{g0})^2 - \delta^2] = K_z^4 c_s^2 v_A^2 |B_{y0}|^2/8\mu_0 n_0 T(1 + k_{x0}^2\lambda_e^2)^2 \,. \tag{165}$$

Equation (165) can be analyzed in two limiting cases. First, for $\Omega \ll K_z c_s$, we have

$$\Omega = K_z v_{g0} \pm \left[\delta^2 - \frac{K_z^2 v_A^2 |B_{y0}|^2}{8\mu_0 n_0 T(1 + k_{x0}^2\lambda_e^2)^2}\right]^{1/2} \,, \tag{166}$$

which predicts an oscillatory instability when

$$|B_{y0}|^2 > 2\mu_0 n_0 T K_z^2(1 + k_{x0}^2\lambda_e^2)/k_{0z}^2 \,.$$

The maximum growth rate of that instability is

$$K_{z0}v_A|B_{y0}|/\sqrt{8\mu_0 n_0 T}(1 + k_{x0}^2 \lambda_e^2) \; .$$

Second, for $\Omega^2 \gg K_z^2 c_s^2$ and $\Omega \gg K_z v_{g0}$, (165) reduces to

$$\Omega^2 = (\delta^2/2) \pm \left[(\delta^4/4) + K_z^4 v_A^2 c_s^2 |B_{y0}|^2 / 8\mu_0 n_0 T (1 + k_{x0}^2 \lambda_e^2)^2\right]^{1/2} \; . \tag{167}$$

Equation (167) also admits an oscillatory instability.

Furthermore, in order to study the long term spatio-temporal evolution of (161) and (162), we must invoke the slowly varying envelope approximation on (161) and solve the pair by means of a numerical scheme. It is likely that the coupled equations admit stationary solutions in the form of supersonic density cavities which may trap spatially localized IAW magnetic fields. Finally, it of interest to mention that the modulation of IAWs by quasi-stationary electromagnetic perturbation has been considered by Shukla (1983). It was found that finite amplitude long (short) wavelength IAW is modulationally stable (unstable). Investigations by Shukla and Stenflo (1985) and Shukla *et al.* (1986c) on the modulation of electromagnetic cyclotron Alfvén waves by ion-sound perturbations along the magnetic field lines are also of interest in this context.

5.8. AMPLITUDE MODULATION OF KAWs

In this section, we consider the nonlinear interaction of a finite amplitude KAW with quasi-stationary density and compressional magnetic field perturbations gives rise to an envelope of waves. Employing the eikonal operator representation, which implies letting $\omega = \omega_0 + i\partial_t$ and $\mathbf{k} = \mathbf{k}_0 - i\nabla$ in Equation (27), where $\omega_0(\mathbf{k}_0)$ is the pump frequency (wavevector), and applying the WKB approximation, viz., $\partial_t B_\perp \ll \omega_0 B_\perp$, we find that the envelope evolves according to (Shukla *et al.*, 1998a)

$$i\left(\frac{\partial}{\partial t} + \mathbf{v}_g \cdot \nabla\right) b_\perp + \frac{\Omega_{A0}^2 \alpha \rho_s^2}{2\omega_0} \nabla_\perp^2 b_\perp - \frac{\Omega_{A0}^2}{2\omega_0} \frac{\delta B_z}{B_0} b_\perp = 0 \; ; \tag{168}$$

here $\mathbf{v}_g = \partial\omega_0/\partial\mathbf{k}_0$ is the group velocity, $\omega_0^2 = \Omega_{A0}^2(1 + \alpha k_{\perp 0}^2 \rho_s^2)$, $\Omega_{A0} = k_{0z}v_A$, $\alpha = 1 + 3T_i/4T_e$, and $B_\perp$ the perpendicular (to $\hat{\mathbf{z}}$) component of the KAW magnetic field. In Equation (168) we have used the frozen-in-field concept and have thus set $n_i/B =$ constant. We have also let $n_i = n_0 + \delta n$ and $B = B_0 + \delta B_z$, where $\delta B_z(\ll B_0)$ is the quasi-stationary compressional magnetic field triggered by the KAW magnetic field pressure. Furthermore, we have also employed the relation $\delta n/n_0 \approx \delta B_z/B_0$.

Combining Equations (147) and (168) we obtain

$$i\left(\frac{\partial}{\partial t} + \mathbf{v}_g \cdot \nabla\right) \hat{b}_\perp + \frac{P}{2}\nabla_\perp^2 \hat{b}_\perp + Q|\hat{b}_\perp|^2 \hat{b}_\perp = 0 \; , \tag{169}$$

where $\hat{b}_\perp = B_\perp/B_0$, $P = \Omega_{A0}^2 \alpha \rho_s^2/\omega_0$, and $Q = \Omega_{A0}^2/4\omega_0(1 + 2\beta)$.

Equation (169) is the standard cubic nonlinear Schrödinger equation, which predicts modulation/filamentation instability of a constant amplitude KAW pump, as well as self-focusing of the KAW.

The nonlinear dispersion relation for the modulational/filamentation instability of a constant amplitude ($B_{\perp 0}$) KAW pump is derived from Equation (169) by decomposing $b_\perp$ as the sum of the pump and the two sidebands. The standard procedure gives

$$(\Omega - \mathbf{K} \cdot \mathbf{v}_g)^2 = P K_\perp^2 (\tfrac{1}{4} P K_\perp^2 - Q|b_0|^2) , \tag{170}$$

where $\Omega(\mathbf{K})$ is the frequency (wave number) of the quasi-stationary modulation, $\mathbf{K} = \hat{\mathbf{z}} K_z + \mathbf{K}_\perp$, and $b_0 = B_{\perp 0}/B_0$. Letting $\Omega = \mathbf{K} \cdot \mathbf{v}_g + i\gamma$ in Equation (170), we observe that the growth rate γ of the modulational instability is positive for $Q|b_0|^2 > P K_\perp^2/4$.

On the other hand, stationary filamentation instability can be investigated on the basis of the nonlinear dispersion relation

$$K_z^2 = \frac{P K_\perp^2}{4 v_A^2 \alpha}(P K_\perp^2 - 4Q|b_0|^2) , \tag{171}$$

where v_{gz} is the z component of the group velocity of the KAW. Equation (171) follows from Equation (170) if we set $\Omega = 0$ and assume that $K_z v_{gz} \gg \mathbf{K}_\perp \cdot \mathbf{v}_{g\perp}$. Setting $K_z = -i K_m (K_m > 0)$ in Equation (171), we see that convective amplification occurs for $|b_0|^2 > P K_\perp^2/4Q$. The mode number of the most unstable wave is $K_m = (2Q b_0/P)^{1/2}$ and the corresponding spatial amplification rate is $K_i = Q|b_0|^2/v_{gz}$. The minimum scalelength over which the KAW filamentation occurs is $2\pi/K_i$.

We now consider the time-independent stationary propagation of KAW along the z axis. Thus, we seek the solution of Equation (169) in the form $\hat{b}_\perp = \hat{b}_\perp(r)$ $\exp(i\lambda z)$ and assume the steady state ($\partial_t b_\perp = 0$), where λ is a constant. Thus, for cylindrically-symmetric KAW beams, we have

$$\frac{1}{r}\frac{\mathrm{d}}{\mathrm{d}r}\left(r \frac{\mathrm{d}\hat{b}_\perp}{\mathrm{d}r}\right) - \frac{2}{P}(v_{gz}\lambda - Q\hat{b}_\perp^2)\hat{b}_\perp = 0 . \tag{172}$$

For $\lambda > 0$, Equation (172) admits cylindrical soliton solutions.

Furthermore, in the steady state Equation (169) can be cast in the form

$$i\partial_\xi \hat{b}_\perp + \frac{1}{2\rho}\frac{\partial}{\partial\rho}\left(\rho \frac{\partial\hat{b}_\perp}{\partial\rho}\right) + D|\hat{b}_\perp|^2 \hat{b}_\perp = 0 , \tag{173}$$

where $\xi = z\Omega_{A0}^2\alpha/v_{gz}\omega_0$, $\rho = r/\rho_s$ and $D = 1/2(1 + 2\beta)\alpha$. Equation (173) has been investigated in detail in the context of self-focusing of laser beams. For a Gaussian beam $|\hat{b}_\perp|^2 = \hat{b}_{\perp 0}^2 \exp(-\rho^2/a^2)$, the threshold for the self-focusing is

$Da^2 \hat{b}_{\perp 0}^2 > 2$, where a is the normalized (by ρ_s) beam width. The filamentation and collapse of KAW beams can constitute a novel mechanism for the plasma heating in an intermediate β-plasma.

5.9. SELF-INTERACTION BETWEEN DAWS

Here, we consider self-interaction between finite amplitude DAWs a nonuniform multicomponent plasma whose constituents are electrons and singly charged ions in an external magnetic field $B_0 \hat{\mathbf{z}}$. The plasma density is assumed to be inhomogeneous along the x-axis. In the electromagnetic fields, the electron and ion fluid velocities are given by (Shukla et al, 1984)

$$\mathbf{v}_e \approx \frac{1}{B_0} \mathbf{E}_\perp \times \hat{\mathbf{z}} - \frac{T_e}{e B_0 n_e} \hat{\mathbf{z}} \times \nabla n_e + v_{ez} \left(\hat{\mathbf{z}} + \frac{\mathbf{b}_\perp}{B_0} \right) \tag{174}$$

and

$$\mathbf{v}_i \approx \frac{1}{B_0} \mathbf{E}_\perp \times \hat{\mathbf{z}} + \frac{T_i}{e B_0 n_i} \hat{\mathbf{z}} \times \nabla n_i + \frac{1}{B_0 \omega_{ci}} \left(\partial_t + \mathbf{v}_i \cdot \nabla \right) \mathbf{E}_\perp , \tag{175}$$

where $\mathbf{E}_\perp = -\nabla_\perp \phi$ is the perpendicular component of the wave electric field, $\mathbf{b}_\perp = \nabla A_z \times \hat{\mathbf{z}}$ the perturbed magnetic field, ϕ the scalar potential, and A_z the parallel (to $B_0 \hat{\mathbf{z}}$) component of the vector potential. The parallel component of the electron fluid velocity is given by

$$v_{ez} \approx \frac{1}{\mu_0 n_e e} \nabla_\perp^2 A_z , \tag{176}$$

where we have ignored the ion motion parallel to $\hat{\mathbf{z}}$, as well as neglected the compressional magnetic field perturbation. Thus, ion- acoustic and magnetosonic waves are decoupled in our low-β ($\beta \ll 1$) system.

Substituting (174) into the electron continuity equation, letting $n_j = n_0(x) + n_1$, where $n_1 (\ll n_0)$ is the particle number density perturbation, and using (176) we obtain

$$d_t n_1 - \frac{1}{B_0} \hat{\mathbf{z}} \times \nabla n_0 \cdot \nabla \phi + \frac{1}{\mu_0 e} d_z \nabla_\perp^2 A_z = 0 , \tag{177}$$

where $d_t = \partial_t + B_0^{-1} \hat{\mathbf{z}} \times \nabla \phi \cdot \nabla$ and $d_z = \partial_z + B_0^{-1} \nabla A_z \times \hat{\mathbf{z}} \cdot \nabla$. We have assumed that $(\omega_{pe}^2 / \omega_{ce}) |\hat{\mathbf{z}} \times \nabla \phi \cdot \nabla| \gg c^2 \partial_z \nabla_\perp^2 A_z$.

On the other hand, substitution of the ion fluid velocity (175) into the ion continuity equation (assuming quasineutrality) yields

$$d_t n_1 - \frac{1}{B_0} \hat{\mathbf{z}} \times \nabla n_0 \cdot \nabla \phi - \frac{n_0}{B_0 \omega_{ci}} \left(d_t + \mathbf{u}_{i*} \cdot \nabla \right) \nabla_\perp^2 \phi -$$

$$- \frac{T_i}{e B_0^2 \omega_{ci}} \nabla_\perp \cdot \left[(\hat{\mathbf{z}} \times \nabla n_1) \cdot \nabla \nabla_\perp \phi \right] = 0 . \tag{178}$$

Subtracting (178) from (177) we obtain the modified ion vorticity equation

$$\left(d_t + u_{i*}\partial_y\right)\nabla_\perp^2\phi + v_A^2 d_z\nabla_\perp^2 A_z +$$

$$+\frac{T_i}{eB_0 n_0}\nabla_\perp\cdot\left[(\hat{\mathbf{z}}\times\nabla n_1)\cdot\nabla\nabla_\perp\phi\right] = 0\ . \tag{179}$$

By using (174) and (176), the parallel component of the electron momentum equation can be written as

$$\left(\partial_t + u_{e*}\partial_y\right)A_z - \lambda_e^2 d_t\nabla_\perp^2 A_z + d_z\left(\phi - \frac{T_e}{en_0}n_1\right) = 0\ . \tag{180}$$

Equations (177), (179) and (180) are the desired nonlinear equations for the coupled drift-Alfvén modes in nonuniform magnetoplasmas. In a uniform cold plasma, they reduce to those derived earlier (Shukla and Stenflo, 1985) *viz.*

$$d_t\nabla_\perp^2\phi + v_A^2 d_z\nabla_\perp^2 A_z = 0\ , \tag{181}$$

and

$$d_t A_z - \lambda_e^2 d_t\nabla_\perp^2 A_z + \partial_z\phi = 0\ , \tag{182}$$

which govern the nonlinear interactions between finite amplitude inertial Alfvén waves.

5.10. QUASI-STATIONARY VORTICES

Let us now consider stationary solutions of the nonlinear Equations (177), (179) and (180) , assuming that all the field variables depend on x and $\eta = y + \alpha z - ut$, where u is the translation speed of the vortex along the y -axis, and α the angle between the wave front normal and the (x, y) plane. Two cases are considered. First, in the stationary η-frame, (180) for $\lambda_e^2|\nabla_\perp^2| \ll 1$ can be written as (Shukla *et al.*, 1986b)

$$\hat{D}_A\left(\phi - \frac{T_e}{en_0}n_1 - \frac{u - u_{e*}}{\alpha}A_z\right) = 0\ , \tag{183}$$

where $\hat{D}_A = \partial_\eta + (1/\alpha B_0)[(\partial_\eta A_z)\partial_x - (\partial_x A_z)\partial_\eta]$. A solution of (183) is

$$n_1 = \frac{n_0 e}{T_e}\phi - \frac{n_0 e(u - u_{e*})}{\alpha T_e}A_z\ . \tag{184}$$

Writing (177) in the stationary frame, and making use of (184) it can be put in the form

$$\hat{D}_A\left(\lambda_{De}^2\nabla_\perp^2 A_z + \frac{u(u - u_{e*})}{\alpha^2 c^2}A_z - \frac{u - u_{e*}}{\alpha c^2}\phi\right) = 0\ , \tag{185}$$

where $\lambda_{De} = v_{te}/\omega_{pe}$ is the electron Debye radius. A solution of (185) is

$$\lambda_{De}^2 \nabla_\perp^2 A_z + \frac{u(u - u_{e*})}{\alpha^2 c^2} A_z - \frac{u - u_{e*}}{\alpha c^2} \phi = 0 \ . \tag{186}$$

The modified ion vorticity Equation (179) for cold ions can be expressed as

$$\hat{D}_\phi \nabla_\perp^2 \phi = 0 \ , \tag{187}$$

where $\hat{D}_\phi = \partial_\eta - (uB_0)^{-1}[(\partial_x \phi)\partial_\eta - (\partial_\eta \phi)\partial_x]$.

Combining (186) and (187) we obtain

$$\hat{D}_\phi \left(\nabla_\perp^2 \phi + \frac{p}{\rho_s^2}\phi + \frac{u - u_{e*}}{\alpha \rho_s^2} A_z \right) = 0 \ , \tag{188}$$

where $p = (u_{e*} - u)/u$. A typical solution of (188) is

$$\nabla_\perp^2 \phi + \frac{p}{\rho_s^2}\phi + \frac{u - u_{e*}}{\alpha \rho_s^2} A_z = C_1 (\phi - uB_0 x) \ , \tag{189}$$

where C_1 is an integration constant.

Eliminating A_z from (186) and (189), we obtain a fourth order inhomogeneous differential equation

$$\nabla_\perp^4 \phi + F_1 \nabla_\perp^2 \phi + F_2 \phi + C_1 \frac{u^2(u - u_{e*})B_0}{\alpha^2 c^2 \lambda_{De}^2} x = 0 \ , \tag{190}$$

where $F_1 = (p/\rho_s^2) - C_1 + u(u - u_{e*})/\alpha^2 c^2 \lambda_{De}^2$,
and

$$F_2 = (u - u_{e*})^2 /\alpha^2 c^2 \lambda_{De}^2 \rho_s^2 + (p - C_1 \rho_s^2)u(u - u_{e*})/\alpha^2 c^2 \lambda_{De}^2 \rho_s^2 \ .$$

We note that the outer solution, where $C_1 = 0$ and $F_2 = 0$, of (190) has a long tail for $(u - u_{e*})(\alpha^2 v_A^2 - u^2) > 0$. In the outer region ($r > R$), where R is the vortex radius, we set $C_1 = 0$ and write the solution of (190) as (Liu and Horton, 1994; Shukla *et al.*, 1986c; Mikhailovskii *et al.*, 1987)

$$\phi = [Q_1 K_1(s_1 r) + Q_2/r]\cos\theta \ , \tag{191}$$

where Q_1 and Q_2 are constants, and $s_{1,2}^2 = -[-\alpha_1 \pm (\alpha_1^2 - 4\alpha_2)^{1/2}/2$ for $\alpha_1 < 0$ and $\alpha_1^2 > 4\alpha_2 > 0$. Here, $\alpha_1 = (p/\rho_s^2) + u(u - u_{e*})/\alpha^2 c^2 \lambda_{De}^2$ and $\alpha_2 = [(u - u_{e*})^2 + u(u - u_{e*})p]/\alpha^2 c^2 \lambda_{De}^2 \rho_s^2$. In the inner region ($r < R$), the solution reads

$$\phi = \left[Q_3 J_1(s_3 r) + Q_4 I_1(s_4 r) - \frac{C_1}{\lambda_{De}^2} \frac{u^2(u - u_{e*})B_0}{\alpha^2 c^2 F_2} r \right] \cos\theta \ , \tag{192}$$

where Q_3 and Q_4 are constants. We have defined $s_{3,4} = [(F_1^2 - 4F_2)^{1/2} \pm F_1]/2$ for $F_2 < 0$.

Second, we present the double vortex solution of (181) and (182). Thus, we write them in the stationary frame as

$$\hat{D}_\phi \nabla_\perp^2 \phi - \frac{v_A^2 \alpha}{u} \hat{D}_A \nabla_\perp^2 A_z = 0 \, , \tag{193}$$

and

$$\hat{D}_\phi \left[\left(1 - \lambda_e^2 \nabla_\perp^2\right) A_z - \frac{\alpha}{u}\phi \right] = 0 \, . \tag{194}$$

It is easy to verify that (194) is satisfied by

$$\left(1 - \lambda_e^2 \nabla_\perp^2\right) A_z - \frac{\alpha}{u}\phi = 0 \, . \tag{195}$$

By using (193) one can eliminate $\nabla_\perp^2 A_z$ from (195), yielding

$$\hat{D}_\phi \left[\nabla_\perp^2 \phi + \frac{\alpha^2 v_A^2}{u^2 \lambda_e^2}\phi - \frac{\alpha v_A^2}{u \lambda_e^2} A_z \right] = 0 \, . \tag{196}$$

A typical solution of (196) is

$$\nabla_\perp^2 \phi + \beta_1 \phi - \beta_2 A_z = C_2 \left(\phi - u B_0 x\right) \, , \tag{197}$$

where $\beta_1 = \left(\alpha^2 v_A^2 / u^2 \lambda_e^2\right)$, $\beta_2 = \alpha v_A^2 / uc\lambda_e^2$, and C_2 is an integration constant.
Eliminating A_z from (193) and (197) we obtain

$$\nabla_\perp^4 \phi + F_1 \nabla_\perp^2 \phi + F_2 \phi - \frac{C_2 u B_0}{\lambda_e^2} x = 0 \, , \tag{198}$$

where $F_1 = \lambda_e^{-2} \left(\alpha^2 v_A^2 / u^2 - 1\right) - C_2$, and

$$F_2 = C_2 / \lambda_e^2 \, .$$

Equation (198) is similar to (189) and its bounded solutions (similar to (191) and (192)) exist provided that $u^2 > \alpha^2 v_A^2$.

5.11. DYNAMICS OF VORTICES

Here we suggest that the observed ray-like forms of the aurora can be understood in terms of the nonlinear IAW in cold plasmas. Assuming that the auroral structures have a very long extension along the magnetic field-lines, we can model nonlinearly interacting parallel electron current sheets by means of the equations

$$\frac{d}{dt} \nabla_\perp^2 \phi + \frac{v_A^2}{B_0} \nabla A_z \times \hat{\mathbf{z}} \cdot \nabla \nabla_\perp^2 A_z = 0 \, , \tag{199}$$

and

$$\frac{d}{dt} \left(A_z - \lambda_e^2 \nabla_\perp^2 A_z\right) = 0 \, , \tag{200}$$

which are derived from (181) and (182) by assuming that $\partial \nabla_\perp^2 A_z / \partial z = 0$ and $\partial \phi / \partial z = 0$. Equations (199) and (200) are numerically analysed by Chmyrev *et al.*, (1992), by taking
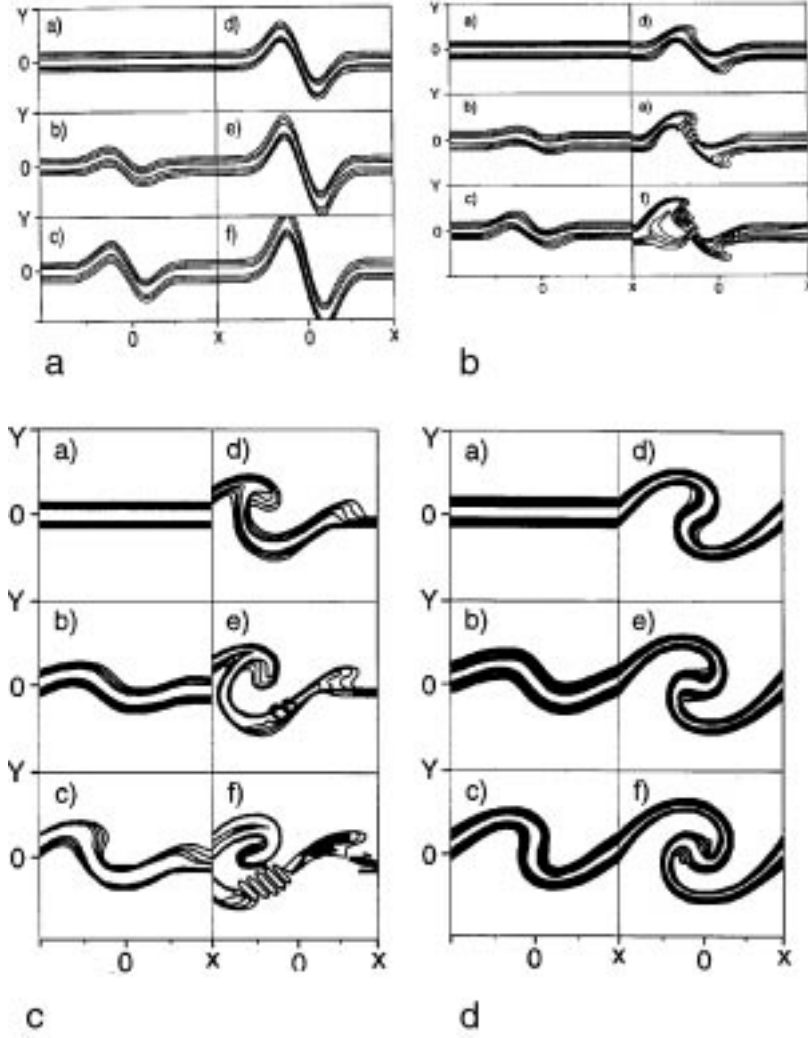
Figure 36. Numerical simulation results of the development and dynamics of folds, spirals and vortices. (After Chmyrev *et al.*, 1992.)

$$\nabla_\perp^2 A_z = A_0 k^2 \ln \cosh(ky) \tag{201}$$

and

$$\phi = \phi_1 \tanh(ky) + \phi_2 \exp(-\gamma x^2) \tag{202}$$

as initial conditions, with $A_0 = 0.1$, $k = 1.18$, $\phi_1 = 1$, $\phi_2 = 5$, and $\gamma = 0.15$. Here, A_z, A_0, ϕ_1, ϕ_2 are in units of T_e/e and the space variables (k) are normalized by ρ_s (ρ_s^{-1}).

Figure 36(a) displays temporal evolution of the parallel electron current sheet. We see the formation of a fold within 2 s for the auroral plasma parameters. Fig-

ure 36(b) exhibits temporal evolution of the parallel current sheet for the same current density as in Figure 36(a), but assuming that $\phi = 5 \tanh(ky)$. Here we see the formation of a fold and the disintegration of a fold into the vortex chain.

Figure 36(c) shows the formation of a spiral (S structure) in the current sheet for the same parameters as in Figure 36(a) but with an axi-symmetric electric field with $\phi = \exp(-0.2x^2)$. The formation of spiral and the generation of a vortex chain in the spiral are depicted in Figure 36(d). Here, the profile of the parallel electron current density and the other parameters are the same as in Figure 36(a), whereas the scalar potential has the same form as in Figure 36(b). The numerical simulations thus demonstrate that within the framework of the nonlinear IAW model, one can describe all the observational stages of the development of folds, spirals, as well as the disintegration of folds and spirals into the vortex chain. Physically, the nonlinear mode coupling of the inertial Alfvén fluctuations self-organize into larger-scale structures, which eventually break into smaller-size coherent vortex structures. The energy transfer from large vortical motion into small vortical motion is thus evident in the low-beta magnetoplasma containing inertial Alfvén wave turbulence. The results have relevance to the structures that are observed in the aurora.

5.12. CHAOS IN ALFVÉNIC TURBULENCE

Finally, in this section, we show that the nonlinear equations governing the dynamics of low-frequency, flute-like Alfvénic disturbances in a nonuniform collisional plasma can be written as a set of three coupled nonlinear equations. The latter are a generalization of the Lorenz–Stenflo equations (Lorenz, 1963; Stenflo, 1996), which admit chaotic fluid behavior of electromagnetic turbulence in a nonuniform magnetoplasma.

The nonlinear dynamics of low-frequency, long wavelength (in comparison with the ion gyroradius) electromagnetic fields in a nonuniform magnetized plasma containing sheared plasma flows is governed by the ion vorticity equation

$$(D_t - \mu \nabla_\perp^2) \nabla_\perp^2 \phi - \frac{\omega_{ci} J_0'}{n_0 e} \partial_y A_z - \frac{v_A^2}{B_0} (\hat{\mathbf{z}} \times \nabla A_z) \cdot \nabla \nabla_\perp^2 A_z = 0 , \qquad (203)$$

and the parallel (to $\hat{\mathbf{z}}$) component of the electron momentum equation

$$\left[(1 - \lambda_e^2 \nabla_\perp^2) D_t - \eta \nabla_\perp^2 \right] A_z + \frac{v_0'}{\omega_{ce}} \partial_y \phi = 0 , \qquad (204)$$

where $D_t = \partial_t + B_0^{-1} \hat{\mathbf{z}} \times \nabla \phi \cdot \nabla$, $\nabla_\perp^2 = \partial_x^2 + \partial_y^2$, $v_0' = \partial v_{e0}/\partial x$, $J_0' = \partial J_0/\partial x$, and $J_0 = n_0 e (v_{i0} - v_{e0})$ is the equilibrium plasma current. Furthermore, $\eta = v_e \lambda_e^2$ is the plasma resistivity, and $\mu = (3/10) v_i \rho_i^2$ is the coefficient of ion gyroviscosity. The electron and ion collision frequencies are denoted by v_e and v_i, respectively, and ρ_i is the ion Larmor radius. We have assumed that the phase velocities of the disturbances are much larger than the electron and ion diamagnetic drift velocities.

Equations (203) and (204) are the nonlinear equations governing the dynamics of finite amplitude Alfvén-like disturbances in a nonuniform magnetoplasma containing equilibrium magnetic field-aligned sheared plasma flows. In the absence of the nonlinear interactions, we readily obtain from (203) and (204) the dispersion relation (Shukla, 1987)

$$\omega^2 + i\omega\Gamma - \Omega^2 + \gamma_0^2 = 0 \, , \tag{205}$$

where $\Gamma = [\mu + \eta/(1 + K^2\lambda_e^2)]K^2$, $\Omega^2 = \mu\eta K^4/(1 + K^2\lambda_e^2)$, $\mathbf{K} = \hat{\mathbf{x}}K_x + \hat{\mathbf{y}}K_y$ is the wave vector, and $\gamma_0^2 = -m_e J_0' v_{e0}' K_y^2/m_i n_0 e(1 + K^2\lambda_e^2)K^2$. In the absence of the equilibrium current and velocity gradients, (205) gives convective cells and magnetostatic modes, which are decoupled. However, when the current and velocity gradients are opposite to each other, we obtain an instability provided that $\gamma_0^2 > \Omega^2 - \Gamma^2/4$. The maximum growth rate of that instability is $|\gamma_0|$.

In the following, we follow Lorenz and Stenflo and derive a set of equations which are appropriate for studying the temporal behavior of chaotic motion involving low-frequency electromagnetic waves in a dissipative magnetoplasma with sources. Accordingly, we introduce the Ansatz

$$\phi = \phi_1(t)\sin(k_x x)\sin(k_y y) \, , \tag{206}$$

and

$$A_z = A_1(t)\sin(k_x x)\cos(k_y y) - A_2(t)\sin(2k_x x) \, , \tag{207}$$

where k_x and k_y are constant parameters, and ϕ_1, A_1 and A_2 are amplitudes which are only functions of time. By substituting (206) and obtain (Mirza and Shukla, 1997) (207) into (203) and (204), we readily

$$k^2 d_t\phi_1 = -\mu k^4\phi_1 + \alpha_1 k_y A_1 - \alpha_2(k^2 - 4k_x^2)k_x k_y A_1 A_2 \, , \tag{208}$$

$$\left(1 + k^2\lambda_e^2\right)d_t A_1 = -\eta k^2 A_1 - \alpha_3 k_y\phi_1 + \frac{c}{B_0}\left[1 + k^2\lambda_e^2 - 6k_x^2\lambda_e^2\right]k_x k_y A_2\phi_1 \tag{209}$$

and

$$(1 + 4k_x^2\lambda_e^2)d_t A_2 = -\frac{c}{2B_0}(1 + 4k_x^2\lambda_e^2)k_x k_y\phi_1 A_1 - 4\eta k_x^2 A_2 \, , \tag{210}$$

where $\alpha_1 = \omega_{ci}J_0'/n_0 e$, $\alpha_2 = v_A^2/B_0$ and $\alpha_3 = v_{e0}'/\omega_{ce}$. We note that the terms proportional to $\sin(3k_x x)$ have been dropped in the derivation of (208) to (210). This approximation is often employed by many authors for deriving the relevant Lorenz-like equations in many branches of physics.

Equations (208) to (210) can be appropriately normalized so that they can be put in a form which is similar to that of Lorenz and Stenflo. We have (Mirza and Shukla, 1997; Shukla *et al.*, 1998b)

$$d_\tau X = -\sigma X + \sigma Y + \delta Y Z \, , \tag{211}$$

$$d_\tau Y = -XZ + \gamma X - Y \tag{212}$$

and

$$d_\tau Z = XY - \beta Z , \tag{213}$$

which describe the nonlinear coupling between various amplitudes. Here, $\sigma = \mu$ $\left(1 + k^2\lambda_e^2\right)/\eta$, $\gamma = -\alpha_1\alpha_3 k_y^2/(\eta\mu k^6)$, $\beta = 4k_x^2\left(1 + k^2\lambda_e^2\right)/(1 + 4k_x^2\lambda_e^2)k^2$, and the new parameter $\delta = \alpha_2(k_y^2 - 3k_x^2)\left(1 + k^2\lambda_e^2\right)\mu^2 k^6 B_0/[\alpha_1^2 k_y^2(1 + k^2\lambda_e^2 - 6k_x^2\lambda_e^2)]$, with $k^2 = k_x^2 + k_y^2$ and $\tau = t/t_0$, where $t_0 = \eta k^2/\left(1 + k^2\lambda_e^2\right)$.

A comment is in order. If we set $\delta = 0$, which happens for $k_y^2 = 3k_x^2$, then (211) to (213) reduce to the Lorenz type equations. However, the normalizations used here (Mirza and Shukla, 1997) are

$$\phi_1 = \left\{ \frac{\sqrt{2}\eta k^2 B_0}{k_x k_y \left[\left(1 + k^2\lambda_e^2\right)\left(1 + k^2\lambda_e^2 - 6k_x^2\lambda_e^2\right)\right]^{1/2}} \right\} X , \tag{214}$$

$$A_1 = \left\{ \frac{\sqrt{2}\eta\mu k^6 B_0}{\alpha_1 k_x k_y^2 \left[\left(1 + k^2\lambda_e^2\right)\left(1 + k^2\lambda_e^2 - 6k_x^2\lambda_e^2\right)\right]^{1/2}} \right\} Y , \tag{215}$$

and

$$A_2 = -\left[\frac{\eta\mu k^6 B_0}{\alpha_1 k_x k_y^2 \left(1 + k^2\lambda_e^2 - 6k_x^2\lambda_e^2\right)} \right] Z . \tag{216}$$

Let us now discuss the chaotic fluid behavior of electromagnetic turbulence that is governed by (211) to (213). We observe that the equilibrium points of the dynamical equations are (Mirza and Shukla, 1997)

$$X_0 = \pm\{\beta(\gamma - 2 + \delta\gamma^2/\sigma) + \tfrac{1}{2}[(\gamma - 2 + \delta\gamma^2/\sigma)^2 + 4(\gamma - 1)]^{1/2}\}^{1/2} , \tag{217}$$

$$Y_0 = \frac{\gamma\beta X_0}{(\beta + X_0^2)} \tag{218}$$

and

$$Z_0 = \frac{X_0 Y_0}{\beta} . \tag{219}$$

In the absence of the δ-term, we note that for $|\gamma| > 1$, the equilibrium fixed points $[X_0 = Y_0 = \pm\sqrt{\beta}(|\gamma| - 1)^{1/2}]$ and $Z_0 = |\gamma| - 1)$ are unstable, resulting in convective cell motions. Thus, the linear instability should saturate by attracting to one of these new fixed states. Furthermore, it is worth mentioning that a detailed behavior of chaotic motion for $k_y \neq \sqrt{3}k_x$ can studied numerically (Sparrow, 1982) by solving (211) to (213).

6. Present Understanding and Outlook

This review is concerned with an eclectic set of observations and theory that have the single underlying theme of being simultaneously related to the small-scale aurora and Alfvén waves. Up to this point we have presented mostly observational facts and theoretical ideas vaguely related to the observational facts. We have yet to integrate our pool of experimental understanding and theoretical knowledge into a revealing picture of the phenomena in question. To do so requires a bit of subjectivity and thus the picture is shaded by the authors' perspective. Nevertheless, a presentation of facts without an attempt to draw conclusions goes counter to the main goal of a review paper which is to assess our understanding of the subject, formulate a picture and point out the gaps in our present understanding. We briefly summarize the observational facts, then summarize the theories which have been motivated by observations and then finally form a picture that seems to be a best fit between observation and theory.

Freja and FAST satellite observations have shown the existence of oblique Alfvén waves which is consistent with a first order structure in the form of a current sheet and which is usually associated with transverse structure resembling vortices or co-axial current channels. Alfvénic structures are often situated within larger scale density cavities and associated with short-scale electrostatic waves, possibly strong parallel electric fields, electron acceleration, and ion heating. The structures are consistent with the optical signature as shown in Figure 1 which is usually referred to as a thin auroral arc. As yet simultaneous measurements of optical signatures and Alfvén features are very rare so that we cannot state with certainty that Alfvénic structures are auroral arcs. However, the optical characteristics are compatible with *in-situ* electric and magnetic field data which show either a sheet-like structure or a vortex-like structure. The non-uniqueness of one-point *in situ* measurements does not allow one to make definitive statements in this regard.

This picture of Alfvénic structure has been formed from the prodigious volume of data collected by *Freja* and FAST, and summarized in Sections 3.3 and 3.4. The main feature in the observations is the widespread presence of dispersive Alfvén waves with intermittent occurrence of electromagnetic singularities, possibly related to auroral arcs.

The experimental facts have motivated theorists to formulate models to explain specific properties of Alfvénic structures. There are many aspects of dispersive Alfvén waves that we understand well and these we have discussed in Section 2. We now summarize our understanding.

It has been noted that dispersive Alfvén waves have a finite electric field parallel to the external magnetic field, and that this electric field is caused by the charge separation arising from the finite ion gyroradius and ion polarization effects. The parallel electric force can be balanced by the parallel electron pressure gradient or the parallel electron inertial acceleration, giving rise to dispersive effects across the magnetic field lines. On the other hand, consideration of the Alfvén wave fre-

quencies close to the ion gyrofrequency provides the possibility of Alfvén wave dispersion (with parallel scale size of the order of collisionless ion skin depth c/ω_{pi}) along the external magnetic field lines.

The two types of dispersive Alfvén waves which can have either a parallel phase velocity either larger or smaller than the electron thermal velocity, are the inertial and kinetic Alfvén waves, These appear in a magnetoplasma with $\beta \ll m_e/m_i$ and $\beta \gg m_e/m_i$, respectively. Both of these waves have the requisite properties to play a very important role with regard to the particle acceleration, particle heating, and they can also initiate a number of nonlinear effects. Dispersive Alfvén waves can be generated by electron beams, cross field pressure gradients, shear flow instability, magnetic reconnection, moving potential and current sources as well as yet to be discovered processes.

The fundamental properties of the dispersive Alfvén wave: the cross field spreading of energy in a conical pattern; the parallel and perpendicular phase velocities; the backward nature of the inertial wave and the forward nature of the kinetic wave have all been firmly established by laboratory studies. Moreover, deep magnetic field-aligned density striations, with cross field scale size on the order of the electron skin depth, have been observed in low beta laboratory plasmas to spontaneously generate Alfvén wave due to the cross field pressure gradient in the wall of the cavity. Thus it is not unexpected that short scale density cavities and Alfvén waves are frequently observed together by spacecraft.

Large amplitude dispersive Alfvén waves can either interact among themselves or with the background plasma, giving rise to such interesting effects as the bare and envelope solitons, density cavities, as well as vortices of various scales. Theoretical studies, which were based on the ion drift approximation, have predicted the existence of planar dispersive Alfvén solitons. The inclusion of higher order ion polarization drift in the nonlinear ion advection term, however, puts a question mark to the planar dispersive Alfvén solitons. The final answer to the existence of planar Alfvén solitons will depend on the inclusion of the full transverse wave magnetic fields and the full ion perpendicular velocities in any realistic theoretical and simulation studies. Most importantly, Alfvénic structures are not observed to be entirely planar and most certainly have important three-dimensional character.

Clearly the observed inhomogeniety of the density, electric and magnetic field provides multiple sources of free energy for the generation of structure through linear instability. Self-organization in the form of folds, curls, and a vortex street in auroral arcs can be described in terms of the three-dimensional nonlinear inertial Alfvén wave models. The dynamical evolution leading to the various auroral forms can be the result of nonlinear shear flow instability or magnetic tearing. Stationary vortex solutions of the nonlinear equations may represent an idealized steady state. Mode coupling equations for nonlinear dispersive Alfvén waves have been developed, which have been use for studying energy cascading and the properties of Alfvén vortices. An energy cascading scenario may explain the generation of short wavelength ($\ll \lambda_e$) electrostatic disturbances due to the parametric processes

involving dispersive inertial Alfvén waves. Auroral plasma density cavity formation may be the result of the combined effects of the ponderomotive force and the electron Joule heating in the IAW fields. Finally, consideration of sources and sinks provides the possibility of chaos in dispersive Alfvén wave turbulence.

A critical evaluation of the literature reveals that while the linear Alfvén wave physics seems to be mostly understood for homogeneous plasma, there is still a good deal to understand about the nonuniform physics of dispersive Alfvén waves and our comprehension of the nonlinear physics is still in its infancy. We believe that further data analysis should be carried out to obtain the complete information on the plasma parameters and on the fields of Alfvénic structures such as the scale sizes along and across the geomagnetic field lines, speed, electric and magnetic field strengths. Theoretical and simulation studies should focus on solving truly three-dimensional problems without resorting to many approximations which may not be relevant to observations. Finally, laboratory experiments should be designed to produce some of the nonlinear effects (*viz.*, parametric instabilities, density cavitation, density bumps, solitons, vortices, shocks, etc.) involving dispersive Alfvén waves.

Acknowledgements

References

Alfvén, H.: 1942, 'Existence of Electromagnetic-Hydromagnetic Waves', *Nature* **150** (3805), 405.

Alfvén, H. and Fälthammar, C. G.: 1963, *Cosmical Electrodynamics*, Clarendon Press, Oxford.

Aikio, A. T., Blomberg, L. G., Marklund, G. T. and Yamauchi, M.: 1996, 'On the Orgin of the High-Altitude Electric Field Fluctuations in the Auroral Zone', *J. Geophys. Res.* **101**, 27,157.

Anderson, B. J., Engebretson, M. J., Rounds, S. P., Zanetti, L. J. and Potemra, T. A.: 1990, 'A Statistical Study of Pc 3-5 Pulsations Observed by the AMPTE/CCE Magnetic Field Experiment', *J. Geophys. Res.* **85**, 10,495.

André, M., Norqvist, P., Anderson, L., Eliason, L., Ericsson, A., Blomberg, L., Erlandson, R. and Waldemark, J.: 1998, 'Ion Energization Mechanisms at 1700 km in the Auroral Region', *J. Geophys. Res.* **103**, 4199.

Bellan, P.: 1998, 'Collisionless Reconnection Using Alfvén Wave Radiation Resistance', *Phys. Plasmas* **5** (9), 3081.

Bellan, P. and Stasiewicz, K.: 1998, 'Fine-Scale Cavitation of Ionospheric Plasma Caused by Inertial Alfvén Wave Ponderomotive Force', *Phys. Rev. Lett.* **80** (16), 3523.

Bellan, P. M.: 1977, 'Plasma Ringing Associated with Pulsed Resonance Cones', *Phys. Fluids* **20**, 649.

Bellan, P. M.: 1994, 'Alfvén Resonance Reconsidered: Exact Equations for Wave Propagation Across a Cold Inhomogenous Plasma', *Phys. Plasmas* **1**, 3523.

Bellan, P. M.: 1996a, 'Mode Conversion into Non-MHD Waves at the Alfvén Layer: The Case Against the Field Line Resonance Concept', *J. Geophys. Res.* **101**, 24,887.

Bellan, P. M.: 1996b, 'New Model for ULF Pc5 Pulsations: Alfvén Cones', *Geophys. Res. Lett.* **23**, 1717.

Belon, A. E., Maggs, J. E., Davis, T. N., Mather, K. B., Glass, N. W. and Hughes, G. F.: 1969, 'Conjugacy of Visual Auroras During Magnetically Quiet Periods', *J. Geophys. Res.* **74**, 1.

Bennett, E. L., Temerin, M. and Mozer, F. S.: 1983, 'The Distribution of Auroral Electrostatic Shocks Below 8000-km Altitude', *J. Geophys. Res.* **88**, 7107.

Benson, R. F. and Calvert, W.: 1979, 'ISIS-1 Observations at the Source of Auroral Kilometric Radiation', *Geophys. Res. Lett.* **6**, 47.

Benson, R. F., Calvert, W. and Klumpar, D. M.: 1980, 'Simultaneous Wave and Particle Observations in the Auroral Kilometric Radiation Source Region', *Geophys. Res. Lett.* **7**, 959.

Berthelier, A., Cerisier, J. C., Berthelier, J. J. and Rezeau, L.: 1991, 'Low Frequency Magnetic Turbulence in the High-Latitude Topside Ionosphere: Low-Frequency Waves or Field-Aligned Currents?', *J. Atmospheric Terrest. Phys.* **53**, 333.

Boehm, M., Paschman, G., Clemmons, J., Höfner, H. and and, R. F.: 1994, 'The Freja Wave and Plasma Density Experiment', *Space Sci. Rev.* **70**, 577.

Boehm, M. H., Carlson, C. W., McFadden, J. P. and Mozer, F. S.: 1990, 'High-Resolution Sounding Rocket Observations of Large-Amplitude Alfvén Waves', *J. Geophys. Res.* **95**, 12,157.

Boehm, M. H., Clemmons, J., Wahlund, J., Eriksson, A., Eliasson, L., Blomberg, L., Kintner, P. and Höfner, H.: 1995, 'Observation of an Upward-Directed Electron Beam with the Perpendicular Temperature of the Cold Ionosphere', *Geophys. Res. Lett.* **22**, 2103.

Bonnell, J., Kintner, P., Wahlund, J.-E., Lynch, K. and Arnoldy, R.: 1996, 'Interferometric Determination of Broadband ELF Wave Phase Velocity Within a Region of Transverse Auroral Ion Acceleration', *Geophys. Res. Lett.* **23**, 3297.

Borg, G. G., Brennan, M. H., Cross, R. C., Giannone, L. and Donnelly, I. J.: 1985, 'Guided Propagation of Alfvén Waves in a Toroidal Plasma', *Plasma Phys. Contr. Fus.* **27**, 1125.

Bostick, W. H. and Levine, M. A.: 1952, 'Experimental Demonstration in the Laboratory of the Existence of Magneto-Hydrodynamic Waves in Ionized Helium', *Phys. Rev.* **94**, 671.

Brown, R. R.: 1966, 'Electron Precipitation in the Auroral Zone', *Space Sci. Rev.* **5**, 311.

Chang, T.: 1982, 'Exact Nonlinear EIC Waves of Arbitrary Amplitude and Cavitons', *Int. J. Eng. Sci.* **20**, 231.

Chaston, C. C., Carlson, C. W., Peria, W. J., Ergun, R. E. and McFadden, J. P.: 1999, 'FAST Observations of Inertial Alfvén Waves in the Dayside Aurora', *Geophys. Res. Lett.* **26**(6), 647.

Chen, L. and Hasegawa, A.: 1974a, 'Plasma Heating by Spatial Resonance of Alfvén Waves', *Phys. Rev. Lett.* **17**, 1399.

Chen, L. and Hasegawa, A.: 1974b, 'A Theory of Long-Period Magnetic Pulsations, 1, Steady State Excitation of Field Line Resonance', *J. Geophys. Res.* **79**, 1024.

Chen, L. and Hasegawa, A.: 1991, 'Kinetic Theory of Geomagnetic Pulsations, 1, Internal Excitations by Energetic Particles', *J. Geophys. Res.* **96**, 1503.

Cheng, C. Z. and Johnson, J. R.: 1999, 'A Kinetic-Fluid Model', *J. Geophys. Res.* **104**, 413.

Chmyrev, V. M., Bilichenko, S. V., Pokhotelov, O. A., Marchenko, V. A., Lazarev, V. I., Streltsov, A. V. and Stenflo, L.: 1988, 'Alfvén Vortices and Related Phenomena in the Ionosphere and the Magnetosphere', *Phys. Scripta* **38**, 841.

Chmyrev, V. M., Marchenko, V. A., Pokhotelov, O. A., Shukla, P. K., Stenflo, L. and Streltsov, A. V.: 1992, 'The Development of Discrete Active Auroral Forms', *IEEE Trans. Plasma Sci.* **20**(6), 764.

Chust, T., Louarn, P., Volverk, M., de Feraudy, H., Roux, A., Wahlund, J.-E. and Holback, B.: 1998, 'Electric Fields with Large Parallel Component Observed by Freja Spacecraft', *J. Geophys. Res.* **103**, 215.

Clark, A. E. and Seyler, C. E.: 1999, 'Electron Beam Formation by Small-Scale Oblique Inertial Alfvén Waves', *J. Geophys. Res.* **104**, 17233.

Cummings, W. D., O'Sullivan, R. J. and P. J. C. Jr.: 1969, 'Standing Alfvén Waves in the Magnetosphere', *J. Geophys. Res.* **74**, 778.

Drell, S. D., Foley, H. M. and Ruderman, M. A.: 1965, 'Drag and Propultion of a Large Satellite in the Ionosphere: An Alfvén Propulsion Engine in Space', *J. Geophys. Res.* **70**, 3131.

Dubinin, E. M., Israelevich, P. I., Kutiev, I., Nikolayeva, N. and Podgorny, I.: 1985, 'Localized Auroral Disturbances in the Morning Sector of the Topside Ionosphere as a Standing Electromagnetic Wave', *Planet. Space Res.* **33**, 597.

Dubinin, E. M., Israelevich, P. L. and Nikolayeva, N. S.: 1990, 'Auroral Electromagnetic Disturbances at an Altitude of 900 km', *Planetary Space Sci.* **38**, 97.

Dubinin, E. M., Volokitin, A. S., Israelevich, P. L. and Nikolayeva, N. S.: 1988, 'Auroral Electromagnetic Disturbances at an Altitude of 900 km: Alfvén Wave Turbulence', *Planet. Space Sci.* **36**, 949.

Eliasson, L., Norberg, O., Lundin, R., Olsen, S., Borg, H., Andre, M., Koskinen, H., Riihela, P., Boehm, M. and Wahlen, B.: 1994, 'The Freja Hot Plasma Experiment-Instrument and First Results', *Space Sci. Rev.* **70**, 563.

Fisher, R. K. and Gould, R. W.: 1971, 'Resonance Cones in the Field Pattern of a Radio Frequency Probe in a Warm Anisotropic Plasma', *Phys. Fluids* **14**, 857.

Gary, J. B., Zanetti, L. J., Potemra, B. J. A. and T. A., Clemmons, J. H., Winningham, J. D. and Sharber, J. R.: 1998, 'Identification of Auroral Oval Boundaries from *in situ* Magnetic Field Measurements', *J. Geophys. Res.* **103** (A3), 4187.

Gavrishchaka, V., Koepke, M. E. and Ganguli, G.: 1996, 'Dispersive Properties of Magnetized Plasma with a Field-Aligned Drift and Inhomogeneous Transverse Flow', *Phys. Plasmas* **3**, 3091.

Gekelman, W.: 1999, 'Review of Laboratory Experiments on Alfvén Waves and Their Relationship to Space Plasmas', *J. Geophys. Res.* **104**, 14417.

Gekelman, W., Leneman, D., Maggs, J. and Vincena, S.: 1994, 'Experimental Observations of Alfvén Wave Cones', *Phys. Plasmas* **1**, 3775.

Gekelman, W., Vincena, S. and Leneman, D.: 1997a, 'Experimental Observations of Shear Alfvén Waves Generated by Narrow Current Channels', *Plasma Phys. Control. Fusion* **39**, A101.

Gekelman, W., Vincena, S., Leneman, D. and Maggs, J.: 1997b, 'Laboratory Experiments on Shear Alfvén Waves and Their Relationship to Space Plasmas', *J. Geophys. Res.* **102**(A4), 7225.

Goertz, C. K.: 1984, 'Kinetic Alfvén Waves on Auroral Field Lines', *Planetary Space Sci.* **32**, 1387.

Goertz, C. K. and Boswell, R. W.: 1979, 'Magnetosphere-Ionosphere Coupling', *J. Geophys. Res.* **84**, 7239.

Greenwald, R. A. and Walker, A. D. M.: 1980, 'Energetics of Long Period Resonant Hydromagnetic Waves', *Geophys. Res. Lett.* **7**, 745.

Greifinger, C. and Greifinger, P.: 1968, 'Theory of Hydromagnetic Propagation in the Ionospheric Waveguide', *J. Geophys. Res.* **73**, 7473.

Gurnett, D., Huff, R. L., Menietti, J. D., Burch, J. L., Winningham, J. D. and Shawhan, S. D.: 1984, 'Correlated Low-Frequency Electric and Magnetic Noise Along the Auroral Field Lines', *J. Geophys. Res.* **89**, 8971.

Haerendel, G.: 1983, in B. Hultqvist and T. Hagfors (eds.), 'An Alfvén Wave Model of Auroral Arcs', *High-Latitude Space Plasma Physics*, Plenum, New York, p. 515.

Hasegawa, A.: 1976, 'Particle Acceleration by MHD Surface Wave and Formation of Aurora', *J. Geophys. Res.* **81**, 5083.

Hasegawa, A. and Chen, L.: 1975, 'Kinetic Process of Plasma Heating Due to Alfvén Wave Excitation', *Phys. Rev. Lett.* **35** (6), 370.

Hazeltine, R. D., Hsu, C. T. and Morrison, P. J.: 1987, 'Hamiltonian Four-Field Model for Nonlinear Tokamak Dynamics', *Physics Fluids* **30**, 3204.

Hilgers, A.: 1992, 'The Auroral Radiating Plasma Cavities', *Geophys. Res. Lett.* **19**, 237.

Hilgers, A., Holback, B., Holmgren, G. and Böstrom, B.: 1992, 'Probe Measurements of Low Plasma Densities with Application to the Auroral Acceleration Region and Auroral Kilometric Raditation Sources', *J. Geophys. Res.* **97**, 8631.

Holback, B., Jansson, S.-E., Åhlen, L., Lundgren, G., Lyngdahl, L., Powell, S. and Meyer, A.: 1994, 'The Freja Wave and Plasma Density Experiment', *Space Sci. Rev.* **70**, 577.

Hui, C.-H. and Seyler, C.: 1992, 'Electron Acceleration by Alfvén Waves in the Magnetosphere', *J. Geophys. Res.* **97** (A4), 3953.

Iijima, T. and Potemra, T. A.: 1978, 'Large Scale Characteristics of Field-Aligned Currents Associated with Substorms', *Geophys. Res.* **83**, 599.

Ishii, M., Sugiura, M., Iyemori, T. and Slavin, J. A.: 1992, 'Correlation between Magnetic and Electric Field Perturbations in the Field-Aligned Current Regions Deduced from DE2 Observations'. *J. Geophys. Res.* **97**, 13,877.

Johnson, J. R. and Cheng, C. Z.: 1997, 'Kinetic Alfvén Waves and Plasma Transport at the Magnetopause', *Geophys. Res. Lett.* **24**, 1423.

Karlsson, T. and Marklund, G. T.: 1996, 'A Statistical Study of Intense Low-Altitude Electric Fields Observed by Freja', *J. Geophys. Res.* **23**, 1005.

Kasha, M.: 1969, *The Ionosphere and Its Interaction with Satellites*, Gordon and Breach, Newark, N. J..

Kelley, M. C.: 1989, *The Earth's Ionosphere*, Academic Press, New York.

Kintner, P. M., Bonnell, J., Arnoldy, R., Lynch, K., Pollack, C. and Moore, T.: 1996, 'SCIEFER - Transverse Ion Acceleration and Plasma Waves', *Geophys. Res. Lett.* **23**, 1873.

Kintner, P. M., Kelley, M. C. and Mozer, F. S.: 1978, 'Electrostatic Hydrogen Cyclotron Waves Near One Earth Radius Altitude in the Polar Magnetosphere', *Geophys. Res. Lett.* **5**, 139.

Kivelson, M. G. and Southwood, D. J.: 1986, 'Coupling of Global Magnetospheric MHD Eigenmodes to Field Line Resonances', *J. Geophys. Res.* **91**, 4345.

Kletzing, C., Cattell, C., Mozer, F. S., Akasofu, S.-I. and Makita, K.: 1983, 'Evidence for Electrostatic Shocks as the Source of Discrete Auroral Arcs', *J. Geophys. Res.* **88**, 41.

Kletzing, C. and Torbert, R. B.: 1994, 'Electron Time Dispersion', *J. Geophys. Res.* **99**, 2159.

Kletzing, C. A.: 1994, 'Electron Acceleration by Kinetic Alfvén Waves', *J. Geophys. Res.* **99**, 11095.

Kletzing, C. A., Mozer, F. S. and Torbert, R. B.: 1998, 'Electron Temperature and Density at High Latitude', *J. Geophys. Res.* **103**, 14837.

Knight, L.: 1973, 'Parallel Electric Fields', *Planetary Space Sci.* **21**, 4326.

Knudsen, D. J.: 1990, 'Distinguishing Alfvén Waves from Quasi-Static Field Structures Associated with He Discrete Aurora: Sounding Rocket and HILAT Satellite Measurements', *Geophys. Res. Lett.* **17**, 921.

Knudsen, D. J., Clemmons, J. H. and Wahlund, J.-E.: 1998, 'Correlation Between Core Ion Energization, Suprathermal Electron Bursts, and Broadband ELF', *J. Geophys. Res.* **103**, 4171.

Knudsen, D. J. and Wahlund, J.-E.: 1998, 'Core Ion Flux Bursts within Solitary Kinetic Alfvén Waves', *J. Geophys. Res.* **103**, 4157.

Lee, L. C.: 1981, 'Non-Linear Ion-Acoustic Waves and Solitons in a Magnetized Plasma', *Phys. Fluids.* **24**, 430.

Leneman, D., Gekelman, W. and Maggs, J.: 1999, 'Laboratory Observations of Shear Alfvén Waves Launched from a Small Source', *Phys. Rev. Lett.* **82**(13), 2673.

Leonovich, A. S. and Mazur, V. A.: 1999, 'Standing Alfvén Waves in the Magnetosphere from a Localized Monochromatic Source', *J. Geophys. Res.* **104**, 2411.

Liu, J. X. and Horton, W.: 1994, 'The Intrinsic Electromagnetic Solitary Vortices in Magnetized Plasma', *J. Plasma Physics* **36**, 1.

Lorenz, E.: 1963, 'Deterministic Nonperiodic Flow', *J. Atmospheric Sci.* **20**, 130.

Lotko, W., Streltsov, A. V. and Carlson, C. W.: 1998, 'Discrete Auroral Arcs, Electrostatic Shock and Suprathermal Electrons Powered by Dispersive, Anomalously Resistive Field Line Resonance', *Geophys. Res. Lett.* **25**, 4449.

Louarn, P., Wahlund, J.-E., Chust, T., de Feraudy, H., Roux, A., Holback, B., Dovner, P. O., Eriksson, A. I. and Holmgren, G.: 1994, 'Observations of Kinetic Alfvén Waves by the FREJA Spacecraft', *Geophys. Res. Lett* **21**, 1847.

Lühr, H., Warnecke, J., Zanetti, L. J., Lindqvist, P. A. and Hughes, T. J.: 1994, 'Fine Structure of Field-Aligned Current Sheets Deduced from Spacecraft and Ground-Based Observations: Initial Freja Results', *Geophys. Res. Lett.* **21**, 1883.

Lundin, R., Haerendel, G. and Grahn, S.: 1994, 'The Freja Science Mission', *Space Sci. Rev.* **70**, 405.

Lyons, L. R.: 1992, 'Formation of Auroral Arcs via Magnetosphere-Ionosphere Coupling', *Rev. Geophys.* **30**, 93.

Lysak, R. L.: 1985, 'Auroral Electrodynamics with Current and Voltage Generators', *J. Geophys. Res.* **90**, 4178.

Lysak, R. L.: 1990, 'Electromagnetic Coupling of the Magnetosphere and Ionosphere', *Space Sci. Rev.* **52**, 33.

Lysak, R. L.: 1991, 'Feedback Instability of the Ionospheric Resonant Cavity', *J. Geophys. Res.* **1553**, 1553.

Lysak, R. L.: 1993, in R. L. Lysak (ed.), 'Generalized Model of the Ionospheric Alfvén Resonator', *Small Rocket Instrumentation Techniques*, Vol. 80,. AGU, Washington, D.C., pp. 121–128.

Lysak, R. L. and Carlson, C. W.: 1981, 'Effect of Microscopic Turbulence on Magnetosphere-Ionosphere Coupling', *Geophys. Res. Lett.* **8**, 269.

Lysak, R. L. and Dum, C. T.: 1983, 'Dynamics of Magnetosphere-Ionosphere Coupling Including Turbulent Transport', *J. Geophys. Res.* **83**, 365.

Lysak, R. L. and Hudson, M. K.: 1979, 'Coherent Anomalous Resistivity in the Region of Electrostatic Shocks', *Geophys. Res. Lett.* **6**, 661.

Lysak, R. L. and Lotko, W.: 1996, 'On the Kinetic Dispersion Relation for Shear Alfvén Waves', *J. Geophys. Res.* **101**, 5085.

Maggs, J. E. and Davis, T. N.: 1968, 'Measurements of the Thickness of Auroral Structures', *Planet. Space Sci.* **16**, 205.

Maggs, J. E. and Morales, G. J.: 1996, 'Magnetic Fluctuations Associated with Field-Aligned Striations', *Geophys. Res. Lett.* **23**, 633.

Maggs, J. E. and Morales, G. J.: 1997, 'Fluctuations Associated with Filamentary Density Depressions', *Phys. Plasmas* **4**, 290.

Maggs, J. E., Morales, G. J. and Gekelman, W.: 1997, 'Laboratory Studies of Field-Aligned Density Striations and Their Relationships to Auroral Processes', *Phys. Plasmas* **4**, 1881.

Makela, J. S., Malkki, A., Koskinen, H., Boehm, M., Holback, B. and Eliasson, L.: 1998, 'Observations of Mesoscale Auroral Plasma Cavity Crossings with the Freja Satellite', *J. Geophys. Res.* **103** (A5), 9391.

Mallinckrodt, A. J. and Carlson, C. W.: 1978, 'Relations between Transverse Electric Fields and Eld-Aligned Currents',. *J. Geophys. Res.* **83**, 1426.

Maltsev, Y. P., Leontyev, S. V. and Lyatsky, W. B.: 1974, 'Pi2 Pulsations as a Result of an Alfvén Impulse Originating in the Ionosphere During the Brightening of Aurora', *Planetary Space Sci.* **22**, 1519.

Marklund, G. T., Blomberg, L. G., Lindqvist, P.-A. and C.-G. F. *et al.*: 1994, 'The Double Probe Electric Field Experiment on Freja: Experiment Description and First Results', *Space Sci. Rev.* **70**, 483.

Maynard, N., Heppner, J. P. and Egeland, A.: 1982, 'Intense Variable Electric Fields at Ionospheric Altitudes as Observed by DE-2', *Geophys. Res. Lett.* **9**, 981.

McFadden, J. P., Carlson, C. W. and Boehm, M. H.: 1986, 'Field-Aligned Electron Precipitation at the Edge of an Arc', *J. Geophys. Res.* **91**, 1723.

Mikhailovski, A., Lakhin, V., Aburdzhaniya, G., Mikhailovskaya, L., Onishchenko, O. and Smolyakov, A. I.: 1987, 'On the Theory of Alfvén Vortices', *Plasma Phys. Contr. Fusion* **29**, (1), 1.

Mikhailovskii, A. B., Petviashvili, V. I. and Fridman, A. M.: 1976, 'Alfvén Soliton', *JETP Lett.* **24**, 43.

Mirza, A. and Shukla, P.: 1997, 'Chaotic Behavior of Nonlinearly Coupled Electromagnetic Modes in Nonuniform Magnetoplasmas', *Phys. Lett.* **A229** (5), 313.

Mishin, E. V. and Förster, M.: 1995, 'Alfvénic Shocks and Low-Altitude Auroral Acceleration', *Geophys. Res. Lett.* **22**, 1745.

Morales, G. J., Loritsch, R. S. and Maggs, J. E.: 1994, 'Structure of Alfvén Waves at the Skin-Depth Scale', *Phys. Plasmas* **1**, 3765.

Mozer, F. S., Cattell, C. A., Temerin, M., Torbert, R. B., Glinsky, S. V., Woldorff, W. and Wygant, J.: 1979, 'The dc and ac Electric Field, Plasma Density, Plasma Temperature, and Field-Aligned Current Experiments on the S3-3 Satellite', *J. Geophys. Res.* **84**, 5875.

Nakamura, M., Hayakawa, H. and Tsuruda, K.: 1989, 'Electric Field Measurement in the Ionosphere Using the Time-of-Flight Technique', *J. Geophys. Res.* **94**, 5283.

Newell, P. T., Feldstein, Y. I., Galperin, Y. I. and Meng, C.-I.: 1996, 'Morphology of Nightside Precipitation', *J. Geophys. Res.* **101**, 10737.

Newton, R. S., Southwood, D. J. and Hughes, W. J.: 1978, 'Damping of Geomagnetic Pulsations by the Ionosphere', *Planetary Space Sci.* **26**, 201.

Norqvist, P., Andre, M., Eliason, L., Eriksson, A., Blomberg, L., Lühr, H. and Clemmons, J.: 1996, 'Ion Cyclotron Heating in the Dayside Magnetosphere', *J. Geophys. Res.* **101**, 13179.

Norqvist, P., Oscarson, T., André, M. and Blomberg, L.: 1998, 'Isotropic and Perpendicular Energization of Oxygen Ions at Energies Below 1 eV', *J. Geophys. Res.* **103**, 4223.

Okuda, H. and Dawson, J.: 1973, 'Theory and Simulation on Plasma Diffusion Across a Magnetic Field', *Phys. Fluids* **16**, 408.

Ono, M.: 1979, 'Cold Electrostatic Ion-Cyclotron Waves and Ion-Ion Hybrid Resonances', *Phys. Rev. Lett.* **42**, 1267.

Penano, J. R., Morales, G. J. and Maggs, J. E.: 1997, 'Properties of Drift Waves in a Filamentary Density Depletion', *Physics Plasmas* **4**(3), 555.

Perraut, S., de Feraudy, H., Roux, A., Décréau, P. M. E., Paris, J. and Matson, L.: 1990, 'Density Measurements in Key Regions of the Earth's Magnetosphere: Cusp and Auroral Region', *J. Geophys. Res.* **95**, 5997.

Persoon, A. M., Gurnett, D. A. and Shawhan, S. D.: 1983, 'Polar Cap Densities from DE-1 Plasma Wave Observations', *J. Geophys. Res.* **88**, 10,123.

Pokhotelov, O., Pokhotelov, D. O., Streltsov, A., Khruschev, V. and Parrot, M.: 1999, 'Dispersive Ionospheric Resonator', *J. Geophys. Res.*, submitted.

Pokhotelov, O. A., Pilipenko, V. A., Nezlina, Y. M., Woch, J., Kremser, G., Korth, A. and Amata, E.: 1986, 'Excitations of High-β Plasma Instabilities at the Geostationary Orbit; Theory and Observations', *Planetary Space Sci.* **34**, 695.

Polyakov, S. and Rapoport, V. O.: 1981, 'The Ionospheric Alfvén Resonator', *Geomagn. Aeron.* **21**, 816.

Radoski, H. R.: 1967, 'A Note on Oscillating Field Lines', *J. Geophys. Res.* **72**, 418.

Rankin, R., Frycz, P., Tikhonchuk, V. T. and Samson, J. C.: 1995, 'Ponderomotive Saturation of Magnetospheric Field Line Resonances', *Geophys. Res. Lett.* **22**, 1741.

Rees, M. H.: 1963, 'Auroral Ionization and Excitation by Incident Energetic Electrons', *Planetary Space Sci.* **11**, 1209.

Ruohoniemi, J. M., Greenwald, R. A., Baker, K. B. and Samson, J. C.: 1991, 'HF Radar Observations of Field Line Resonances in Midnight/Early Morning Sector', *J. Geophys. Res.* **96**, 15,697.

Samson, J. C., Cogger, L. L. and Pao, Q.: 1996, 'Observations of Field Line Resonances, Auroral Arcs, and Auroral Vortex Structures', *J. Geophys. Res.* **101**, 17,373.

Samson, J. C., Hughes, T. J., Creutzberg, F., Wallis, D. D., Greenwald, R. A. and Ruohoniemi, J. M.: 1991, 'Observations of a Detached Discrete Arc in Association with Field Line Resonances', *J. Geophys. Res.* **96**, 15,683.

Sato, T.: 1978, 'A Theory of Quiet Auroral Arcs', *J. Geophys. Res.* **83**, 1042.

Scholer, M.: 1970, 'On the Motion of Artificial Ion Clouds in the Magnetosphere', *Planetary Space Sci.* **18**, 977.

Seyler, C. E.: 1988, 'Nonlinear 3-D Evolution of Bounded Kinetic Alfvén Waves Due to Shear Flow and Collisionless Tearing Instability', *Geophys. Res. Lett.* **15**, 756.

Seyler, C. E.: 1990, 'A Mathematical Model of the Structure and Evolution of Small-Scale Discrete Auroral Arcs', *J. Geophys. Res.* **95**, 17199.

Seyler, C. E., Clark, A. E. and Bonnell, J.: 1998, 'Electrostatic Broadband ELF Wave Emission by Alfvén Wave Breaking', *J. Geophys. Res.* **103**, 7027.

Seyler, C. E. and Wahlund, J.-E.: 1996, 'Theory of Nearly Perpendicular Electrostatic Plasma Waves and Comparison to Freja Satellite Observations', *J. Geophys. Res.* **101**, 21795.

Seyler, C. E., Wahlund, J.-E. and Holback, B.: 1995, 'Theory and Simulation of Low-Frequency Plasma Waves and Comparison to Freja Satellite Observations', *J. Geophys. Res.* **100**, 21,453.

Shukla, P., Yu, M. and Stenflo, L.: 1986a, 'Electromagnetic Drift Vortices', *Phys. Rev.* **A34**, 3478.

Shukla, P., Yu, M. and Stenflo, L.: 1986b, 'Growth Rates of Modulationally Unstable Ion-Cyclotron Alfvén Waves', *Phys. Scripta.* **34**(2), 169.

Shukla, P., Yu, M. and Stenflo, L.: 1986c, 'Modulational Instabilities of Electron Cyclotron Waves', *Phys. Rev.* **A34** (2), 1582.

Shukla, P. K.: 1983, 'Nonlinear Propagation of Kinetic Alfvén Waves in a Plasma', *Phys. Rev.* **A27**, 1702.

Shukla, P. K.: 1987, 'Current Gradient Driven Flute Vortices in Magnetized Plasmas', *Phys. Fluids* **30** (7), 1901.

Shukla, P. K., Anderson, D., Lisak, M. and Wilhelmsson, H.: 1985, 'Shear Alfvén Vortices in a Very-Low-Beta Plasma', *Phys. Rev.* **A31**, 1946.

Shukla, P. K., Bingham, R. and Dendy, R. O.: 1998a, 'Amplitude Modulation of Kinetic Alfvén Waves and the Formation of Nonlinear Structures', *Phys. Lett.* **A239**, 369.

Shukla, P. K., Mirza, A. M. and Faria, R.: 1998b, 'Nonlinear Dynamics of Electromagnetic Turbulence in a Nonuniform Magnetized Plasma', *Phys. Plasmas* **5**, 616.

Shukla, P. K. and Stenflo, L.: 1985, 'Nonlinear Propagation of Electromagnetic Ion-Cyclotron Alfvén Waves', *Phys. Fluids* **28**, 1576.

Shukla, P. K. and Stenflo, L.: 1995, 'Nonlinear Alfvén Waves', *Phys. Scripta* **T60**, 32.

Shukla, P. K. and Stenflo, L.: 1999a, in T. Passot and P. L. Sulem (eds), 'Nonlinear Phenomena Involving Dispersive Alfvén Waves', *Nonlinear MHD Waves and Turbulence*, Springer-Verlag, Berlin, in press.

Shukla, P. K. and Stenflo, L.: 1999b, 'Plasma Density Cavitation Due to Inertial Alfvén Wave Heating', *Phys. Plasmas* **6**, 4120.

Shukla, P. K., Stenflo, L. and Bingham, R.: 1999, 'Nonlinear Propagation of Inertial Alfvén Waves in Auroral Plasmas', *Phys. Plasmas* **6**, 1677.

Shukla, P. K., Yu, M. Y., Rahman, H. U. and Spatschek, K. H.: 1984, 'Nonlinear Convective Motion in Plasma', *Phys. Rep.* **105**, 227.

Simonutti, M. D.: 1976, 'Transient Response from a Small Antenna in an Anisotropic Plasma', *Phys. Fluids* **19**, 608.

Singh, N.: 1999, 'Field Patterns of Alfvén Wave Resonance Cones', *J. Geophys. Res.* **104**, 6999.

Southwood, D. J.: 1974, 'Some Features of Field Line Resonances in the Magnetosphere', *Planetary Space Sci.* **22**, 483.

Sparrow, C.: 1982, *The Lorenz Equations: Bifurcations, Chaos and Strange Attractors*, Springer-Verlag, Berlin.

Stasiewicz, K.: 1985a, 'Generation of Magnetic-Field Aligned Currents, Parallel Electric Fields, and Inverted-V Structures by Plasma Pressure Inhomogeneities in the Magnetosphere', *Planetary Space Sci.* **33**, 1037.

Stasiewicz, K.: 1985b, 'The Influence of a Turbulent Region on the Flux of Auroral Electrons', *Planetary Space Sci.* **33**, 591.

Stasiewicz, K., Gustafsson, G., Marklund, G., Lindqvist, P.-A., Clemmons, J. H. and Zanetti, L.: 1997, 'Cavity Resonators and Alfvén Resonance Cones Observed on Freja', *J. Geophys. Res.* **102**, 2565.

Stasiewicz, K., Holback, B., Krasnoselskikh, V., Boehm, M., Boström, R. and Kintner, P. M.: 1996, 'Parametric Instabilities of Langmuir Waves Observed by Freja', *J. Geophys. Res.* **101**, 21515.

Stasiewicz, K., Holmgren, G. and Zanetti, L.: 1998, 'Density Depletions and Current Singularities Observed by Freja', *J. Geophys. Res.* **103** (A3), 4251.

Stasiewicz, K., Khotyaintsev, Y., Berthomier, M. and Wahlund, J.-E.: 2000a, 'Identification of Widespread Turbulence of Dispersive Alfvén Waves', *Geophys. Res. Lett.* **27**, 173.

Stasiewicz, K., Lundin, R. and Marklund, G.: 2000b, 'Stochastic Ion Heating by Orbit Chaotization on Electrostatic Waves and Nonlinear Structures', *Phys. Scripta* **T84**, 60.

Stasiewicz, K. and Potemra, T.: 1998, 'Multiscale Current Structures Observed by Freja', *J. Geophys. Res.* **103** (A3), 4315.

Stefant, J. R.: 1970, 'Alfvén Wave Damping from Finite Gyroradius Coupling to the Ion Acoustic Mode', *Phys. Fluids* **13**, 440.

Stenbaek-Nielsen, H. C., Hallinan, T. J., Osborne, D. L., Kimball, J., Chaston, C., McFadden, J., Delory, G., Temerin, M. and Carlson, C. W.: 1998, 'Aircraft Observations Conjugate to FAST: Auroral Arc Thicknesses', *Geophys. Res. Lett.* **25**, 2073.

Stenflo, L.: 1996, 'Generalized Lorenz Equations for Acoustic-Gravity Waves in the Atmosphere', *Phys. Scripta* **53** (1), 83.

Streltsov, A. and Lotko, W.: 1995, 'Dispersive Field Line Resonances on Auroral Field Lines', *J. Geophys. Res.* **100**, 19,457.

Streltsov, A. V. and Lotko, W.: 1999, 'Small-Scale, 'Electrostatic' Auroral Structures and Alfvén Waves', *J. Geophys. Res.* **104**, 4411.

Streltsov, A. V., Lotko, W., Johnson, J. R. and Cheng, C. Z.: 1998, 'Small-Scale, Dispersive Field Line Resonances in the Hot Magnetospheric Plasma', *J. Geophys. Res.* **103**, 26,559.

Stringer, T.: 1963, 'Low-Frequency Waves in an Unbounded Plasma', *J. Nuclear Energy C* **5**, 89.

Sugiura, M.: 1984, 'A Fundamental Magnetosphere-Ionosphere Coupling Mode Involving Field-Aligned Currents as Deduced from DE-2 Observations', *Geophys. Res. Lett.* **11**, 877.

Temerin, M. and Lysak, R. L.: 1984, 'Electromagnetic Ion Cyclotron Mode (ELF) Waves Generated by Auroral Electron Precipitation', *J. Geophys. Res.* **89**, 2849.

Temerin, M. M., Waldorf, M. and Mozer, F. S.: 1979, 'Nonlinear Steepening of the Electrostatic Ion Cyclotron Wave', *Phys. Rev. Lett.* **43**, 1941.

Trakhtengertz, V. Y. and Feldstein, A. Y.: 1984, 'Quiet Auroral Arcs: Ionospheric Effect of Magnetospheric Convection Stratification', *Planetary Space Sci.* **32**, 127.

Trondsen, T. S. and Cogger, L. L.: 1998, 'A Survey of Small-Scale Spatially Periodic Distorsions of Auroral Forms', *J. Geophys. Res.* **103**, 9405.

Trondsen, T. S., Cogger, L. L. and Samson, J.: 1997, 'Asymetric Multiple Auroral Arcs and Inertial Alfvén Waves', *Geophys. Res. Lett.* **24**, 2945.

Vincena, S. and Gekelman, W.: 1999, '3D Observations of Electromagnetic Ion Cyclotron Wave Propagation in a Laboratory Plasma Column', *IEE-Trans. Plasma Sci.* **27**, 144.

Vogt, J. and Haerendel, G.: 1998, 'Reflection and Transmission of Alfvén Waves at the Auroral Acceleration Region', *Geophys. Res. Lett.* **25**, 277.

Volokitin, A. S. and Dubinin, E. M.: 1989, 'The Turbulence of Alfvén Waves in the Polar Magnetosphere of the Earth', *Planetary Space Sci.* **37**, 761.

Volwerk, M., Louarn, P., Chust, T., Roux, A., de Feraudy, H. and Holback, B.: 1996, 'Solitary Kinetic Alfvén Waves: A Study of the Poynting Flux', *J. Geophys. Res.* **101**, 13,335.

Voronkov, V., Rankin, R., Tikhonchuk, V. T. and Samson, J. C.: 1997, 'Nonlinear Shear Alfvén Resonances in a Dipolar Magnetic Field', *J. Geophys. Res.* **102**, 27,137.

Wahlund, J.-E., Eriksson, A. I., Holback, B., Boehm, M., Bonel, J., Kintner, P. M., Seyler, C. E., Clemmons, J. H., Eliasson, L., Knudsen, D., Norqvist, P. and Zanetti, L.: 1998, 'Broadband ELF Plasma Emission During Auroral Energization 1. Slow Ion Acoustic Waves', *J. Geophys. Res.* **103**, 4343.

Wahlund, J.-E., Louarn, P., Chust, T., de Feraudy, H., Roux, A., Holback, B., Cabrit, B., Ericsson, A., Kintner, P., Kelley, M. C., Bonel, J. and Chesney, S.: 1994a, 'Observations of Ion Acoustic Fluctuations in the Auroral Topside Ionosphere by the Freja s/c', *Geophys. Res. Lett.* **21**, 1835.

Wahlund, J.-E., Louarn, P., Chust, T., de Feraudy, H., Roux, A., Holback, B., Dovner, P.-O. and Holmgren, G.: 1994b, 'On Ion-Acoustic Turbulence and the Nonlinear Evolution of Kinetic Alfvén Waves in Aurora', *Geophys. Res. Lett.* **21**, 1831.

Walker, A. D., Ruohoniemi, J. M., Baker, K. B. and Greenwald, R. A.: 1992, 'Spatial and Temporal Behaviour of ULF Pulsations Observed by the Goose Bay HF Radar', *J. Geophys. Res.* **97**, 12,187.

Walker, A. D. M.: 1980, 'Modelling of Pc5 Pulsation Structure in the Magnetosphere', *Planetary Space Sci.* **28**, 213.

Watanabe, T., Oya, H., Watanabe, K. and Sato, T.: 1993, 'Comprehensive Simulations Study on Local and Global Development of Auroral Arcs and Field-Aligned Potentials', *J. Geophys. Res.* **98**, 21,391.

Weimer, D. R., Goertz, C. K., Gurnett, D. A., Maynard, N. C. and Burch, J. L.: 1985, 'Auroral Zone Electric Fields for DE 1 and 2 at Magnetic Conjunctions', *J. Geophys. Res.* **90**, 7479.

Weimer, D. R. and Gurnett, D. A.: 1993, 'Large-Amplitude Auroral Electric Fields Measured with DE-1', *J. Geophys. Res.* **98**, 13,557.

Whalen, B. A., Knudsen, D. J., Yau, A. W., Pilon, A. M. and Cameron, T. A.: 1994, 'The Freja F3C Cold Plasma Analyzer', *Space Sci. Rev.* **70**, 541.

Wilcox, J. M., Boley, F. I. and DeSilva, A. W.: 1960, 'Experimental Study of Alfvén Wave Properties', *Phys. Fluids* **3**, 15.

Xu, B.-L., Samson, J. C., Liu, W. W., Creutzberg, F. and Hughes, T. J.: 1993, 'Observations of Optical Aurora Modulated by Resonant Alfvén Waves', *J. Geophys. Res.* **98**, 11,531.

Zanetti, L. *et al.*: 1994, 'Magnetic Field Experiment on the Freja Satellite', *Space Sci. Rev.* **70**, 465.

Zhu, X. and Kivelson, M. G.: 1991, 'Compressional ULF Waves in the Outer Magnetosphere, 1, Statistical Study', *J. Geophys. Res.* **96**, 19,451.